ELECTROCHEMICALLY ACTUATED CAPILLARY FLOW CONTROL FOR THE DEVELOPMENT OF INTEGRATED MICROFLUIDIC DEVICES

Alemayehu Paulos Washe

Dipòsit Legal: T. 475-2013

Doctoral Thesis

Alemayehu Paulos Washe

**ELECTROCHEMICALLY ACTUATED CAPILLARY FLOW CONTROL
FOR THE DEVELOPMENT OF
INTEGRATED MICROFLUIDIC DEVICES**

Universitat Rovira i Virgili

Department of Chemical Engineering

Tarragona, 2013

Alemayehu Paulos Washe

ELECTROCHEMICALLY ACTUATED CAPILLARY FLOW CONTROL FOR THE DEVELOPMENT OF INTEGRATED MICROFLUIDIC DEVICES

Doctoral Thesis

Supervised by:

Dr. Ioanis Katakis
Dr. Pablo Lozano-Sanchez

Department of Chemical Engineering

Universitat Rovira I Virgili

Tarragona

2013

UNIVERSITAT
ROVIRA I VIRGILI

ESCOLA TÈCNICA SUPERIOR D'ENGINYERIA
QUÍMICA DEPARTAMENT D'ENGINYERIA QUÍMICA
Av. Països Catalans 18
Campus Sescelades
43007 Tarragona (Spain)
Tel. 34 977 556955
Fax 34 977 55 86 23

Dr. Ioanis Katakis and Dr. Pablo Lozano,

Certify that:

The doctoral thesis entitled "Electrochemically actuated capillary flow control for the development of integrated microfluidic devices" presented by Alemayehu Paulos Washe to obtain the degree of doctor by the Universitat Rovira I Virgili has been carried out under my supervision at the Department of Chemical Engineering.

Dr. Ioanis Katakis

Dr. Pablo Lozano

Tarragona, 25 January 2013

To my family
Jada, Juliet & Bezuayehu

ACKNOWLEDGEMENT

It gives me great pleasure to express my sincere gratitude to my PhD supervisor Dr. Ioanis Katakis who accepted me and trusted me for the great scientific intent to be realized. It was great opportunity for me to work with Dr. Katakis. He guided me properly and encouraged me to exercise the scientific attitude freely that gave me the opportunity to develop confidence for independent thinking-Many thanks! I am also grateful to my co-supervisor Dr Pablo Lozano who encouraged me and helped me during the PhD.

I would like to thank Dr. Ciara O' Sullivan for kind guidance during my incorporation into the BBG group and also for recommending me for a PhD student position under Dr. Katakis. I am also grateful to Professor F. Xavier Rius for unreserved guidance and training during my Master studies and initial periods of the PhD. I am grateful to Dr. Santiago Macho and Dr. Enrique J. Parra for kind collaborations and friendly atmosphere in Tarragona and URV. My appreciation and thanks to all current and previous members of the INTERFIBIO group including Dr. Bruno Dias, Dr. Mayreli Ortiz, Dr. Angel González, Dr. Valerio Beni, Dr. Alex Fragoso, Dr. Teresa Mairal for friendly approaches and collaborations. I am thankful to Mr. Diego Bejarano-Nosas who helped me a lot with my activities in Lab 214. I thank Dr. Olivier Henry for helping me with the video set ups for my experiments. I would like to thank Dr. Sergio Martínez Montequín for training on screen-printing during initial periods of the PhD. I have special thanks to my lab-mates Mabel Torrens and Ewelina Wajs and of course our colleague Oumaya Msehli for collaborations and friendly atmosphere in Lab214. I would like to extend my appreciation to Dr. Mayreli Ortiz and Mabel Torrens for showing responsibility from their own initiation and taking time to correct my Spanish on the "Resumen" section-lots of thanks!!!

I would like to acknowledge the University of Rovira I Virgili (URV), and the Autonomous Government of Catalunya for BRDI and FIDGR doctoral fellowships respectively. The Dilla University, my home University in Ethiopia, is also acknowledged for granting me study leave permission and providing financial support to my family during this PhD. I am thankful to Ms. Barbara Vastenavond and Ms. Sira Durán for assistance in the administrative works.

My deepest gratitude and appreciation goes to my family, my daughters (Jada Alemayehu and Juliet Alemayehu) and to my wife Bezuayehu Assefa, who showed relentless patience and endurance taking care of the kids and encouraging me to concentrate of my study. I would like to thank also Ato Harkiso Haile and my mother W/ro Ferenj Abebe for encouragements.

Summary

Microfluidics may be defined as the study of the behavior, and manipulation of very small volume of fluid in microchannels of dimensions 10s to 100s of micrometers. Microfluidics offers very fascinating features with some interesting challenges to overcome in the device development. In addition to the improved analytical performance related to the high surface area-to-volume ratio resulting from miniaturization, the ability to perform analysis on a very small volume of samples with economy of reagents and time makes microfluidics cost effective solution to the realization of current needs for ASSURED (a term introduced by A. Guiseppi-Elie: Affordable, Sensitive, Specific, User-friendly, Rapid and robust, Equipment-free and Deliverable) devices for distributed diagnostics and home-health care (D$_2$H$_2$) applications.

A good example of diagnostic devices that can be considered as a starting point for the development of ASSURED microfluidic devices are Lateral flow Devices (LFDs). Because LFDs have been successfully commercialized and used in point-of-care (POC) diagnostics. They owe their success to their simplicity that significantly depends on the capillary-driven flow and versatile technological platform that lends itself to fast and low cost product development. However, these devices are often limited to screening applications. They are not sensitive enough for certain applications that require highly sensitive and quantitative analysis such as that of allergies. Microfluidic devices, particularly capillary driven microfluidic devices, are expected to outperform LFDs and overcome their limitation if flow rate is precisely controlled in microchannels given current state of the art in microfabrication techniques.

In this thesis the design, fabrication and implementation of three different electrochemically actuated capillary flow control schemes have been developed through low voltage electrowetting/electrochemical actuation of the flow using i) electrical stimuli responsive superhydrophobic surfaces based on intelligent polymers ii) superhydrophobic nanoporous carbonaceous surfaces, and iii) superhydrophobic electrodes coupled to other electrodes that facilitate the generation of gradients to propel the liquid. The developed schemes are expected to facilitate the realization of ASSURED devices for bioanalytical applications where an analytical response depends on the dissolution of previously deposited reagents, the kinetics of biological affinity and enzymatic reactions, and mass transport of products to a transducer in the microchannels. The thesis unravels the mechanism of response of such systems and demonstrates ways for reduction to practice of such devices for the "democratization" of theranostics.

The valving configuration in all the three schemes involves a pair of screen printed electrodes (SPEs) transversal to the flow. One of the electrodes in each pair is superhydrophobic to provide passive stopping and facilitate low-voltage actuation of the flow by virtue of: electrically tunable wettability based on intelligent polymers, low voltage electrowetting transition from the less wetted Cassie to more wetted Wenzel or on-chip generated concentration gradient.

In the first scheme the fabrication of polymer based superhydrophobic surface by electropolymerization required pretreatment of screen printed carbon electrodes (SPCEs) to amplify the roughness and enhance electrochemical performance. The activation as well as roughness amplification strategy was controlled to avoid nucleophilic functionalities on the surface of the electrodes. Such functionalities as hydroxyl groups can render nucleophilic attack to the growing polymeric chain or reactive intermediates during the electropolymerization and destroy the conjugation- the key requirement for the expected electrically tunable property of the polymer. In this work we achieved this by a new procedure that involves controlled and selective subtraction of nonelectroactive components from the electrode's surface based on solubility principles. The selective subtraction enhances surface roughness and also activates the electrodes for electropolymerization by increasing graphitic loading and exposure (electrochemical accessibility) of the graphitic edges with electrocatalytic property. Electrodeposition of the polymer was then performed on the previously roughened and activated SPCE surface through controlled cycling of potential to produce poly(3-methylthiophene) based superhydrophobic surface that displays passive stopping of capillary flow and facilitate low voltage actuation of the flow.

The second approach boasts simplicity and is based on the favorable wettability transition from the less stable Cassie-Baxter wettability regime of superhydrophobic nanoporous electrode with no further modification to a more stable and more wettable Wenzel regime by electrowetting. By virtue of superhydrophobicity the electrode stops the flow and by virtue of the high conductivity, large potential window and intrinsic charge accumulation capacity of carbonaceous material it facilitates the low voltage actuation through electrowetting transitions at extremely low voltage. In this case both electrodes involved in the valving operation are based on screen printed carbon-one wettable and the other superhydrophobic nanoporous in each stop/go valving electrode pair.

The third scheme also exploits the superhydrophobic nanoporous carbon electrode but couples it to screen printed silver. The superhydrophobic electrode as usual provides passive stopping of

the flow and facilitates low voltage actuation of the flow via on-chip generated gradients of concentration.

All the three schemes have been successfully implemented to demonstrate multiple and sequential stop/go fluidic operations in microchannels using different aqueous solutions including biological buffers containing proteins of interest such as lactoglobulins. Such operations, unlike the previously reported methods, allow precise control of the flow at specific locations in the microchannels and are simple, low cost and miniaturizable.

Resumen

La microfluídica se define como el estudio del comportamiento y la manipulación de pequeños volúmenes de fluidos en microcanales de dimensiones entre las decenas y centenas de micrómetros. Esta tecnología ofrece grandes ventajas para el desarrollo de nuevos dispositivos en diversas áreas de investigación. Un importante avance de la aplicación de la microfluídica es el incremento del rendimiento analítico del dispositivo resultante de la miniaturización del sistema, debido al aumento de la relación área superficial/volumen. En este sentido, las pequeñas dimensiones de los microcanales hacen posible el empleo de poca cantidad de muestra, así como la disminución del tiempo de análisis, respecto a otras técnicas. Lo que representa una ventaja desde el punto de vista económico y una opción muy interesante para lograr mejorar las actuales necesidades de los dispositivos *ASSURED* (término introducido por A. Guiseppi-Elie: *Affordable, Sensitive, Specific, User-friendly, Rapid and robust, Equipment-free and Deliverable)* para tratamientos a domicilio.

Los dispositivos de flujo lateral (LFDs) pueden ser considerados como el punto de partida en el desarrollo de dispositivos de microfluídica *ASSURED*. Éstos se han comercializado y utilizado exitosamente con fines diagnósticos. Los LFDs deben su éxito a su sencillez, que depende fundamentalmente del manejo del flujo capilar y versatilidad de su plataforma tecnológica, lo que los hace productos económicos. Sin embargo, presentan limitaciones en investigaciones que requieran elevada sensibilidad y análisis cuantitativos, como los dedicados a estudios de alergia. Los dispositivos de microfluídica, específicamente los conducidos mediante capilaridad es una de las opciones para superar las limitaciones del los LFDs mediante el control preciso de la velocidad de flujo en los microcanales utilizando técnicas de microfabricación.

En esta Tesis se ha desarrollado el diseño, fabricación e implementación de tres alternativas diferentes de dispositivos con control de flujo mediante técnicas electroquímicas. El flujo se maneja mediante electroquímica y *electrowetting* de bajo voltaje. Las tres alternativas presentadas son i) superficies superhidrofóbicas basadas en polímeros que responden inteligentemente a los estímulos eléctricos, ii) superficies de carbono nanoporosas superhidrofóbicas, y iii) electrodos con superficies superhidrofóbicas acoplados a otros electrodos que facilitan la generación de gradientes que pueden impulsar el líquido. Con estos sistemas propuestos se espera lograr la fabricación de futuros dispositivos *ASSURED* para aplicaciones bioanalíticas; donde la respuesta analítica depende de la disolución de los reactivos previamente depositados, la cinética de afinidad biológica, las reacciones enzimáticas, y el transporte de masa del productos al transductor en los microcanales. La tesis estudia el mecanismo de la respuesta en cada caso en estos sistemas y demuestra opciones para la reducción a la práctica de herramientas que pueden "democratizar" la "teranostica" (*theranostics).*

Uno de los electrodos de cada par es superhidrofóbico para permitir la detención pasiva del flujo y facilitar el control del mismo por bajo voltaje mediante la humidificación controlable eléctricamente basada en polímeros inteligentes, la transición electro-humidificante de bajo voltaje desde el menos húmedo *Cassie* al más húmedo *Wenzel*, y el gradiente de concentraciones generado en el chip.

En el primer esquema, la fabricación del polímero basado en una superficie superhidrofóbica requirió el pretratamiento de los electrodos de carbono impresos (SPCEs) para aumentar la rugosidad mejorar sus características electroquímicas. La activación, así como la estrategia de amplificación de la rugosidad, fue controlada para evitar la aparición de grupos funcionales nucleofílicos en la superficie del electrodo. Debido a que grupos funcionales como hidroxilos pueden realizar ataques nucleofílicos en la cadena polimérica en formación o reaccionar con intermediarios durante la electropolimerización, destruyendo la conjugación que es el elemento clave de las propiedades eléctricamente controlables del polímero. En este trabajo nosotros conseguimos este propósito empleando un nuevo procedimiento que comprende el control y la sustracción selectiva de componentes no electroactivos de la superficie del electrodo basados en principios de solubilidad. La selectiva sustracción incrementa la rugosidad superficial y activa los electrodos mediante electropolimerización por incremento de la carga del grafito y exposición (accesibilidad electroquímica) de los vértices de la superficie del grafito con propiedades electrocatalíticas. La electrodeposición del polímero fue entonces realizada, en las superficies de los SPCE previamente activados, mediante voltametría cíclica produciendo poli(3-metiltiofeno), debido a la superficie superhidrofóbica que muestra detención pasiva del flujo capilar y facilita la actuación del bajo voltaje sobre el flujo.

El segundo enfoque muestra una mayor simplicidad y se basa en la transición favorable desde el menos estable régimen de humidificación *Cassie-Baxter* de electrodos nanoporosos superhidrofóbicos sin modificación al régimen más estable y humidificable *Wenzel* mediante *electrowetting*. Gracias a la superhidrofobicidad, el electrodo detiene el flujo y debido a la alta conductividad, al amplio rango de potenciales y a la capacidad intrínseca de acumulación de carga de estos materiales, se facilita la acción de bajo voltaje mediante transiciones de *electrowetting* a voltajes extremadamente bajos. En este caso, cada par de electrodos implicados en la operación de válvulas se basan en electrodos impresos de carbono, siendo uno humidificable y el otro nanoporoso con carácter superhidrofóbico.

El tercer esquema utiliza nuevamente electrodos de carbono nanoporosos con carácter superhidrofóbico pero emparejado con un electrodo impreso de plata. El electrodo superhidrofóbico aporta la detención pasiva del flujo y facilita la actuación del bajo voltaje sobre el flujo a través de gradientes de concentración generados en el chip.

Los tres esquemas han sido implementados exitosamente, demostrando así posibilidad de realizar secuencialmente operaciones fluídicas de parada y continuación del flujo en los microcanales, utilizando diferentes soluciones acuosas como tampones biológicos que contienen proteínas de interés como lactoglobulinas. Dichas operaciones, contrario a lo reportado previamente en la literatura, ofrecen un control preciso del flujo en posiciones específicas en los microcanales y constituyen una alternativa simple, de bajo coste y fácilmente miniaturizable.

List of abbreviations

EW: Electrowetting

EWOD: Electrowetting on dielectric

η: viscosity

γ: interfacial tension

μ: chemical potential

ρ: density of liquid

ζ: zeta potential

ψ: surface potential

θ: contact angle in degree

ε: permittivity of a dielectric

λ: Debye length

Å: angstrom unit

σ: charge density

V: Voltage

R: resistance

R_{ct}: charge transfer resistance

d: depth of a microchannel

w: width of a microchannel

R_{soln}: solution resistance

W: Warburg diffusion

C: Capacitance

Q: constant phase element

SPCE: Screen printed carbon electrode

DMF: N, N-Dimethylformamide

CH3CN: acetonitrile

DMSO: Dimethylsulfoxide

i_{ct}: Faradic current (charge transfer current)

i_{dl}: Capacitive current (double layer charging current)

i_{pa}: anodic peak current

i_{pc}: cathodic peak Current

AFM: Atomic force Microscopy

ESEM: Environmental scanning electron microscopy

3-MeT: 3-methylthiphene

P3MeT: Poly(3-methylthiophene)

List of publications

Title: SMART electrodes for stop-go fluidic manipulation in analytical microsystems

Authors: Alemayehu P. Washe, P. Lozano, D. Bejarano, and Ioanis Katakis

Journal: Electrochemistry Communications (Submitted)

Title: Electrochemically actuated stop-go valves for capillary force-operated diagnostic microsystems (Article in press, accepted as VIP)

Authors: Alemayehu P. Washe, P. Lozano, D. Bejarano, and Ioanis Katakis

Journal: ChemPhysChem

Title: Electrochemically actuated passive stop-go microvalves for flow control in microfluidic systems (accepted)

Authors: Alemayehu P. Washe, P. Lozano, D. Bejarano, B. Teixeira-Dias and Ioanis Katakis

Journal: Microelectronic Engineering

Title: Facile and versatile approaches to enhancing electrochemical performance of screen printed electrodes (Published)

Authors: Alemayehu P. Washe, P. Lozano, D. Bejarano, and Ioanis Katakis

Journal: Washe et al., Electrochimica Acta 91 (2013) 166– 172

Scientific contributions to congresses

1. Electrochemically actuated passive stop-go microvalves for Flow control in microfluidic systems (POSTER)

Authors: Alemayehu P. Washe, P. Lozano, D. Bejarano, B. T. -Dias and Ioanis Katakis, 38th International Conference on Micro and Nano Engineering, Sep. 2012, Toulouse (France).

2. Flow control in microfluidic systems using electrochemically actuated passive stop-go valves (ORAL PRESENTATION)

Authors: Alemayehu P. Washe, P. Lozano, D. Bejarano, B. Teixeira-Dias and Ioanis Katakis

 XVII Trobada Transfronterera de Sensors i Biosensors. Sep. 20, 2012, Tarragona Spain

3. Activation of mass fabricated screen-printed carbon electrodes for biosensor development (POSTER)

Authors: Alemayehu P. Washe, P. Lozano, Ioanis Katakis

XVIèmes Rencontres Transfrontalières « Capteurs et Biocapteurs » – Toulouse 2011

4. Electrochemically actuated passive stop-go microvalves for flow control in microfluidic systems *(Invited Paper)*

Authors: Ioanis Katakis, <u>Alemayehu P. Washe</u>, P. Lozano, D. Bejarano, and B. Teixeira-Dias "Microfluidics, BioMEMS, and Medical Microsystems XI" conference, 2 February 2013 to 7 February 2013 in San Francisco, California USA.

5. Electrochemically Actuated, Capillarity-Driven Biodetection Devices for Food Safety and Clinical Analysis (Invited presentation)

Authors: Ioanis Katakis, <u>Alemayehu P. Washe</u>, Luis Carlos Rosales-Rivera, Pablo Lozano-Sánchez, Diego Bejarano-Nosas, Bruno Teixeira-Dias, Bioelectrochemistry 2013, Bochum, Germany, 17-21 March 2013.

Author´s scientific contributions not related to this thesis

1. Paper
Title: Potentiometric online detection of aromatic hydrocarbons in aqueous phase using carbon nanotube based sensors

Authors: <u>Alemayehu P. Washe</u>, Santiago Macho, Gastón A. Crespo and F. Xavier Rius

Journal: *Anal. Chem.* **2010,** *82,* 8106–8112

2. Contributions to congresses

Title: Potentiometric On-line Detection of Aromatic Hydrocarbons in Aqueous Phase Using Carbon Nanotube-based Sensors

Authors: <u>Alemayehu P. Washe</u>, Santiago Macho, Gastón A. Crespo and F. Xavier Rius

Congress: IV Workshop Analytical Nanoscience and Nanotechnology. Sep. 2010, Zaragoza, Spain

Format: Oral presentation and poster

Table of Contents

CHAPTER 1

INTRODUCTION

1.1 Microfluidics: Background and Applications

Microfluidics refers to manipulation and analysis of tiny volume of fluids (usually nanolitres or less) at a size scale of microchannel dimensions in the order of tens to hundreds of micrometers.[1] The distant origins of microfluidics for analytical applications can be traced back to microanalytical methods for chromatographic techniques [gas chromatography (GC) and high pressure liquid chromatography (HPLC)] and capillary electrophoresis (CE). In the mid 1950s Golay[2] and van Deemter[3] showed the importance of scaling parameters on the performance of GC and HPLC, respectively. Scaling down of packed column particle sizes and open column diameters was shown to improve the separation performance of the columns. Around the same time the microelectronics industry started miniaturization and integration of circuit elements of multiple functionalities to enhance the performance of electronic devices through its silicon-based micromachining processes using photolithography, etching, and bonding techniques.[4, 5] Thus the merging of advances in analytical methods and microelectronics industry can be considered to have given birth to microfluidics. The first miniaturized silicon-based GC air analyzer on a silicon wafer was published in 1979 by Terry et al. from Stanford University.[6] But the concept of miniaturization and integration of several analytical operations involved in a typical bioassay including sampling, transport, pretreatment, and detection on a chip in what is generally known as "lab-on-a-chip (LOC)" or miniaturized total analysis systems (µTAS) was introduced by Manz et al in 1990s.[7-9]

In 1992 Manz et al. heralded a new microfluidic era in separation sciences through the first on-chip CE system. In that same year, Mathies et al. proposed high-throughput electrophoretic sequencing on arrays of microfluidic devices.[10] In 1993, Harrison et al. demonstrated a micro-CE system in glass.[11] The next year, Woolley and Mathies successfully miniaturized a microfluidic capillary gel electrophoresis system for DNA analysis, which allowed to accomplish separation in as little as 2 minutes.[12] It was in the mid 1990s that microfluidics started to show a boom with new concepts and devices to investigate microfluidic solutions not only for separations, but also other applications notably due to the analytical and economic advantages of miniaturizations.

Miniaturization brings improved analytical performance associated with the high surface area to volume ratio resulting from scaling down of the size. These include separation efficiency,

higher specificity, high throughput, and in-situ monitoring. The high surface area-to-volume ratio of microfluidic channels increases effective thermal dissipation which in turn aids in reducing power consumption of devices. On the other hand, the ability to make analysis on a very small volume of samples with economy of reagents and time, less waste, parallelization and portability makes microfluidics a cost effective solution for the realization of current needs for ASSURED devices for distributed diagnostics and home-health care or in general POC applications.

Considering that most biological processes involve small-scale fluidic transport, microfluidics seems especially relevant to bioanalytical applications. The rise of water in trees from the ground through roots to the leaves via capillaries (xylem), material exchange through capillary walls in human body, molecular transfer across cellular membranes, oxygen diffusivity through the lungs and blood flow through microscale arterial networks are among relevant examples. Fig 1.1 provides the comparative relevant size scales of device dimensions or volume of liquids to that of molecules/particles.
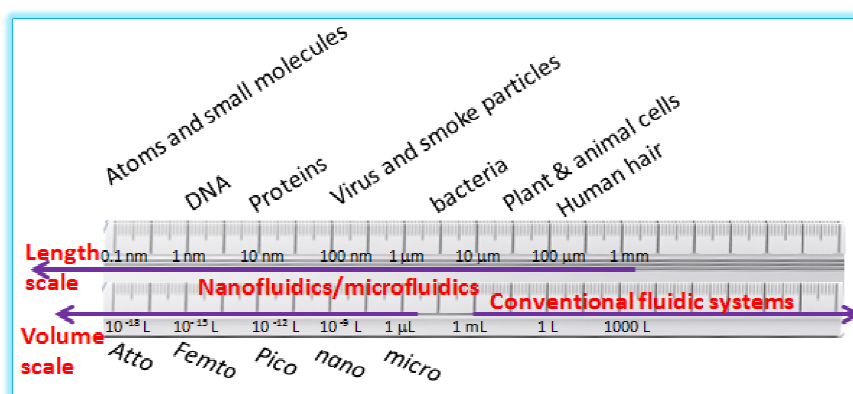
Fig. 1.1 Comparative size scales for several biological and microfluidic systems as compared to conventional world of analysis.

The advent of microfluidics from separation to other applications was facilitated by advances in microfabrication technologies of microelectronics and microelectromechanical systems (MEMS) giving rise to microarray technology which found its way to microfluidics.[13, 14] In 1990s use of standard lithography to immobilize probe molecules on microarrays as individual spots that may hybridize with the target to make extremely large numbers of parameters to be screened at short time was reported.[15] In 1995 the well known 96 microwell array was used to detect an organism's gene expressions.[16, 17] Aside from relatively simple reactions on microarrays, on-chip polymerase chain reaction (PCR) that uses enzymatic transcription to systematically amplify parts or all of a DNA strand, triggered via thermal fluctuations was reported by Northrup et al. in 1995 and

1996.[18] In addition to the inspiring progress in basic research in academia, microfluidics started to develop as practical technology by life science companies such as Caliper Life Sciences in 1995. Founded in 1996, Cepheid commercialized rapid biothreat detection systems. Other diagnostic companies such as the Biosite Triage appeared in the 2000s.[19] Inspired by such practical demonstration of microfluidics, researchers continued extensive investigation of microfluidics in chemical and system biology,[20-22], genetic (DNA/RNA) analysis,[23-26] proteomics,[27-32] cell/molecule analysis [33-44] and clinical diagnostics,[45] sample preconcentration,[46] drug delivery,[49-50] point-of-care (POC) diagnostics, [51-55] environmental monitoring and other applications.[56]

1.2 Microfluidics: Challenges and Opportunities

The unique feature of microfluidics that is also the hope of microfluidic community is the integration and automation of various analytical operations on a chip so that users who are not experts in the field such as the patient, clinicians, and police officers can operate it easily. This hope can only be achieved if the key operations, i.e various fluid manipulation components such as pumps and valves and analytical separation and detection techniques are integrated on a device. In addition to the simplicity of operation, integration provides distinct advantages to µTAS devices including avoiding sample contamination, reducing error caused from human contact, reduced sample-processing time and allow for a fully-automated analysis. Indeed virtually all LOC systems rely upon some microfluidic components to control, transport, and manipulate small volume of liquid in the microchannels. However, the fabrication of the structural (the microchannels) and functional components (pumps, valves, detectors etc) and their integration and automation on a chip have not been so easy. The first microfluidic devices were made from silicon (of silicon industry) and glass by adapting the lithographic techniques used in the microelectronics industry such as Micro-Electro-Mechanical Systems (MEMS) or Micro-Opto-Electro-Mechanical Systems (MOEMS) for creating features needed in the device.[57] Conventional machining methods (i.e. milling, drilling, cutting, and turning) that remove material from metals and hard plastics have been used to create simple microstructures, primarily for molding applications.[58, 59] Traditional method of producing microfluidic systems on silicon and glass require long and costly processing procedures such as wet and dry etching, metal evaporation and anodic bonding.[59] Current microfluidic fabrications are, however, usually made on plastic than silicon or glass partly because it is much easier to fabricate the components required for microanalytical systems-especially pumps and valves-in elastomeric plastics than rigid materials and partly due to the prohibitive prices of silicon and its opaque nature to visible and ultraviolet light (i.e it cannot be used with conventional optical methods of detection). Polymeric microfluidic platforms can easily be

produced using soft lithography, hot embossing, injection molding, laser ablation, in-situ construction[60] and plasma etching.[61] The most popular method used in the production of polymeric microfluidic devices is injection molding.[62-63] A polymer melt is injected under high pressure into an evacuated mold to completely fill a cavity or cavities, and subsequently chilled (cooled and solidified) such that it can be separated from the mold. Likewise polymers can be embossed to a master to produce desirable features.[64] In the embossing machine, the master and the polymer substrate are heated separately under vacuum to a temperature just above the glass transition temperature T_g of the polymer material. The master is then brought into contact with the substrate and embossed with a controlled force for several seconds. The master-substrate sandwich is then cooled to just below T_g while still applying the embossing force. After reaching a specific temperature, the master is mechanically separated from the substrate which now contains the desired features which may require further processing, e.g. by drilling holes or bonding it to a cover lid to close the channels. Bonding of a planar matting material to cover microfluidic channels are accomplished by anodic bonding (glass-silicon), fusion bonding (silicon-silicon), or by depositing a thin film of polymer or through interlayer of adhesive and the substrates.[65] The primary advantage of polymeric materials for microfluidic applications is their sharply reduced costs, both in terms of raw material costs and manufacturing costs.[66-68] This is particularly important for diagnostic applications where the risk of cross contamination is best managed by simply disposing of the device.[69] However, polymers are generally considered to lack the functionality and are often used only as structural materials defining the microchannel geometry.[70, 71] To overcome this problem, efforts have been made to increase the functionality of polymer-based devices while maintaining their cost advantages.[72–74] Some surface treatment strategies including plasma oxidation have been tried to give hydrophilicity and functionality to some elastomeric polymers such as PDMS.[75] But such treatments often lead to reduction of stability due to sensitivity to environment such as changes in pH due to ionizable functionalities such as silanol groups. Moreover the oxidized surface of PDMS, for instance, is unstable in air-quickly reverting to hydrophobic.

Thick-film (screen printing) technology is an ideal and simple technique to reproducibly and inexpensively modify any substrates through ink deposites that can be functionalized seamlessly.[76-77] It offers distinct advantages over conventional fabrication in that almost any substrate (plastic, glass, silicon, paper) can be used. It offers easy miniaturization, is low cost and has fast prototyping cycle and proved appropriate for mass production as has already been demonstrated in some biosensor applications.[78-86] The flexibility, versatility, and possibility of

printing different layers with various inks allows an unlimited variety of designs and the incorporation of different active elements into microchannels. Given current state of the art in microfabrication, however, the most important challenge that requires innovative approaches is challenges related to the flow behavior resulting from miniaturization.

1.3 Miniaturization and the Flow Behavior

The behavior of fluids at the microscale differs from that of macro-scale. Microscale flow is characterized by low Reynolds number (Re) and consequently is laminar (Re < 2000). Re, which compares the effect of momentum (or body force) of a fluid to that of viscosity:

$$R_e = \frac{\rho D_h v}{\eta} \dots\dots\dots\dots\dots.. Eqn. 1$$

where ρ is the fluid density, v is the average fluid velocity, η is the dynamic viscosity, and D_h is the hydraulic diameter of the capillary is even lower than 1 for microfluidic channels. The very low values of R_e signifies viscous forces domination over inertial forces and factors such as surface tension, fluidic resistance, and energy dissipation that are not of prime importance at larger scales start to dominate the flow behavior. A key consequence of this is that fluids do not mix in the traditional convective sense of large scale flow. Two laminar liquid streams in adjacent channels, for instance, can flow in parallel without eddies or turbulence.[87] Moreover, since flow rate (volume V transported per unit time t, laminar), which according to the law of Hagen-Poiseuille for laminar incompressible and viscous flow is given by:

$$\frac{V}{t} = \frac{r^4{}_c \Delta P}{8\eta L} \dots\dots\dots\dots.. Eqn. 2$$

where r_c is the radius and L the length of the capillary tube, depends strongly on the radius of the microchannel, an enormous amount of pressure needs to be applied to keep a significant flow at the microscale. The laminar nature of flows in microfluidic channels can have positive or negative impacts on analytical operation. Since molecular transport occurs mainly by diffusion in absence of turbulence between two liquid streams, diffusion based separation and detection can be realized in microchannels as the liquids flow next to each other across adjacent microchannels without a separating wall.[88] Laminar flow is advantageous in electrophoretic separations for reducing band broadening due to dispersion. But it is a nuisance in processes where mixing is necessary. Mixing is an important precondition for most bio/chemical reactions. When dissolution, mixing, and reaction are expected to occur simultaneously as a horizontal laminar flow passes over the chemical previously deposited in the microchannels, lack of turbulent mode of mixing affect the extent of such operations and hence the sensitivity of detection. In such application, therefore, the

expected improvements in analytical performances such as high-throughput resulting from high surface area-to-volume ratio and decreased diffusion length of the reacting species in microsystems are compromised by the bad mixing nature of the flow. In most LOC devices, thus, control of flow rate or residence time of the liquid in the microchannels is critical expected operation. Flow control is provided by using pumps and valves. Pumps are used to introduce fluids into the microchannel at decided flow rate whereas valves provide flow control by delaying or stopping the flow at a specific location in the microchannels for expected duration of time to enhance other microfluidic operations such as dissolution, mixing, reaction, analysis and detection. A wide variety of active and passive pumping and valving flow control mechanisms have been developed.[89-91]

1.4 Active Pumps

Active pumps may be classified as mechanical and nonmechanical. Mechanical pumping driven by pressure differential is an obvious method to induce flow of liquid in microchannels. The most straightforward mechanical method of pumping involves pressure differentials generated via externally employed devices such as syringe pumps or vacuum pumps.[92] Most active pumps couple mechanically moveable parts such as serially deflectable PDMS membranes or piezoelectric material placed above liquid chamber in the microchannel to pneumatic[93-100] or voltage sources.[101-103] As the membranes deflect by air supplied externally through a dedicated channel it pushes portion of the liquid forward. Two or more such membranes coupled with pneumatic sources through separate or same channels can work together to generate a peristaltic type movement of the membrane in a manner that drives liquid or open or close the channel to gate the flow movement of liquid along the channel (Fig. 1. 2). Various microchannel design architectures in either normally open or normally closed modes of operation have been used with pneumatic pumping. Instead of pneumatic source, mechanical movements can also be achieved by employing piezoelectric operations. Piezoelectric materials, such as lead zirconate titanate (PZT),[102] can undergo significant shape changes when subjected to stress, e.g. electrical current. The piezoelectric material, as it bends, transfers the stress to the material coupled to it such as a thin diaphragm or membrane and causes the liquid pump.[101-105] Most membrane material for microfluidic pumps and valves are based on an elastomers, particularly PDMS. The use of pressure-driven flow with either elastomeric microfluidic devices or external pumps has its drawbacks. Because the elastomers respond capacitively to applied pressure, it results in high dead time (time delay between the application of differential pressure and the corresponding change in flow rate). Moreover, the use of external pump (e.g. a syringe pump) is not compatible with the

very aim of microfluidics- the integration and miniaturization of all necessary components onto a single chip. Such mechanical pumps require moving parts that need to be tethered to pressure/vacuum sources or in the case of piezoelectric micropumps to a high voltage source.
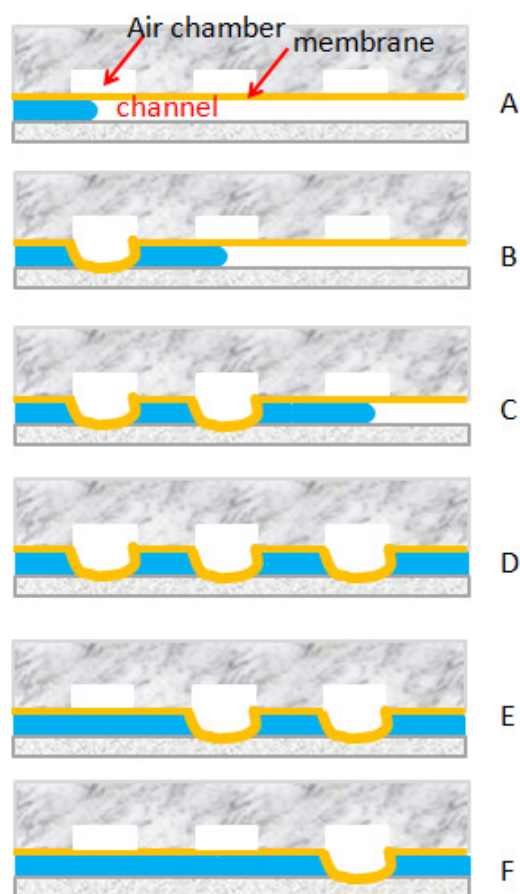
Fig. 1. 2 Representative pneumatic pumping schemes as reported in Wang et al, 2006.

Alternatively on chip micropumps with no moving parts utilizing electrochemical,[106-107] electrokinetic,[108-126] acoustic,[127-134] or magnetohydrodynamic,[135, 136] forces have been developed. In electrochemical pumps gas generated by electrolysis reaction using electrodes embedded in the pumping chamber is used to create pressure differentials to pump the liquids in microchannels. Among these methods electrokinetic method is advantageous as a nonmechanical and miniaturizable on-chip pumping mechanism. It can pump the liquid continuously and can precisely and rapidly control the flow rate. Electrophoresis, electroosmosis and electrowetting are collectively known as electrokinetic flows.[108] The principle of electrokinetics involves direct conversion of electrostatic or electromechanical energy into motion of charged particles or conductive media by application of electric fields. Because electrokinetic pumps depend on the electric double layer at the solid-liquid interface, a prior introduction about electric double layer (EDL) may be helpful for understanding electrokinetic phenomena.

1.5 The Electric Double Layer

Most solids acquire surface charges through specific ion adsorption, dopants, impurities, isomorphous substitution, or through ionization of surface groups when brought into contact with aqueous electrolytes. The charged surface electrostatically attracts counter ions from the liquid towards the electrode´s surface giving rise to Electric Double Layer (EDL). Fig. 1.3 illustrates the common mechanism of charging-the formation of surface charges by ionization of surface groups.
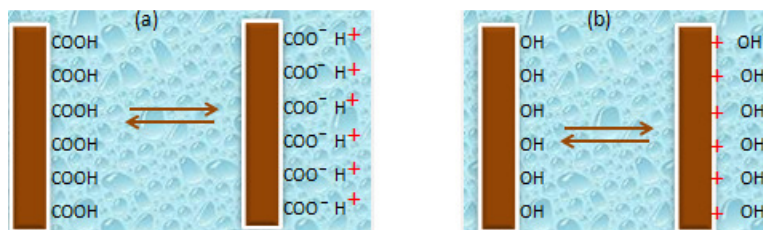
Fig. 1.3 surface charges by ionization of surface groups such as carboxyl (a) and hydroxyl (b).

The interpretation of EDL began with the von Helmholtz[137] model of a plate capacitor. A more comprehensive picture of EDL was developed by Gouy-Chapman in the years 1910-1917.[138-139] According to this model the double layer capacitance is dependent on the applied potential and electrolyte concentration. Thus, the double layer would not be compact as in Helmholtz's description but of variable thickness. The ions are subject to thermal motions, and their distribution in the double layer follows Boltzmann law:

$$\rho(x) = -N_A e \sum Z_i c_i e^{-Z_i e \psi(x)/kT} \dots\dots\dots\dots\dots Eqn.\,3$$

Where $N_A e$ if the Faraday constant, Z_i and c_i are the charge and concentration of ith ion, ψ surface potential, k Boltzmann's constant and T temperature. Close to the electrode´s surface there is immobile layer of counter ions called Stern layer. Next to the stern layer in the bulk side of the EDL is called the mobile (diffuse) portion of the EDL known as the Gouy-Chapman layer. The potential is not the same at and away from the electrode´s surface and is given by the Poisson–Boltzmann law. The linearized Poisson–Boltzmann equation under proper boundary conditions (ψ (x = 0) = ψ_0 and ψ (x→ ∞) = 0 is:[140]

$$\psi = \psi_0 . e^{-kx} \dots\dots\dots\dots\dots\dots Eqn.\,4$$

The potential decays exponentially as one move from the electrode´s surface into the bulk. The decay length also called Debye length is given by $\lambda_D = k^{-1}$ where[141]

$$k = \sqrt{\frac{2c_0 e^2}{\varepsilon \varepsilon_0 k_B T}} \dots\dots\dots\dots. Eqn.\,5$$

Where c_0 is bulk concentration of the monovalent salt and the others have usual significance. Quantifying all factors at 25 ^{0}C, the Debye length for monovalent ions is:[140]

$$\lambda_D = \frac{3.04 \mathring{A}}{\sqrt{c_0 \frac{L}{mol}}} \ldots\ldots\ldots\ldots Eqn.6$$

1.6 Electrokinetic flows

The purpose of this section is to provide brief introduction on different electrokinetic modes of flow so that the reader will know the context of current work in relation to existing knowledge. Electrokinetic methods including electroosmosis, electrophoresis, and dielectrophoresis involves electrostatic (columbic) interaction of externally applied electric field with the charged species. The migration of charged species forms a basis for separation of such species or movement of bulk liquid induced thereoff. Electrowetting, on the other hand, involves effect of the electric filed applied by means of electrodes in contact with the liquid either directly or through a thin interlayer of dielectric as in electrowetting on dielectric (EWOD).

1.6.1. Electrophoresis and Dielectrophoresis

Electrophoresis (EP) refers to migration of charged species under the influence of electric field. This technique is mainly used for separation of species based on their different mobility in electric field. The technique was introduced by Reus (1807) and has been used for electrophoretic separation of proteins and DNA analysis. The sample containing one or more such constituents with different mobility is dispensed on a support medium (usually a gel, a porous medium or flat sheets) placed between two opposite electric poles. When an electric field (~800 V/cm) is applied the charged species move according to their charge and size towards the corresponding electrode. The columbic force acting on the species is:

$$F = q_i E \ldots\ldots\ldots\ldots\ldots\ldots. Eqn.7$$

where F is the electric force on the ith ion with charge q in the electrostatic field E. The velocity of the species towards the corresponding oppistely charged pole is given by:

$$v_i = \mu_i E \ldots\ldots\ldots\ldots\ldots\ldots\ldots Eqn.8$$

v is the velocity of the ith ion, μ its mobility and E the applied field strength. Electrophoresis generally involves the action of electric field on charged species. However, the phenomenon was extended to the separation of uncharged species making use of nonuniform electric field. Uncharged species that can be polarized under nonuniform electric field can show directional motion facilitating separation. The method involved is known as dielectrophoresis. Due to the non uniformity of the electric field the particle experience different electric (columbic) force from

different sides giving rise to induce dipole moment. The side of the particle in the stronger direction of the electric field experiences stronger electric force than the side in the direction of weaker electric field giving rise to a net force that moves the particle. Dielectrophoresis (DEP) may thus be defined as motion of particles toward or away from regions of high electric-field intensity by the action of a non uniform electric field on so induced dipole moments in the particle and the suspending fluid. The technique is intensively studied to trap, manipulate, and separate particles ranging from large DNA strands to blood cells and larger particles in microfabricated devices. For a spherical dielectric particle, the time-averaged force on the particle in AC electric field is given by:

$$F_{DEP} = 2\pi\varepsilon_m r^3 Re(f_{CM})\nabla E^2 \dots\dots\dots\dots\dots\dots Eqn. 9$$

where ε_m is the permittivity of the surrounding medium, r is the particle radius, E is the root-mean square (RMS) value of the electric field, and f_{cm} is the Clausius-Mossotti factor. The Clausius-Mossotti factor

$$f_{CM} = \frac{\varepsilon_p - \varepsilon_m}{\varepsilon_p + 2\varepsilon_m}\dots\dots\dots\dots Eqn.10$$

refers to the relative polarizability of the particle relative to the medium and predicts the direction of movement of the particle-in the direction of high electric field (positive DEP) or in the opposite (negative DEP) as shown in Fig. 1.4.
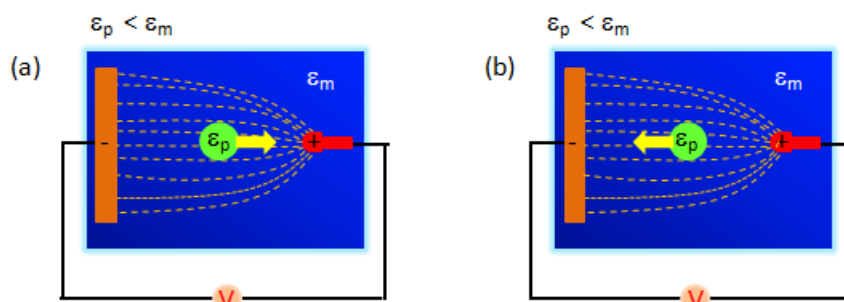
Fig. 1.4. Positive dielectrophoresis (a) and negative DEP (b)

1.6.2 Electroosmotic Pumps

Electroosmotic pumps (EOPs)[142] are based on electroosmosis. Electroosmosis refers to the motion of bulk liquid with respect to a stationary charged solid surface in response to externally applied electric field parallel to the surface. Quite often, porous media are used instead of capillaries (microchannels), as the flow rate in a single microchannel is not sufficient in many applications. The surface charges are intrinsically generated by the aforementioned mechanisms. When an electric field is applied tangential to the EDL, electric body force are exerted on the counter ions at the diffuse zone of the EDL setting them into motion towards the corresponding electrode, usually

in the direction of applied electric field. The electric force (body force) exerted on the counter ion at the EDL is transferred to the bulk through viscous stress, i.e. the counterions drag the bulk liquid with them through viscous force and the liquid starts to flow. Electroosmotic technique was first developed for flow control with capillary electrophoresis (CE). Electrophoresis is the most widely used electrokinetic method in analysis wherein separation and analysis of charged species including DNA, proteins, and amino acids is achieved as they electrophoretically move towards oppositely charged electrode. It was around mid-1990s that EOP developed as a technique for fluid pumping and controlling applications in microfluidic systems as distinct from capillary electrophoresis (CE).[142-146] Details on EOP can be found in Ref. 147. Reuss (1809) was the first to discover the phenomenon of electroosmosis, wherein bulk flow was induced by the application of an electric field across a porous dielectric material. Conventionally electric field is directed from positive to negative terminal. If the counter ions in the diffuse layer of the EDL are cations electroosmosis takes place in the direction of the electric field. Otherwise it can take place in the direction opposite to the direction of the electric field. The liquid molecules close to the electrode´s surface may bind tightly with the surface possibly like the ions and may remain intact. Bulk molecules only at a distance ´d´ away from the electrode´s surface are free to move. An imaginary plane parallel to the EDL at this distance is called a shear plane. The potential at this distance is called the zeta potential ζ. The magnitude of ζ determines the EO flow rate. The electroosmotic velocity may be estimated in terms of the zeta-potential using the Helmholtz-Smoluchowski Equation:[147]

$$v_{eo} = -\frac{\varepsilon \zeta E_x}{\eta} \quad \text{.................} Eqn.11$$

where v is fluid velocity, ε is the permittivity, E_x is the x-component of applied electric field, η is viscosity of the liquid. Clearly the flow velocity is proportional to the zeta potential and to the applied field. From the relation of zeta potential with the Debye length which decreases with increasing concentration, it follows that electroosmotic velocity decreases with increasing concentration. Since surface ionization and hence surface charge depends on the pH of the solution, the EO velocity can vary with pH of solution. EOPs offer a number of advantages including: a) creation of constant pulse-free flows and elimination of moving parts. b) a plug-like, non-parabolic fluid velocity profile that eliminates dispersion caused by parabolic pressure-driven flow. c) ability to control the flow simply by adjusting the potential of electrodes at different locations in a microchannel. d) can pump continuously from an open reservoir e) EOPs can be fabricated using standard microfabrication technologies and thus is readily integrateable with LOC devices. Despite these advantages, electroosmotic pumps have certain drawbacks. Often very high

electric fields (100s of V/cm) are required to achieve appreciable flow rates. Reproducibility in flow rates is challenged by the sensitivity of the method to changes in both type and composition[147] of the solvent and the electrolyte[148]. High voltage operations may unavoidably lead to gas formation at the electrodes because of electrolysis. Joule heating due to the high voltage can also form gases. The gas bubbles, if become sufficiently large, can break the electrical continuity and then the pump no longer functions. Continuous efforts have been made to alleviate the problems of EOP methods including isolating the electrode and solvent reservoir with a membrane that permits the flow of ions but limits the flow of gas and bulk liquid.[146, 149] However, such solutions often complicates the design and fabrication of the devices obliging the microfluidic community to seek for power free (passive pumping) methods.

Pumping in microchannels require high-pressure differentials to induce flow. Such Poiseuille flow depends strongly on the applied pressure differential (ΔP), size of the tube [radius and length], and the viscosity of the solution. Generally Poiseuille flow rate decreases as microchannel dimension decrease-a situation opposite to EOP and other pumping modes such as capillary. Another limitation of differential pressure pumping (Poiseuille flow) is related to the inhomogeneous velocity profile.
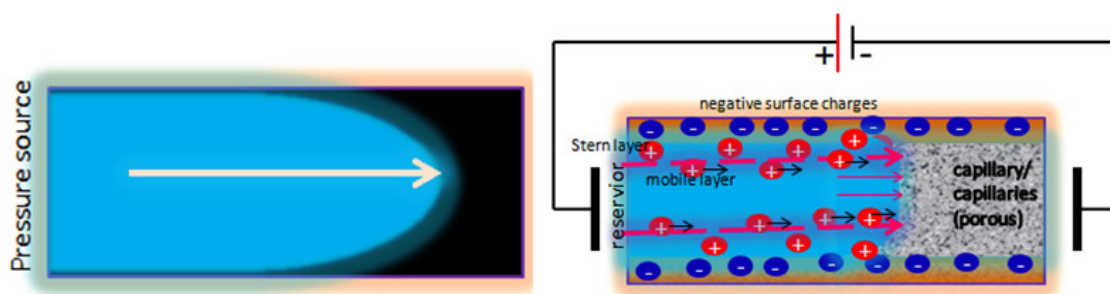
Fig. 1.5 Parabolic flow profile of Poiseuille flow (left) and plug like (flat) electroosmotic flow induced by counter ions migration in the direction of externally applied electric field (right). Co-ions in the liquid are not indicated for clarity reasons.

The velocity of the flow varies with position across the channel, as fluid near the center of the channel moves at a faster rate than fluid near the channel walls, resulting in a parabolic flow profile unlike plug like flow in EOP (Fig. 1.5). The disadvantage of a parabolic flow is that it spreads out a given volume of analyte causing sample dispersion, which is undesirable in separations. Fig.1.5 provides comparative schematics of Poiseuille flow and electroosmotic flow resulting from migration of counter ions in the direction of externally applied electric field.

1.7 Active Valves

Mechanical movement of membranes or other moving parts coupled to mechanical,[150-153] pneumatic,[154-162] and electrokinetic,[163-166] have been used for valving operations. Non mechanical

active valves operated by electroosmotic,[167, 168] thermocapillary, and electrowetting effects,[169-175] have also been reported. Most of these solutions however, require mechanical moving parts that require bulky peripherals or high energy sources. Alternatively active valving methods requiring relatively lower energy have been built based on electrochemical,[176, 177] thermal,[178] phase change,[179–191] and rheological[192–193] actuations. Electrochemically generated gas by electrolysis can provide force to deflect the membrane with relatively low voltages. Actuation by using stimuli-responsive or smart materials such as hydrogel or polymers,[179–189] paraffin[190, 191] and ice[191] is achieved by taking advantage of reversible change in the volume as the material undergoes solid-liquid or vice versa or simple swelling or collapsing with respect to applied stimulus such as temperature, pH, electric fields or light, and is very useful in disposable biochip applications due to its relatively low cost.[194] Nonmechanical pumping by centrifugal force as a disc containing liquids in microchannels spins[194-197] have been used coupled to capillary burst valves,[194, 195] which can passively stop the flow as the spin ceases and allows the liquid to flow when a rotation frequency exceeds threshold value.

1.8 Passive Pumps and Valves

Passive pumping takes advantage of the dominance of the interfacial energy over body forces at the microscale and couples it to geometrical considerations to generate autonomous filling of the microchannels by the liquid. The most common passive pumping mechanism is based on capillarity. Capillary driven devices are simple to construct and operate, low cost and miniaturizable. But for a practical capillary force operated microfluidic devices a precise on-chip capillary flow control, particularly that provides stop/go operations are critical expected capacities. Flow control strategies that fulfill the basic requirements of ASSURED devices is greatly needed if microfluidic devices are to have success in D_2H_2.

1.9 Capillarity and Applications

Capillarity may be defined as autonomous flow of liquid in narrow channels/tube or porous media. The significance of capillary phenomena in nature and in technological applications was realized during the mid 1920s by Fisher[198] and Haines[199]. Capillarity is very common in our daily life and facilitates life process. Exchange of materials (oxygen, carbon dioxide, heat etc) in our body between blood and tissue occurs through capillaries connecting arteries and veins. The uptake of water by trees from the ground by roots to leaves of formidably tall trees happens by capillary action coupled to transpiration.[200] The use of paper towel to wipe wet table involves capillary wicking of the liquid into the pores in the paper. The famous technique of separation in chemistry-

chromatography be it paper, thin layer or column chromatography partially or entirely depends on capillary migration of bulk (mobile phase) through porous media (capillaries) that serves as stationary phase. Other areas of technological applications of capillarity include the printing industry.[199-201]

The most successful analytical applications of capillarity are in diagnostic applications. Among the capillary driven analytical devices, the most prominent are lateral flow devices. The Lateral flow tests,[202] also known as lateral flow immunochromatographic strip test introduced in 1988 by Unipath has been the commonest commercially available diagnostic devices most of which used in POC diagnostics. LFAs are an extension of latex agglutination tests which were developed in 1956 by Singer and Plotz.[203] Lateral flow assays are widely used for the qualitative/semiquantitative detection of several analytes in pregnancy tests (β-chorionic gonadotropin), fertility and ovulation tests (luteinizing hormone and follicle stimulating hormone), infectious diseases, cancer diagnostics, cardiac or drugs-of-abuse markers (amphetamines, cocaine and benzodiazepines) sold by companies such as Unipath, Abbott, or Quidel. The most common lateral flow assays are immunoassays. The device has a serially classified zones dedicated for specific and integrated operations. Basically appropriate detection antibodies are immobilized in detection and control testing zone on a porous membrane such as nitrocellulose near the middle of the device. Labeled detection antibodies labeled with reporter particles including colloidal gold, carbon black, dyed latex particles or fluorescent markers (or redox markers as in recently reported devices) are used as either separately mixed with the sample or directly bound to the membrane on the conjugate pad.[204-205] A sample-pad at the entry part of the device (usually placed above conjugate pad) pre-filters the sample. When a sample such as blood or urine is added, pre-filtration occurs on sample pad, and the sample liquid then migrates by capillary force toward the absorbent pad through conjugate pad then detection zone followed by control test zone towards the absorbent-pad at the opposite side of the membrane which wicks the liquid facilitating the capillary flow through the membrane as shown in Fig. 1.6. The affinity reaction between the detection antibodies labeled with the reporter molecules and analyte in the sample forms an immunocomplex that moves to detection zone followed by control test zone where other affinity reaction of the complex with surface confined capture antibodies provides a read-out analytical signal. Incorporated in most of the devices is also a control line where a suitable ligand previously deposited on the surface captures excess reporter molecules ensuring that the fluid migrated through the test device.
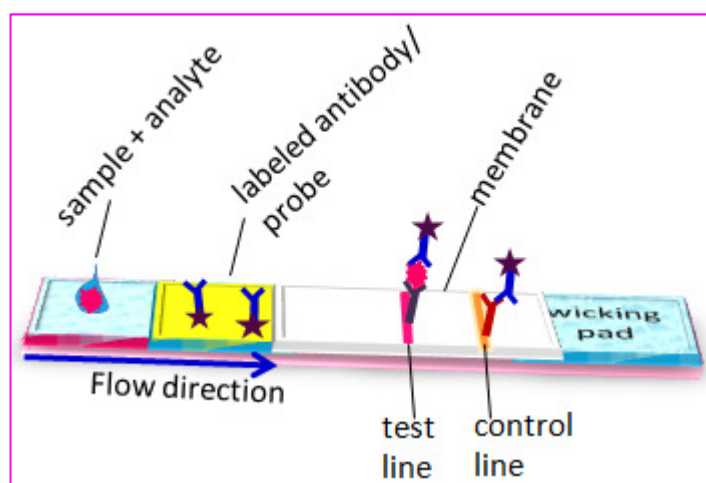
Fig. 1.6 Standard layout of a lateral flow immunoassay device

The attractive features of these devices include their simplicity and that they fulfill most of the requirement of the ASSURED devices. They can be operated wherever the user is, are simple and fast to operate, low cost and portable. They can provide reliable analytical information, mainly qualitative. They owe their success to their simplicity that significantly depends on the capillary-driven flow and versatile technological platform that lends itself to fast and low cost product development. However, these devices are often limited to screening applications. They provide only qualitative or semiquantitative results. They are not sensitive enough for certain applications that require highly sensitive quantitative analysis because most of the analytical information is lost in the porous matrix as only lateral information is detected. Some of the factors that affect the sensitivity are: 1) the type of detection technique employed that only lateral information is acquired 2) the efficiency of mixing and reaction as the components wick through the porous membrane. The latter is affected critically by, among others, the flow rate "wicking rate" through the membrane which is set during design and not precisely controlled. Generally, the higher the wicking rate, the lower the sensitivity, i.e sensitivity is related to residence time which determines extent of dissolution, mixing and reaction of the previously surface confined labeled immunochemical with the analyte, if any, suspended in the flow.

Microfluidic devices, particularly capillary force operated microfluidic devices are expected to outperform and overcome the limitations of LFDs if flow rate is precisely controlled in microchannels given current state of the art in microfabrication to incorporate highly sensitive detection schemes such as electrochemical techniques. The first convincing implementation of capillary based microfluidic systems as an alternative to LFIAs was developed by the Biosite Triage in 2000s. The chip has a sample metering area, hydrophobic patches to control flow rates

(i.e by delaying the sample in the vicinity of surface dried detection antibody), patterned receptor areas and a microfluidic channel. The microchannel forms a loop around the main channel to facilitate wicking of the sample through the device and keeping the device small. Inspired by such successful realization of capillary based POC devices, researchers and companies have shown great interest in capillary driven microfluidic devices that mimic lateral flow devices.[206, 207] Progress in the development of microfluidic systems that retain the simplicity and user friendly advantages of lateral flow devices and tries to overcome their intrinsic limitations include the pioneering work of Whitesides[208-211] and other authors[212-223] including the BBG group led by Katakis[224-225] at the University of Rovira i Virgili on papers and plastics. Similar to porous membranes in LFAs, papers provide a 3D passive/capillary movement of reagents and facilitate separation, mixing and reaction. The 3D nature of the capillaries in paper is suitable for immobilization of chemicals by simple adsorption. The adsorbed and dried chemical can dissolve readily and become activated as liquid passes over it. The important step in these devices is to produce microfluidic channels to direct liquid movement in the desired direction on the paper which is accomplished by hydrophobic patterns obtained by either wax printing or impregnating the paper with photoresist and exposing it to UV light. However, paper based microfluidic devices still has the drawbacks of the LFDs and do not provide reliable fluid operations. Using screen printing for fabrication of components and constructing microchannels on plastics have been demonstrated as simple and low cost approach to develop analytical microsystems. The progress in such work should included effective exploitation of capillary phenomena and innovations to precisely control capillary flow in microchannels.

1.10 Capillary Flow/Control Principles

Capillary flow arises from the interplay of the wettability and dimensions of the microchannel. Fig.1.7 illustrates the different level of capillary rise in capillaries of different dimension. Such differences may also result from variations in wettability of inner walls of the tubes or from the surface energy of liquids, i.e different liquids may rise different heights. Clearly the capillary phenomena depend on the surface energies (of both the liquid and the microchannels) and the dimensions of the microchannels (or capillaries).
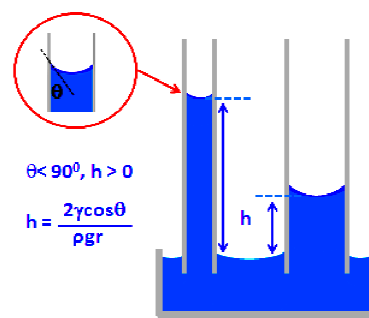
Fig. 1.7 Rise of water up column capillaries of different diameter

Capillary phenomena involve two immiscible phase, often the liquid and its vapor (or air) above the liquid. When the vapor phase of a liquid is confined between two surfaces (particles) so close to each other, capillary condensation occurs which gives rise to liquid menisci. The force caused by such a liquid meniscus is called "capillary force" also termed meniscus force. The corresponding pressure difference ΔP also called capillary pressure for rectangular capillaries of height h and width w is related to the surface tension and dimension of the microchannel by the Young–Laplace Equation.

$$\Delta P = -\gamma.\left(\frac{Cos\theta_b + Cos\theta_t}{h} + \frac{Cos\theta_l + Cos\theta_r}{w}\right) + \rho gh$$

Where γ is the surface tension of liquid (= 72 mN/m for water) and the indices b, t, l, r referring to bottom, top, left and right walls, respectively. The right term can be neglected in the absence of gravitation or body force (e.g. with very small objects or dimension). $Cos\theta$ refers to the cosine of the water contact angle which is a measure of wettability. According to the Young-Laplace equation capillary flow can be controlled via control of wettability or geometry of the microchannel. Most of the capillary flow controls reported to date are based on delay valves by means of hydrophobic patches or geometrical grooves or foldings. On the other hand, both theoretical and experimental works have indicated stringent dependence of microfluidic immunoassays on flow rate pointing to the importance of tight control of flow rate in microchannels if such systems are to have success.[226, 227] Sudden changes in geometry can provide passive stopping of the flow that can be actuated by means of liquid triggering or centrifugal actuation.[194-197] The dependence of capillary flow on wettability provides attractive opportunity for on-chip manipulation of the flow. Based on wettability control it is possible to fabricate surfaces in microchannels that can provide passive stopping.[207] If the passive stop valve is coupled to a fast actuation mechanism such as that based on electrical signal an effective stop/go operations of capillary flow can be achieved.

1.10.1 Control of surface wettability

Wettability of a surface is a function of the surface energy of the liquid and the surface itself. When a droplet of a liquid is dispensed on a solid surface, the droplet may spread on the surface to form a thin wetting film or it may remain as a drop exhibiting specific contact angle with the surface. A contact angle is an angle at which a liquid-vapor interface meets the sold-liquid interface. The degree of wetting depends on the balance of forces acting at the three phase contact line: the liquid-vapor, the solid-liquid, and the solid-vapor, Fig. 1.8. The first one-the liquid-vapor interfacial energy, commonly called surface tension, has a horizontal component given by $\gamma_{lv}\cos\theta$ (Fig. 1.8). The second one is the force corresponding to the interaction of the liquid with the solid is called solid-liquid interfacial energy. The third is the solid-vapor interfacial energy.
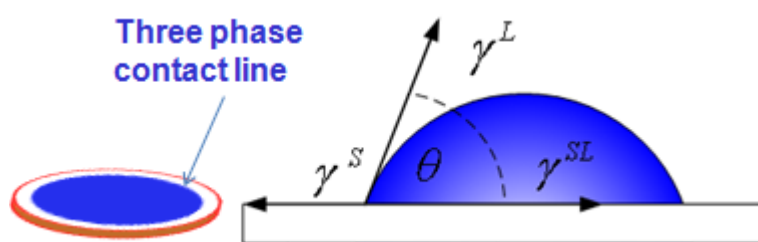
Fig. 1.8 three forces acting at the three phase contact line

In 1805, Thomas Young developed a thermodynamic description of wetting phenomena considering the balance of the three forces acting on the TCL by the equation called in honor of his name-Young´s equation:[228-229]

$$\gamma_L \cos\theta = \gamma_S - \gamma_{SL} \ldots\ldots\ldots\ldots\ldots\ldots. Eqn.\,12$$

If the solid-vapor interfacial tension is higher than that of the solid–liquid interface ($\gamma_S > \gamma_{SL}$), the right hand side of Young's equation is positive. This implies that the contact angle has to be smaller than 90^0, in which case the surface is classified as hydrophilic. On low surface energy materials ($\gamma_S < \gamma_{SL}$), the contact angle will exceed 90^0, such solid surfaces are classified as hydrophobic. Different surfaces display different contact angles ranging from 0 to 180^0, Fig. 1.9, depending on the properties of the solid and the liquid, particularly their surface energies. Surfaces that display water contact angles above 150^0 are called superhydrophobic. Those that display water contact angles close to 0^0 are called superhydrophilic.
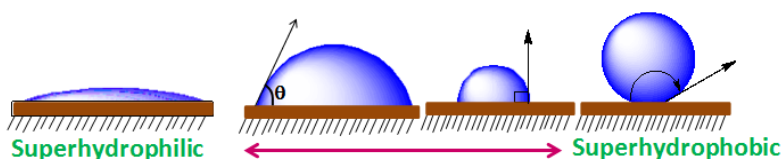
Fig. 1.9 Possible profiles of a liquid droplet when dispensed on a solid surface

Young's description of wetting holds only for liquid droplets on smooth surfaces and at equilibrium. The water contact-angles of smooth surfaces are governed mainly by surface chemistry. For rough surfaces Wenzel[230] and Cassie[231] developed theories that take into account the roughness factor. When the surface is highly rough and porous it leaves an open air space beneath a droplet dispensed on it. In contrast to smooth surfaces which often have a maximum contact angle not exceeding 120° and thus a narrow range for the dynamic control of surface wettability, superhydrophobic nanostructured surfaces have recently drawn considerable interest because of large range of contact angle changes that can be achieved as the wettability changes from superhydrophobic to superhydrophilic. A model surface for superhydrophobicity is provided by the leaves of the Lotus plant (*Nelumbo nucifera*), which have an intrinsic hierarchical structure, built by convex cell papillae and randomly oriented hydrophobic wax tubules on it.[232] Water on such surface forms a spherical droplet, and both the contact area and the adhesion to the surface are dramatically reduced giving the surface self-cleaning property. The droplet is described as being in a "fakir" state lying solely on the top of the pillars resulting in rather very large values of water contact angle. Superhydrophobicity, therefore, could be achieved by mimicking the leaves of Lotus plant.[233] Inspired by their applications in self cleaning windows, windshields, exterior paints for buildings, navigation-ships and utensils, roof tiles, textiles, corrosion protection, solar panels and flow control in microfluidic systems, researchers have shown great effort to produce artificial superhydrophobic surfaces.[234] Superhydrophobic surfaces are fabricated by controlling the surface energy and microscale roughness as engineered by nature, e.g. in Lotus leaves. Although the notion of superhydrophobicity was coined by Wenzel and Cassie decades ago, the first report of artificial superhydrophobic surface was made by the group at Kao in 1996.[235] Since then a great number of researchers produced artificial superhydrophobic surfaces through different methods including electrochemical reaction and deposition,[236-239] layer-by-layer and colloidal assembly[240-244] sol–gel process,[245-249] phase separation,[250] lithography (photolithography, electron beam lithography etc)[251-254] and different etching methods including plasma etching,[255-256] laser etching,[257, 258] and chemical etching,[259] and physical and chemical vapor deposition.[260-262] These methods fall under either one or both of the two key strategies: constructing micro/nanoscale roughness on a low surface energy material (hydrophobic) or modifying a highly rough surface with hydrophobic material.[230] In phase separation, for instance, a hardening process is adapted to produce porous structures by removing a second phase from materials that consist of a solid phase and a second phase that could be liquid or solid. Conductive superhydrophobic surfaces, on the other hand, have been obtained through combination of conducting polymers and low-surface-energy materials such as fluorinated molecules during electropolymerization.[263-265] Li et al have

recently reported conductive superhydrophobic inorganic ZnO films prepared via electrochemical deposition method.[266]

1.10.2 Dynamic wettability

Wettability of a surface can be modulated by external signals such as temperature,[267-269] light,[270-271] pH,[272] solvent,[273-274] counterion exchange[275-279], and electrical potential[280-286] by modifying the surface with appropriate stimuli responsive material. Despite such wide range of possibilities to switch wettability only few reports demonstrated the application of switchable wettability for flow control in microfluidic systems based on temperature[287] and light[288] responding polymers. Electrical control of wettability (electrowetting) is attractive for flow actuation in microfluidic systems. It is fast, miniaturizable and low cost. Electrowetting is a phenomenon of enhancing wettability of a nonwetting or partially wetting liquid on a surface and hence change in macroscopic contact angle by means of locally generated electric field. Electrowetting involves bulk motion induced by changes in interfacial energy corresponding to changes in charge density at the interface due to applied potential in accordance with Gibbs adsorption isotherm. The alteration in charge density at the interface causes rearrangement of ions at the EDL. As the counterions moves towards the electrode surface at applied potential the process induces motion of the bulk (electrocapillarity). The basis for electrowetting is the electrocapillarity experiment first described in 1875 by Gabriel Lippmann.[289] The set up for electrowetting consists of at least two electrodes (working and counter) and a liquid/liquid droplet contacting the electrodes either: directly (Fig. 1.10, (a)) or via a dielectric (Fig. 1.10, (b)). The limitation of direct electrowetting is electrolytic decomposition of water at higher potentials. Under this condition the potential drops not only at the EDL but also in the solution associated with the faradaic process. In early 1990s Berge[290] introduced the idea of using a thin insulating layer to separate the conductive liquid from the metallic electrode which is known as electrowetting on dielectric (EWOD), Fig. 1.10 (b).
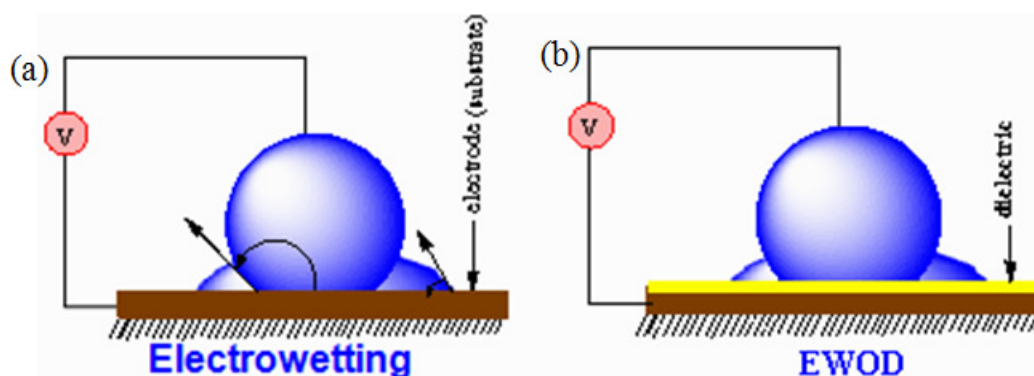
Fig. 1.10 Direct electrowetting (a) and electrowetting on dielectric (b).

In absence electrolysis, the effect of the applied potential on the interfacial energy, at constant electrochemical potential (μ), pressure (P) and temperature (T) is related to the charge density at the EDL by Lippmann equation:

$$\left(\partial_{\gamma sl}/\partial_V\right)_{\mu,P,T} = -\sigma \ldots\ldots\ldots\ldots\ldots\ldots. Eqn. 13$$

Where σ is the surface charge density of the counter-ions at applied potential V. Eqn. 13 can be rewritten as:

$$d\gamma_{sl} = -\sigma_{sl}dV \ldots\ldots\ldots\ldots\ldots\ldots. 14$$

The voltage dependence of γ_{sl} is calculated by integrating Eqn. 14. Applying Helmholtz Model for voltage dependent distribution of counter-ions near the interface, i.e. $C = Q/V = \varepsilon\varepsilon_0 A/d = cA$ where ´c´ is the specific capacitance and that the charge density $q = Q/A = cV$ we obtain:

$$\gamma_{sl}(V) = \gamma_{sl}^0 - \int_{V_{pzc}}^V \sigma_{sl}dV = \gamma_{sl}^0 - \int_{V_{pzc}}^V cVdV \ldots\ldots\ldots Eqn. 15$$

Evaluation of the integral of Eqn. 15 gives the voltage dependence of γ_{sl}.

$$\gamma_{sl}(V) = \gamma_{sl}^0 - \frac{1}{2}\frac{\varepsilon_0\varepsilon}{d}\left(V - V_{pzc}\right)^2 \ldots\ldots\ldots\ldots. Eqn. 16$$

Eqn. 16 represents a parabola with maxima at V = V_{pzc}. The position of maxima may vary depending on the surface charge and the nature of adsorption (specific cation adsorption or anion adsorption). Substituting the expression of $\gamma_{sl}(V) = \gamma_s - \gamma_L\cos\theta(V)$ and $\gamma^0_{sl} = \gamma_s - \gamma_L\cos\theta_0$ from Young´s equation in Eqn. 16 affords the well known Young-Lippmann Equation.

$$Cos\theta(V) = Cos\theta_0 + \frac{1}{2d\gamma_{lv}}\varepsilon_0\varepsilon\left(V - V_{pzc}\right)^2 \ldots\ldots\ldots\ldots. Eqn. 17$$

Where V_{pzc} is the potential of zero charge as any surface acquire a spontaneous charge when immersed into electrolyte solutions in absence of any applied voltage. The voltage required to compensate for this spontaneous charging is V_{pzc}. Contemporary works explained force for the lateral displacement of liquid to be of electromechanical[291] origin and not due to contact angle changes. As a pumping mechanism electrowetting has been used mainly for droplet manipulation. But it is even more appropriate to valving operations with continuous flows in microchannels such as capillary driven flows.

Thus through control of surface energy such as by electrowetting capillary flow can be controlled. Control of the wettability of either one or more walls of the microchannel could provide passive stopping of the flow. Superhydrophobic surface is often required to provide passive stopping of capillary flow if only one of the microchannel walls is considered. Superhydrophobic surfaces provide additional advantages: a large range of contact angle changes can be achieved as the

surface wettability changes from superhydrophobic to superhydrophilic. The corresponding change in capillary pressure, according to the Young-Laplace equation, is expected to facilitate flow actuation in capillary operated microfluidic systems.

It was thus proposed that a stop-go control of capillary flow might be achieved by coupling the dependence of capillary flow on surface properties to a conveniently integrated low-voltage electrowetting/electrochemical actuation. Through hydrophilic/superhydrophobic patterning of microchannel surfaces a patterned flow behavior including stopping and restarting can be achieved. By incorporating electrical stimuli responsive superhydrophobic electrodes into microfluidic systems a stop/go fluidic operation can be performed. Such electrodes can be constructed through proper engineering of electrode surfaces with conducting polymers that display reversible redox property with the different oxidation states displaying different wettability. Alternatively superhydrophobic nanoporous graphitic electrodes can be used directly to provide passive stopping and facilitate low voltage actuation of the flow via facile electrowetting transition from the relatively less stable Cassie wettability state to more stable Wenzel state at low voltage electrowetting.[292]

A different approach may include the use of gradients that might be created along fluidics by means of planar microelectrode arrays placed transversal to the flow direction. Asymmetry due to geometry or electrochemical processes is possible way of generating gradients (e.g. potential, concentration) across electrodes placed in contact with the liquid. The electric force associated with such gradients can propel the liquid and facilitate flow actuation. This can be achieved by using superhydrophobic electrode and other electrode that couples it asymmetrically.

1.11 Objective of the Study

☞ Develop electrochemically actuated stop/go capillary flow controls

☞ Characterize the performance of the electrochemically actuated capillary flow control

☞ Demonstrate the utility of the flow control in a capillary force operated integrated microfluidic systems that simulate lateral flow devices.

Sub objectives:

☞ Develop microfluidic systems that display capillarity

☞ Investigate different approaches to low voltage electrowetting/electrochemical actuation of capillary flows.

☞ Integrate the electrochemically actuated capillary flow controls into a microfluidic system operated by capillarity and characterize the performance in stop/go modes.

1.12 Electrochemically Actuated Capillary Flow Control

The dependence of capillary flow on surface property provides attractive opportunity for on-chip control of the flow. If such dependence of capillary flow is coupled a fast actuation mechanism such as electrical methods, a precise control of capillary flow including stopping and restarting might be achieved. Passive stopping and restarting have been demonstrated using superhydrophobic surfaces using thermal,[287] light[288] or electrical actuations.[293-294] Thermal actuations are costly and naturally slow due to a slow thermal response of materials/systems. Light driven actuations require bulky peripherals that are costly and limit miniaturization, integration, and automations. Among these methods electrical control of wettability is very attractive due to its simplicity to fabricate and operate and expediency to perform stop-go fluidic operations in microchannel. It can conveniently be applied in a programmable and automated fashion via individually addressable electrodes. Superhydrophobic surfaces provide distinct advantage to develop electrically actuated capillary flow controls. On one hand they provide reliable passive stopping. On the other hand they allow large range of contact angle changes to modulate wettability and control the flow. However, a low voltage actuation of the flow that stops at the superhydrophobic surface is not trivial. The surface has to be such that it provides not only passive stopping but also facilitate actuation of the flow at extremely low voltage. Only few reports have demonstrated electrically actuated flow using electrowetting on dielectric (EWOD).[293-294] Electrowetting techniques employed so far use mainly the famous hydrophobic dielectric material-the poly (tetrafluoroethylene) (PTFE). However EWOD often requires high voltages (100s) and has associated problems including dielectric breakdown and contamination to the system, joule heating, and contact angle saturation. These limitations deter the application of EWOD actuation mechanism to the realization of the ASSURED. In this thesis it was proposed that surface-engineered electrodes incorporated into microfluidic channels at specific locations can provide simple, low cost and yet effective on-chip capillary flow control. Since screen printing is proposed as a simple, low cost, flexible method to incorporate electrodes with proper post printing surface modifications, a hydrophilic/superhydrophobic patterning of the microchannel can be achieved. While the hydrophilic part of the microchannel provides autonomous capillary flow, the superhydrophobic surface provides a passive stopping. The stopped flow can be resumed by just pressing a button to activate the battery and create gradient that can propel the liquid. To this end

the superhydrophobic surface itself has to be prone to low voltage modulation of its wettability. Superhydrophobic surfaces based on electrical stimuli responsive conducting polymers, when incorporated into a capillary force operated microsystems, were envisaged to provide both passive stopping and low voltage actuation of the flow by virtue of their electrically tunable wettability. As a simple strategy and taking advantage of the naturally hydrophobic nature of screen printed carbon electrodes the fabrication of electrical stimuli responsive superhydrophobic surface was envisaged to be carried out by nanostructuring of the previously roughness amplified SPCE surface with electropolymerized polythiophenes which are hydrophobic in neutral state and turn hydrophilic upon applied potential. Two challenges to face: on one hand, electropolymerization requires clean and electrochemically active electrode surface. Activation of electrode surface for electrochemical applications including electropolymerization has been accomplished usually by oxidative procedures that introduce exotic functionalities such as hydroxyl or carboxyl groups. Such procedure is a nuisance to our intention because the surface groups can render nucleophilic attacks to the growing polymeric oligomers or charged intermediates during polymerization and destroy the required conjugation of the polymeric chain. On the other hand, fabrication of superhydrophobic surface requires a previously roughness amplified surface. SPCE is a composite material generally composed of the electroactive graphitic particles and other agents such as polymeric resins and solvents for binding and dispersion of the particles. Due to the constraints of screen printing such agents including thinning agents are often used in excess and block the charge transfer process at the electrode´s surface. Thus the expected level of activation and roughness without modifying the intrinsic characteristic of graphitic particles which are naturally hydrophobic but has high electrocatalytic activity were envisaged to be achieved via a surface activation strategy that simultaneously amplifies the roughness of the electrode´s surface. Controlled and selective superficial subtraction of nonelectroactive surface deactivating components can afford electrode´s surface with desired enhanced electrochemical performance and roughness. The expected level of activation to the electrode´s surface, in this case, takes advantage of the native electrocatalytic characteristic of the graphitic particles whose loading and exposure (electrochemical accessibility) increases as surface blocking agents are selectively removed. Solubility principles can be adapted to partially remove only the contaminants and not the graphitic particles. Control over the duration of exposure will be very important to achieve what is required. Depending on the duration of exposure to the solvent and as the solvent action extends to the interstices between particles than just etching surfaces a highly porous structure that will grow to superhydrophobicity could be achieved; which also can be exploited as advantage given the ability to control the exposure time. Alternatively thus superhydrophobic porous carbon

based surface was proposed to provide the expected solutions of passive stopping and a low voltage actuation of the capillary flow through low voltage electrowetting transition to a more wettable regime by virtue of their high conductivity, high surface area and intrinsic charge accumulation behavior. In addition to flow actuation based on tunable wettability of stimuli responsive materials and low voltage wettability transitions of superhydrophobic porous surfaces, gradients in pH, surfactants, potential, and concentration along the fluidics can be used for flow actuation.[297-302] Such approaches, however, should always be coupled to a superhydrophobic surface to provide a prior reliable stopping of the flow. Thus superhydrophobic electrode was envisaged to be coupled to a judiciously selected counter electrode to simulate asymmetric electrochemical processes that can generate on-chip gradients that can stimulate the stopped flow to resume.

1.13 Organization of the Thesis

This thesis is organized into seven chapters including an introductory chapter followed by four article based chapters (chapter 2 to chapter 5) and the last two chapters (chapter 6 and chapter 7) providing general conclusions and future outlook.

Chapter 1 is an introduction where the state-of-art in different areas of scientific development in the field of microfluidics and related researches including surface wettability control strategies is discussed. The state of art in microfluidics or integrated microfluidics systems including a brief touch of historical perspective and potential application areas are provided. Following this the state of art in microfabrication is briefly discussed. Also presented is the key challenges in microfluidic development-the science of miniaturization is briefly discussed. As microfluidic development always requires functional components to control flows in microchannels, different pumping and valving strategies including electrokinetic and pneumatic were briefly reviewed. Special emphasis is given to capillary phenomena, capillary pumps and valves. Some interesting capillary force operated devices-Lateral flow devices that have been successfully implemented for practical applications is discussed. As capillary flow control requires control of surface properties, particularly wettability, various approaches including electrowetting developed to modify or control wettability of solid surfaces were reviewed briefly.

Following the brief introduction on the state of the art of relevant subjects, the overall and subobjectives of the study followed by hypothesis formulated as guiding tentative solutions to the stated scientific problems were presented.

CHAPTER 2 (Article 1, submitted):

TITLE: **SMART electrodes for stop-go fluidic manipulation in analytical microsystems**

Journal: Electrochemistry communications

In this chapter a simple strategy is developed to demonstrate a stop/go operation of capillary flows through the application of the electrically tunable wettability property of conducting polymers. Two closely spaced electrodes (one of which has electrical stimuli responsive superhydrophobic surface) were fabricated by screen printing followed by surface structuring in a microchannel. The fabrication of the stimuli responsive superhydrophobic surface was performed by controlled potential cycling electropolymerization to coat the previously roughness amplified screen printed carbon electrode surface with P3MeT. Presented also is a simple strategy to fabricate stimuli responsive superhydrophobic surface. The existing procedure for the development of stimuli responsive surface involves very lengthy steps of layer-by-layer deposition and intensive instrumentation including lithographic techniques and clean room facility that are costly and difficult to miniaturize and integrate into microfluidic systems. The performance of the valve was characterized in terms of response time. Response time is defined in this thesis as the time elapsing between the application of the potential and the moment the meniscus front reaches and crosses the end of the 1 mm hydrophobic barrier of the valve.

Chapter 3 (Article 2, in press):

Title: Electrochemically actuated stop-go valves for capillary force-operated diagnostic microsystems

Journal: *ChemPhysChem*

This chapter presents the fabrication and implementation of superhydrophobic carbonaceous material for stop/go fluidic operations in microfluidic systems. Unlike the polymer modified surface presented in chapter 3, this approach is more simple and robust and takes advantage of unique electrowetting phenomena on superhydrophobic nanoporous surfaces. The fabrication strategy is simple and is a continuation of roughness amplification strategy developed in chapter 2. Depending on the duration of exposure to the solvent the roughness and hence hydrophobicity of the SPCEs surface can be tuned proportionally. Therefore by just increasing durations of exposure

from the 5 minutes used in chapter 2 to 40 minutes and beyond a superhydrophobic nanoporous surface was obtained. The process increased the roughness and porosity of the surface that caused the superhydrophobic effect. The superhydrophobic surface of the carbon electrode, in addition to functioning as passive stop valve (PSV), facilitates the flow actuation using low applied voltage avoiding observable electrochemical reactions in aqueous solutions. When a low voltage (~ - 1 V) was applied at the carbon electrode against a second wettable carbon electrode, the flow of such solutions (e.g. 0.01 M phosphate buffer saline solution) that was stopped at the PSV, resumed, crossing the 1 mm pitch of hydrophobic barrier of the PSV in 1 sec and reestablishing capillary flow downstream. The low cost and flexibility of fabrication, facile integration and miniaturization, and reproducible performance of such on/off valves make this configuration promising for the development of low cost microfluidic devices for point-of-care diagnostics, food analysis, and environmental monitoring. The selective etching action of organic solvent on a composite material surface is developed as a versatile and simple technique to produce superhydrophobicity on naturally hydrophobic composite surfaces. Interesting mechanistic investigations on the low voltage actuation of the valves based on such surfaces is presented.

Chapter 4 (Article 3, Accepted)

Title: Electrochemically actuated passive stop-go microvalves for flow control in microfluidic systems

Journal: Microelectronic Engineering

In this chapter new electrode configuration was employed with the objective of improving the response time. Similar to scheme 2 discussed under chapter 4 the superhydrophobic nanoporous carbon electrode was used but in this case coupled to screen printed silver electrode. The superhydrophobic electrode as usual provides passive stopping of the flow and facilitates low voltage actuation of the flow but in this case in different manner. The asymmetric electrode configuration is expected to cause asymmetric electrochemical process giving rise to gradients across the two electrodes that can propel the liquid. Consistent with the proposed mechanism this valving configuration displays positive concentration dependence, particularly of chloride salts. The operation revealed a chloride adsorption on silver electrode as a driving mechanism.

CHAPTER 5 (Article 4, published):

TITLE: Facile and versatile approaches to enhancing electrochemical performance of screen printed electrodes

This chapter is a prerequisite to chapter 2. It presents a new electrode surface activation strategy specifically relevant to overcome some of the challenges related to electropolymerization. Since an electrically responsive polymer based superhydrophobic surface was envisaged to be developed for a stop/go fluidic operations and that this requires electropolymerization as a simple approach to be performed on a low cost electrode material-screen printed carbon a prior steps of activation of screen printed carbon surface in a way that simultaneously enhances roughness of the electrode was performed. Because the fabrication of superhydrophobic surface is accomplished by modification of a previously roughness amplified surface with low surface energy or hydrophobic (in this case the polymer) material. Screen printed carbon is a typical composite material composed of the important electroactive graphitic particles and other agents including polymeric resins and solvents or thinners for binding and dispersion of the particles. Due to the constraints of screen printing such agents are often included in excess in the ink formulation. These agents block the electrode´s performance. Thus the electrode always requires activation procedure. Existing activation procedures electrochemical, photochemical, and plasma activation of the surface introduces exotic functionalities that are nuisance when the expected property of the polymer is expected to be achieved by electropolymerization. Moreover the preamble of the work-development of user friendly devices obliges us to opt for all low cost and simple approaches in all the fabrication steps. Presented in chapter two is thus an extremely simple and low cost strategy to activate screen printed carbon electrode´s in a way that also enhances the roughness appropriate for chapter 3. In this procedure a controlled and subtractive etching of the electrode´s surface were performed based on solubility principles to remove the contaminants, activate the electrode and simultaneously increase the roughness.

All the three schemes have been successfully implemented to demonstrate multiple and sequential stop/go fluidic operations in microchannels. Such operations, unlike the previously reported methods, allows precise control of the flow at specific locations in the microchannels to realize the successful accomplishment of each elementary operations expected to be performed along the fluidics in the foreseen capillary force operated integrated microfluidic systems for diagnostic applications. Such fluidic operations are simple, low cost and miniaturizable and are expected to advance microfluidics a step forward to fully utilize its potential to outperform lateral flow devices. The low cost and flexibility of fabrication, facile integration and miniaturization make this configuration promising for the development of low cost microfluidic devices for point-of-care diagnostics, food analysis, and environmental monitoring.

CHAPTER 6 and CHAPTER 7

Chapter 6 provides summaries main findings and general conclusions of overall work. Chapter 7 presents the future outlook based on current findings. Possible areas where the findings of this thesis could be applied are presented.

1.14 Bibliography

1. Whitesides G. M. *Nature* **2006**, *442*, 368-373.

2. Golay MJE. *Anal Chem* **1957**, *29*, 928-932.

3. van Deemter J. J., Zuiderweg F. J., Klinkenberg A. *Chem. Eng. Science* **1956**, *5*, 271-289.

4. Kilby J. S. *Proc. IEEE* **2000**, *88* 109–11.

5. Petersen K. E. *Proc. IEEE* **1982**, *70*, 420-457.

6. Terry S. C., Jerman J. H., Angell J. B. *IEEE T Electron Dev* **1979**, *26*, 1880-1886.

7. Manz A., Graber N., Widmer H. M. *Sensors and Actuators B: Chemical* **1990**, *1*, 244-248.

8. Manz A., Miyahara Y., Miura J., Watanabe Y., Miyagi H., Sato K. *Sensors and Actuators B: Chemical* **1990**, *1*, 249-255.

9. Manz A., Harrison D. J., Verpoorte E. J., Fettinger J. C., Paulus A., Lüdi H., Widmer H. M. *Journal of Chromatography A* **1992**, *593*, 253-258.

10. Mathies R. A., Huang X. C. *Nature* **1992**, *359*, 167-169.

11. Harrison D. J., Fluri K., Seiler K., Fan Z., Effenhauser C., Manz A. *Science* **1993**, *261*, 895-897.

12. Woolley A., Mathies R. *Proc. National Academy of Sciences* **1994**, *91*, 11348-11352.

13. Reyes D. R., Iossifidis D., Auroux P.-A., Manz A. *Anal. Chem.* **2002**, *74*, 2623-2636.

14. Arora A., Simone G., Salieb-Beugelaar G. B., Kim J. T., Manz A. *Anal. Chem.* **2010**, *82*, 4830–4847.

15. Fodor S., Read J., Pirrung M., Stryer L., Lu A., Solas D. *Science* **1991**, *251*, 767-773.

16. Schena M., Shalon D., Davis R., Brown P. *Science* **1995**, *270*, 467-470.

17. Schena M., Shalon D., Heller R., Chai A., Brown P., Davis R. *Proc. National Academy of Sciences* **1996**, *93*, 10614-10619.

18. Northrup M. A., Gonzalez C., Hadley D., Hills R. F., Landre P., Lehew S., Saw R., Sninsky J. J., Watson R. *Solid-State Sensors and Actuators and Eurosensors IX* **1995**, *1*, 764-767.

19. Buechler K. F. *Diagnostic Devices For the Controlled Movement Of Reagents Without Membranes*, **1995** , U.S. Patent 5458852.

20. Bringer, M. R.; Gerdts, C. J.; Song, H.; Tice, J. D.; Ismagilov, R. F. *Phil. Trans. R. Soc. Lond. A.* **2004**, *362*, 1087–1104.

21. Weibel D. B., Whitesides G. M. *Curr. Opin. Chem. Biol.* **2006**, *10*, 584–591.

22. Breslauer D. N., Lee P. J., Lee L. P. *Mol. Biosyst.* **2006**, *2*, 97–112.

23. Senturia S.D. Microsystem Design. Kluwer Academic Publishers, Boston, 2001.

24. Krishnan M., Ugaz V., Burns M. *Science* **2002**, *298*, 793.

25. Rasmussen K. H., Marie R., Lange J. M., Svendsen W. E., Kristensen A., Mir K. U. *Lab Chip* **2011**, *11*, 1431-1433.

26. Hong J., Edel J. B., deMello A. J. *Drug Discovery Today* **2009**, *14*, 134–146.

27. Sanders G. W., Manz A. *Trends in Analytical Chemistry* **2000**, *19*, 364-378.

28. Lion N., Reymond F., Girault H. H., Rossier J. S. *Current Opinion in Biotechnology* **2004**, *15*, 31-37.

29. Freire S. L. S., Wheeler A. R. *Lab Chip* **2006**, *6*, 1415-1423.

30. Srinivasan V., Pamula V. K., Fair R. B. *Lab Chip* **2004**, *4*, 310-315.

31. Herr A. E., Hatch A. V., Throckmorton D. J., Tran H. M., Brennan J. S., Giannobile W. V., Singh A. K. *PNAS* **2007**, *104*, 5268-5273.

32. Koster S., Verpoorte E. *Lab Chip* **2007**, *7*, 1394-1412.

33. El-Ali J., Sorger P. K., Jensen K. F. *Nature* **2006**, *442*, 403-411.

34. Takayama S., Ostuni E., LeDuc P., Naruse K., Ingber D. E., Whitesides G. M. *Nature* **2001**, *411*, 1016-1016.

35. Tourovskaia A., Masot X., Folch A., *Lab Chip* **2005**, *5*, 14-19.

36. Balagadde F. K., You L., Hansen C. L., Arnold F. H., Quake S. R. *Science* **2005**, *309*, 137-140.

37. Roman G., Chen Y., Viberg P., Culbertson A., Culbertson C. *Anal. Bioanal. Chem.* **2007**, *387*, 9-12.

38. Hunt T. P., Issadore D., Westervelt R. M. *Lab Chip* **2008**, *8*, 81-87.

39. Ahn K., Kerbage C., Hunt T. P., Westervelt R. M., Link D. R., Weitz D. A. *Appl Phys Lett* **2006**, *88*, 024104.

40. Li Y., Dalton C., Crabtree H. J., Nilsson G., Kaler K. V. I. S. *Lab Chip* **2007**, *7*, 239-248.

41. Wheeler A. R., Throndset W. R., Whelan R. J., Leach A. M., Zare R. N., Liao Y. H., Farrell K., Manger I. D., Daridon A. *Anal. Chem.* **2003**, *75*, 3581–3586.

42. Werdich A. A., Lima E. A., Ivanov B., Ges I., Anderson M. E., Wikswo J. P., Baudenbacher F. J., *Lab Chip* **2004**, *4*, 357–362.

43. Dittrich P. S., Manz A. *Anal. Bioanal. Chem.* **2005**, *382*, 1771–1782.

44. Stavis S. M., Edel J. B., Samiee K. T., Craighead H. G. *Lab Chip* **2005**, *5*, 337–343.

45. Sato K., Mawatari K., Kitamori T. *Lab Chip*. **2008**, *8*, 1992–1998.

46. Lin C.-C., Hsu J.-L., Lee G.-B. *Microfluid Nanofluid* **2011**, *10*, 481–511.

47. Razzacki Z. S., Thwar P. K., Yang M., Ugaz V. M., Burns M. A. *Advanced Drug Delivery Reviews* **2004**, *56*, 185-198.

48. McAllister D., Wang P., Davis S., Park J., Canatella P., Allen M., Prausnitz M., *Proc. National Academy of Sciences* **2003**, *100*, 13755-13760.

49. Receveur R. A. M., Lindemans F. W., Rooij N. F., *J Micromech Microengineering* **2007**, *17*, R50-R80.

50. Santini Jr. JT, Cima MJ, Langer R. *Nature* **1999**, *397*, 335-338.

51. Gervais L., Rooij N., Delamarche E. *Adv. Mater.* **2011**, *23*, H151-H176.

52. Warsinke A. *Anal. Bioanal. Chem.* **2009**, *393*, 1393–1405.

53. Gubala V., Harris L. F., Ricco A. J., Tan M. X., Williams D. E. *Anal. Chem.* **2012**, *84*, 487–515.

54. Choi S., Goryll M., Sin L.Y. M., Wong P. K., Chae J. *Microfluid Nanofluid* **2011**, *10*, 231–247.

55. Chin C. D., Linder V., Sia S. K. *Lab Chip* **2012**, *12*, 2118–2134.

56. Gardeniers J. G. E., Berg A.v.d. *Anal. Bioanal. Chem.* **2004**, *378*, 1700–1703.

57. Harrison D.J., Manz A., Fan Z., Luedi H., Widmer H.M. *Anal. Chem.* **1992**, *64*, 1926-1932.

58. Martynova L., Locascio L. E., Gaitan M., Kramer G. W., Christensen R. G., MacCrehan W. A. *Anal Chem* **1997**, *69*, 4783-4789.

59. Locascio L. E., Gaitan M., Hong J., Eldefrawi M. *Proc Micro-TAS* **1998**, *98*, 367-370.

60. Beebe D.J., Moore J.S., Yu Q., Liu R.H., Kraft M.L., Jo B.H., Devadoss C. Proc. Natl. Acad. Sci. USA **2000**, *97*, 13488-13493.

61.Rossier, J.S., Vollet C., Carnal A., Lagger G., Gobry V., Girault H. H., Michel P., Reymond F. *Lab Chip* **2002**, *2*, 145-150.

62. McCormick R. M., Nelson R. J., Alonso-Amigo M. G., Benvegnu D. J., Hooper H. H. *Anal. Chem.* **1997**, *69*, 2626-2630.

63. Paulus A., Williams S. J., Sassi S. J., Kao P. H., Tan H., Hooper H. H. *Proc. SPIE* **1998**, *3515*, 94-103.

64. Becker H., Dietz W., Dannberg P. *Proc. Micro-TAS* **1998**, 98.

65 Becker H., Gärtner C. *Electrophoresis* **2000**, *21*, 12–26.

66 Webster J. R., Burns M. A., Burke D. T., Mastrangelo C. H. *Proc. µTAS* **1998**, 249–252.

67. Verpoorte E. *Electrophoresis* **2002**, *23*, 677–712.

68. Wang J., Chen Z., Corstjens P. L. A. M., Mauk M. G., Bau H. H. *Lab Chip* **2006**, *6*, 46–53.

69. Kim D. S., Lee S. H., Ahn C. H., Lee J. Y., Kwon T. H. *Lab Chip* **2006**, *6*, 794–802.

70. Qi S., Liu X., Ford S., Barrows J., Thomas G., Kelly K., McCandless A., Lian K., Goettert J., Soper S. A. *Lab Chip* **2002**, *2*, 88–95.

71. Kameoka J., Craighead H. G., Zhang H., Henion J. *Anal.Chem.* **2001**, *73*, 1935–1941.

72. Yang Y., Li C., Kameoka J., Lee K. H., Craighead H. G. *Lab Chip* **2005**, *5*, 869–876.

73. Liu R. H., Yang J., Lenigk R., Bonanno J., Grodzinski P., *Anal.Chem.* **2004**, *76*, 1824–1831.

74. Roman G. T., Kennedy R. T. *J. Chromatogr. A* **2007**, *1168*, 170–188.

75. Thorsen T., Maerkl S. J., Quake S. R. *Science* **2002***, 298*, 580–584.

76. Alvarez-Icaza M., Bilitewski U. *Anal. Chem.* **1993**, *665*, 525.

77. Bejarano D., Lozano P., Mata D., Cito S., Constanti M., Katakis I. J. Micromech. Microeng. **2009**, *19*, 115007.

78. Wring S. A., Hart J. P. *Analyst* **1992**, *117*, 1281.

79. Cagnini A., Palchetti I., Lionti I., Mascini M., Turner A. P. F. *Sens.Actuators B* **1995**, *24*, 85.

80. Green M., Hildrich P. *Anal. Proc.* **1991**, *28*, 374.

81. Lewis B. D., Clin. Chem. 1992, 38, 2093.

82. Ng R., Martin L., Halpin M., Bernstein R., Fischer J., Taylor E., Schroder S., Clin. Chem. **1995**, *41*, S181.

83. Nie Z., Deiss F., Liu X., Akbulut O., Whitesides G. M. *Lab Chip*, **2010**, *10*, 3163–3169.

84. Martinez A. W., Phillips S. T., Whitesides G. M. *Anal. Chem.* **2010**, *82,* 3–10.

85. Cui G., Yoo J. H., Yoo J., Lee S. W., Nam H., Cha G. S. *Electroanalysis* **2001**, *13*, 224-228.

86. Zhang C., Haruyama T., Kobatake E., Aizawa M. *Analytica Chimica Acta* **2001**, *442*, 257–265.

87. Tabeling, P. *Introduction to Microfluidics*. Oxford University Press, 2005.

88. Weigl B. H., Yager P. *Science* **1999**, *283*, 346-347.

89. Laser D. J., Santiago J. G., *J. Micromech. Microeng.* **2004**, *14*, R35–R64.

90. Au A. K., Lai H., Utela B. R., Folch A. *Micromachines* **2011**, *2*, 179-220.

91. Oh K. W., Ahn C. H. *J. Micromech. Microeng.* **2006**, *16*, R13–R39.

92. Moscovici, M, Chien, W.Y., Abdelgawad, M., Sun, Y. *Biomicrofluidics* **2010**, *4*, 046501.

93. Lee S. J., Chan J. C. Y., Maung K. J., Rezler E., Sundararajan N. *J. Micromech. Microeng.* **2007**, *17*, 843-851.

94. Kim J., Baek J., Lee K., Park Y., Sun K., Lee T., Lee S. *Lab Chip* **2006**, *6*, 1091-1094.

95. Jeong O.C., Konishi S. *J. Micromech. Microeng.* **2008**, *18*, 025022.

96. Wang C. H., Lee G. B. *J. Micromech. Microeng.* **2006**, *16*, 341-348.

97. Huang S.B., Wu M. H., Cui Z. F., Cui Z., Lee G. B. *J. Micromech. Microeng.* **2008**, *18*, 12, 045008.

98. Kim J. Y., Park H., Kwon K. H., Park J. Y., Baek J. Y., Lee T.S., Song H. R., Park Y. D., Lee S. H. *Biomed. Microdevices* **2008**, *10*, 11-20.

99. Zhang C., Xing D., Li Y. *Biotechnol. Adv.* **2007**, *25*, 483-514.

100. Lai H., Folch A. *Lab Chip* **2011**, *11*, 336-342.

101. Vanlintel H. T. G., Vandepol F. C. M., Bouwstra S. *Sens. Actuat.* **1988**, *15*, 153-167.

102. Smits J.G. *Sens. Actuat. A* **1990**, *21*, 203-206.

103. Koch M., Evans A. G. R., Brunnschweiler A. *J. Micromech. Microeng.* **1998**, *8*, 119-122.

104. Nguyen N. T., Huang X. Y. *Sens. Actuat. A* **2001**, *88*, 104-111.

105. Johnston I. D., Tracey M. C., Davis J. B., Tan C. K. L. *Lab Chip* **2005**, *5*, 318-325.

106. Bohm S., Olthuis W., Bergveld P. *Biomed. Microdevices* **1999**, *1*, 121-130.

107. Bohm S., Timmer B., Olthuis W., Bergveld P. *J. Micromech. Microeng.* **2000**, *10*, 498-504.

108. Jacobson S. C., Hergenroder R., Koutny L. B., Ramsey J. M. *Anal. Chem.* **1994**, *66*, 2369-2373.

109. Ramsey R.S., Ramsey J. M. *Anal. Chem.* **1997**, *69*, 1174-1178.

110. McKnight T. E., Culbertson C. T., Jacobson S. C., Ramsey J. M. *Anal. Chem.* **2001**, *73*, 4045-4049.

111. Chen C. H., Santiago J. G. *J. Microelectromech. Syst.* **2002**, *11*, 672-683.

112. Ajdari A. *Phys. Rev. E* **2000**, *61*, R45-R48.

113. Brown A. B., Smith C. G., Rennie A. R. *Phys. Rev. E* **2001**, *63*, 016305.

114. Studer V., Pepin A., Chen Y., Ajdari A. *Microelectron. Eng.* **2002**, *61*, 915-920.

115. Mpholo M., Smith C. G., Brown A. B. D. *Sens.Actuat.B* **2003**, *92*, 262-268.

116. Debesset S., Hayden C. J., Dalton C., Eijkel J. C., Manz A. *Lab Chip* **2004**, *4*, 396-400.

117. Pollack M. G., Fair R. B., Shenderov A. D. *Appl. Phys. Lett.* **2000**, *77*, 1725-1726.

118. Lee J., Moon H., Fowler J., Schoellhammer T., Kim C. J. *Sens. Actuat. A* **2002**, *95*, 259-268.

119. Cho S. K., Moon H. J., Kim C. J. *J. Microelectromech. Syst.* **2003**, *12*, 70-80.

120. Barbulovic-Nad I., Yang H., Park P. S., Wheeler A. R. *Lab Chip* **2008**, *8*, 519-526.

121. Barbulovic-Nad I., Au S. H., Wheeler A. R. *Lab Chip* **2010**, *10*, 1536-1542.

122. Pollack M. G., Shenderov A.D., Fair R. B. *Lab Chip* **2002**, *2*, 96-101.

123. Batchelder J. S. *Rev. Sci. Instrum.* **1983**, *54*, 300-302.

124. Jones T. B. *J. Electrostat.* **2001**, *51*, 290-299.

125. Schwartz J. A., Vykoukal J. V., Gascoyne, P. R. *Lab Chip* **2004**, *4*, 11-17.

126. Zeng J., Korsmeyer T. *Lab Chip* **2004**, *4*, 265-277.

127. Rife J. C., Bell M. I. *Proc. SPIE* **1998**, *358*, 125-135.

128. Rife J. C., Bell M. I., Horwitz J. S., Kabler M. N., Auyeung R. C. Y., Kim W. J. *Sens. Actuat. A* **2000**, *86*, 135-140.

129. Yuan H., Prosperetti A. *J. Micromech. Microeng.* **1999**, *9*, 402-413.

130. Geng X., Yuan H., Oguz H. N., Prosperetti A. *J. Micromech. Microeng.* **2001**, *11*, 270-276.

131. Dijkink R. J., van der Dennen J. P., Ohl C. D., Prosperetti A. *J. Micromech. Microeng.* **2006**, *16*, 1653-1659.

132. Tovar A. R., Lee A. P. *Lab Chip* **2009**, *9*, 41-43.

133. Lee A. P., Patel M. V., Tovar A. R., Okabe Y. *J. Assoc. Lab.Autom.* **2010**, *15*, 449-454.

134. Tovar A. R., Patel M. V., Lee A. P. *Microfluid Nanofluid* **2011**, *10*, 1269–1278.

135. Jang J. S., Lee S. S. *Sens. Actuat. A* **2000**, *80*, 84-89.

136. Lemoff A. V., Lee A. P. *Sens. Actuat. B* **2000**, *63*, 178-185.

137. von Helmholtz H. L. F. *Ann. Physik* **1879***, 7, 337.*

138. Gouy G., *Journ. de Phys.* **1910**, *9*, 457.

139. (a) Chapman D. L. *Phil. Mag.* **1913**, *25*, 475. (b) G. Gouy, *Ann. Phys.***1917**, *7*, 129.

140. Butt H.-J., Graf K., Kappl M. *Physics and Chemistry of Interfaces*, Wiley, New York, **2003**.

141. Debye P., Hückel E. *Physikalische Zeitschrift* **1923**, *24*, 185.

142. (a) Wang X., Cheng C., Wang S., Liu S., *Microfluid Nanofluid* **2009**, *6*, 145-162. (b) Seller K., Fan Z. H., Flurl K., Harrison D. J. *Anal. Chem.***1994***, 66,* 3485–91.

143. Ocvirk G., Munroe M., Tang T., Oleschuk R., Westra K., Harrison D. J. *Electrophoresis* **2000***, 21*, 107–15.

144. Selvaganapathy P., Ki Y.-S. L., Renaud P., Mastrangelo C. H. *J. Microelectromech. Syst.* **2002**, *11*, 448-453.

145. Takamura Y., Onoda H., Inokuchi H., Adachi S., Oki A., Horiike Y., *Electrophoresis* **2003**, *24*, 185-192.

146. Lazar I. M., Karger B. L., *Anal. Chem.* **2002**, *74*, 6259-6268.

147. Chen L., Ma J., Tan F., Guan Y. *Sens. Actuators, B* **2003**, *88*, 260-265.

148. Reichmuth D. S., Chirica G. S., Kirby B. J. *Sens. Actuators, B* **2003**, *92*, 37-43.

149. Dasgupta P. K., Liu S. *Anal.Chem.***1994**, *66*, 1792-1798.

150. Pemble C. M., Towe B. C. *Sens. Actuat. A* **1999**, *77*, 145-148.

151. Weibel D. B., Siegel A. C., Lee A., George A. H., Whitesides G. M. *Lab Chip* **2007**, *7*, 1832-1836.

152. Weibel D. B., Kruithof M., Potenta S., Sia S. K., Lee A., Whitesides G. M. *Anal. Chem.* **2005**, *77*, 4726-4733.

153. Pilarski P. M., Adamia S., Backhouse C. J. *J. Immunol.Meth.***2005**, 3*05*, 48-58.

154. Sundararajan N., Kim D., Berlin A. A. *Lab Chip* **2005**, *5*, 350-354.

155. Studer V., Hang G., Pandolfi A., Ortiz M., Anderson W. F., Quake S. R. *J. Appl. Phys.* **2004**, *95*, 393-398.

156. Hosokawa K., Maeda R. *J. Micromech. Microeng.* **2000**, *10*, 415-420.

157. Grover W. H., Skelley A. M., Liu C. N., Lagally E. T., Mathies R. A. *Sens. Actuat. B* **2003**, *89*, 315-323.

158. Unger M. A., Chou H. P., Thorsen T., Scherer A., Quake S. R. *Science* **2000**, *288*, 113-116.

159. Yang B. Z., Lin Q. *Sens. Actuat. A* **2007**, *134*, 194-200.

160. Yoo J. C., Choi Y. J., Kang C. J., Kim Y. S. *Sens. Actuat. A* **2007**, *139*, 216-220.

161. Irimia D., Toner M. *Lab Chip* **2006**, *6*, 345-352.

162. van der Wijngaart W., Chugh D., Man E., Melin J., Stemme G. *J. Microelectromech. Syst.* **2007**, *16*, 765-774.

163. Lee D. E., Soper S., Wang W. J. *Microsyst. Technol.* **2008**, *14*, 1751-1756.

164. Kaigala G. V., Hoang V. N., Backhouse C. J. *Lab Chip* **2008**, *8*, 1071-1078.

165. Jacobson S. C., Ermakov S. V., Ramsey J. M. *Anal. Chem.***1999**, *71*, 3273-3276.

166. Schasfoort R. B. M., Schlautmann S., Hendrikse L., Berg A. v. d. *Science* **1999**, *286*, 942-945.

167. Harrison D. J., Fluri K., Seiler K., Fan Z. H., Effenhauser C. S., Manz A. *Science* **1993**, *261*, 895-897.

168. Jacobson S. C., Ermakov S. V., Ramsey J. M. *Anal. Chem.***1999**, *71*, 3273-3276.

169. Taniguchi T., Torii T., Higuchi T., *Lab. Chip* **2002**, *2*, 19–23.

170. Lee J., Moon H., Fowler J., Schoellhammer T., Kim C-J. *Sensors Actuators* A **2002**, *95*, 259–68.

171. Pollack M. G., Shenderov A. D., Fair R. B. *Lab. Chip* **2002***, 2*, 96–101.

172. Paik P., Pamula V. K., Pollack M. G., Fair R. B. *Lab. Chip* **2003***,3*, 28–33

173. Gascoyne P. R. C., Vykoukal J. V., Schwartz J. A., Anderson T. J., Vykoukal D. M., Current K. W., McConaghy C., Becker F. F., Andrews C., *Lab. Chip* **2004**, *4*, 299–309.

174. Srinivasan V., Pamula V. K., Fair R. B. *Lab. Chip* **2004**, *4*, 310–315.

175. Yi U.-C., Kim C.-J. *Sensors Actuators* A **2004**, *114*, 347–54.

176. Suzuki H., Yoneyama R. *Sensors Actuators* B **2003**, 96, 38–45.

177. Hua S. Z., Sachs F., Yang D. X., Chopra H. D. *Anal. Chem.* **2002**, *74*, 6392–6396.

178. Takahashi K., Yoshino K., Hatano S., Nagayama K., Asano T. *Proc. IEEE MEMS* **2001**, 286–289.

179. Beebe D. J., Moore J. S., Bauer J. M., Yu Q., Liu R. H., Devadoss C. Jo B. H. *Nature* **2000**, *404*, 588–590.

180. Liu R., Yu Q., Beebe D. J. *J. Microelectromech. Syst.* **2002***, 11*, 45–53.

181. Richter A., Kuckling D., Howitz S., Gehring T., Arndt K.-F. *J. Microelectromech. Syst.* **2003***, 12* 748–753.

182. Yu C., Mutlu S., Selvaganapathy P., Mastrangelo C. H., Svec F. Frechet J. M. J. *Anal. Chem.* **2003**, *75*, 1958–61

183. Hu Z., Zhang X., Li Y. *Science* **1995**, *269*, 525–7.

184. Low L.-M., Seetharaman S., He K.-Q., Madou M. J. *Sensors Actuators* B **2000**, *67*, 149–60.

185. Tanaka T., Nishio I., Sun S.-T., Ueno-Nishio S. *Science* **1982**, *218*, 467–9.

186. Suzuki A., Tanaka T. *Nature* **1990**, *346*, 345–7.

187. Kataoka K., Miyazaki H., Bunya M., Okano T., Sakurai Y. *J. Am. Chem. Soc.* 1998, *120*, 694–5.

188. Miyata T., Asami N., Uragami T. *Nature* **1999**, *399*, 766–9.

189. Carlen E. T., Mastrangelo C. H. *J. Microelectromech. Syst.*2002, *11*, 408–20.

190. Liu R. H., Yang J., Lenigk R., Bonanno J., Grodzinski P. *Sensors Actuators* B **2004**, *98*, 328–36.

191. Gui L., Liu J. *J. Micromech. Microeng.* **2004**, *14*, 242–6.

192. Yoshida K., Kikuchi M., Park J.-H., Yokota S. *Sensors Actuators* A **2002**, *95*, 227–33.

193. Yamahata C., Chastellain M., Parashar V. K., Petri A., Hofmann H., Gijs M. A. M. *J. Microelectromech. Syst.***2005**, *14*, 96–102.

194. Eddington D. T., Beebe D. J. Advanced Drug Delivery Reviews **2004**, *56*, 199–210.

195. Park J., Sunkara V., Kim T.-H., Hwang H., Cho Y.-K., *Anal. Chem.* **2012**, *84*, 2133–2140.

196. Gustafsson M., Hirschberg D., Palmberg C., Jornvall H., Bergman T., *Anal. Chem.* **2004**, *76*, 345-350.

197. Chen J. M., Huang P. C., Lin M. G. *Microfluid. Nanofluid.* **2008**, *4*, 427-437.

198. Fisher R. A. J. Agric. Sci. **1926**, *16*, 492.
199. Haines W. B. J. Agric. Sci. **1927**, *17*, 264.

200. Kramer P. J. Water relations of plants, Academic Press, New York, **1983**.

201. Villanueva W., Amberg G., International Journal of Multiphase Flow **2006**, *32*, 1072-1086.

202. Weiss, A. Concurrent engineering for Lateral-Flow diagnostics. *IVD Technol.* **1999**, *7*, 48–57.

203. Plotz C. M., Singer J. M. *Am. J. Med.* **1956**, *21*, 888–892.

204. Lonnberg M., Carlsson J. *Anal. Biochem.* **2001**, *293*, 224–231.

205. Posthuma-Trumpie G. A., Korf J., Amerongen A. *Anal Bioanal Chem* **2009**, *393*, 569–582.

206. Stevens D. Y., Petri C. R., Osborn J. L., Spicar-Mihalic P., McKenzie K. G., Yager P. Lab Chip **2008**, *8*, 2038–2045.

207. Juncker D., Schmid H., Drechsler U., Wolf H., Wolf M., Michel B., de Rooij N., Delamarche E., *Anal. Chem.* **2002**, *74*, 6139 – 6144.

208 Martinez A. W., Philips S. T., Butte M. J., Whitesides G. M. *Angew Chem Int Ed* **2007**, *46*, 1318–1320.

209 Martinez A. W., Philips S. T., Carrilho E., Thomas S. W., Sindi H., Whitesides G. M. *Anal. Chem.* **2008**, *80*, 3699–3707.

210 Martinez A. W., Phillips S. T., Whitesides G. M., Carrilho E. *Anal. Chem.* **2009**, *82*, 3–10.

211 Martinez A. W., Philips S. T., Whitesides G. M. *Anal Chem* **2010**, *82*, 3–10.

212. Gubala V., Harris L. F., Ricco A. J., Tan M. X., Williams D. E. *Anal. Chem.* **2012**, *84*, 487–515.

213. Delamarche E., Juncker D., Schmid H. *Adv. Mater.* **2005**, *17*, 2911–2933.

214. Warsinke A. *Anal Bioanal Chem* **2009**, *393*, 1393–1405.

215. Choi S., Goryll M., Sin L.Y.M., Wong P. K., Chae J. *Microfluid Nanofluid* **2011**, *10*, 231–247.

216. Delaney J. J., Hogan C. F., Tian J., Shen W. *Anal. Chem.* **2011**, *83*, 1300–1306

217. Lin C.-C., Wang J.-H., Wu H. W., Lee G. B. *JALA* **2010**, 253-274.

218. Ng A. H. C., Uddayasankar U., Wheeler A. R. *Anal Bioanal Chem* **2010**, *397*, 991–1007.

219. Bange A., Halsall H. B., Heineman W. R. *Biosensors and Bioelectronics* **2005**, *20*, 2488–2503.

220. Chin C. D., Linder V., Sia S. K. *Lab Chip* **2012**, *12*, 2118–2134.

221. Henares T. G., Mizutani F., Hisamoto H. *analytica chimica acta* **2008**, *611*, 17–30.

222. Dungchai W., Chailapakul O., Henry C. H. *Analyst* **2011**, *136*, 77.

223. Du D., Wang J., Wang L., Lu D., Lin Y. *Anal. Chem.* **2012**, *84*, 1380–1385.

224. Mata D., Bejarano D., Botero M. L., Lozano P., Constantí M., Katakis I. *Electrochim. Acta* **2010**, *55*, 4261.

225. Santiago L., Bejarano D., Lozano P., Katakis I. Analyst **2010**, *135*, 1276.

226. Zimmermann M., Delamarche E., Wolf M., Hunziker P. *Biomed. Microdevices* **2005**, *7*, 99–110.

227. Rossier J. S., Gokulrangan G., Girault H. H., Svojanovsky S., Wilson G. S. *Langmuir* **2000**, 16, 8489.

228. Young T., *Phil. Trans. Roy. Soc. London* **1805**, 95, 65.

229. P.S. de Laplace, *Mécanique Céleste*, suppl. au X. Livre, Croucier, Paris, 1805.

230. Wenzel R. N. *Industrial and Engineering Chemistry* **1936**, *28*, 988-994

231. Cassie A. B. D., Baxter S. *Trans. Faraday Soc.* **1944**, *40*, 546-551.

232. Ma M., Hill R. M. *Current Opinion in Colloid & Interface Science* **2006**, *11*, 193–202.

233. Li X.-M., Reinhoudt D., Crego-Calama M. *Chem. Soc. Rev.* **2007**, *36*, 1350–1368.

234. McHale G., Shirtcliffe N. J., Newton *M. I, Analyst* **2004**, *129*, 284-287.

235. Onda T, Shibuichi S, Satoh N, Tsujii K. Langmuir **1996**,*12*, 2125–7.

236. Shi F., Song Y. Y., Niu J., Xia X. H., Wang Z. Q., Zhang X. *Chem. Mater.* **2006**, *18*, 1365–1368.

237. Shirtcliffe N. J., McHale G., Newton M. I., Chabrol G., Perry C. C. *Adv Mater* **2004**, *16*, 1929–32.

238. Han J. T., Jang Y., Lee D. Y., Park J. H., Song S. H., Ban D. Y., J *Mater Chem* **2005**, *15*, 3089–92.

239. Hosono E., Fujihara S., Honma I., Zhou H. S. *J Am Chem Soc* **2005**, *127*, 13458–9.

240. Zhang L. B., Chen H., Sun J. Q., Shen J. C. *Chem. Mater.* **2007**, *19*, 948–953.

241. Shi F., Wang Z. Q., Zhang X. *Adv Mater* **2005**, *17*, 1005–9.

242. Zhao N., Shi F.,Wang Z. Q., Zhang X. *Langmuir* **2005**, *21*, 4713–6.

243. Jisr R. M., Rmaile H. H., Schlenoff J. B. *Angew Chem Int Ed* **2005**, *44*, 782–5.

244. Han J. T., Zheng Y., Cho J. H., Xu X., Cho K. *J Phys Chem B* **2005**, *109*, 20773–8.

245. Lu S. X., Chen Y. L., Xu W. G., Liu W. *Appl. Surf. Sci.* **2010**, *256*, 6072–6075.

246. Feng X. J., Zhai J., Jiang L. *Angew Chem Int Ed* **2005**, *44*, 5115–8.

247. Hikita M., Tanaka K., Nakamura T., Kajiyama T., Takahara A. *Langmuir* **2005**, *21*, 7299–302.

248. Shang H. M., Wang Y., Limmer S. J., Chou T. P., Takahashi K., Cao G. Z. *Films* **2005**, *472*, 37–43.

249. Wu X., Zheng L., Wu D. *Langmuir* **2005**, *21*, 2665–7.

250. Wei Z. J., Liu W. L., Tian D., Xiao C. L., Wang X. Q. *Appl. Surf. Sci.* **2010**, *256*, 3972–3976.

251. Furstner R., Barthlott W., Neinhuis C., Walzel P. *Langmuir* **2005**, *21*, 956–61.

252 Callies M., Chen Y., Marty F., Pepin A., Quere D. *Microelectron Eng* **2005**, *78–79*, 100–5.

253. Abdelsalam M. E., Bartlett P. N., Kelf T., Baumberg J. *Langmuir* **2005**, *21*, 1753–7.

254. Notsu H., Kubo W., Shitanda I., Tatsuma T., *J Mater Chem* **2005**,*15*, 1523–7.

255. Shiu J.-Y., Kuo C.-W., Chen P. *Proc. SPIE* **2005**, *5648*, 325–32.

256. Teshima K., Sugimura H., Inoue Y., Takai O., Takano A. *Appl Surf Sci* **2005**, *244*, 619–22.

257. Jin M. H., Feng X. J., Xi J. M., Zhai J., Cho K. W., Feng L. *Macromol Rapid Commun* **2005**, *26*, 1805–9.

258. Song X. Y., Zhai J., Wang Y. L., Jiang L.. *J Phys Chem B* **2005**, *109*, 4048–52.

259. Wang Q., Zhang B. W., Qu M. N., Zhang J. Y., He D. Y. *Appl. Surf. Sci.* **2008**, *254*, 2009–2012.

260. Liu H., Feng L., Zhai J, Jiang L, Zhu DB. *Langmuir* **2004**, *20*, 5659–61.

261. Zhu L. B, Xiu Y. H., Xu J. W., Tamirisa P. A., Hess D. W., Wong C. P. *Langmuir* **2005**, *21*, 11208–12.

262. Huang L, Lau S. P., Yang H. Y., Leong E. S. P., Yu S. F., Prawer S. *J Phys Chem, B* **2005**, *109*, 7746–8.

263. Mecerreyes D., Alvaro V., Cantero I., Bengoetxea M., Calvo P. A., Grande H., Rodriguez J., Pomposo J. A., *Adv. Mater.* **2002**, *14*, 749.

264. Zhang Z., Gu L., Shi G., *J. Mater. Chem.* **2003**, *13*, 2858.

265. Jin Y., Zhang Z., Men X., Xu X., Zhu X. *Langmuir* **2010**, *26*, 10198–10202.

266. Li J., Wan H., Liu X., Ye Y., Zhou H., Chen J. *Applied Surface Science* **2012**, *258*, 8585– 8589.

267. Wang C. H., Liao C S., Kuo S. W., Lin H. C. *Applied Surface Science* **2011**, *257*, 9152– 9157.

268. Chen L., Liu M., Lin L., Zhang T., Ma J., Song Y., Jiang L. *Soft Matter* **2010**, *6*, 2708–2712.

269. Fu, Q.; Rao, G. V. R.; Basame, S. B.; Keller, D. J.; Artyushkova, K.; Fulghum, J. E.; Lopez, G. P. *J. Am. Chem. Soc.* **2004**, *126*, 8904.

270. Lim H. S., Han J. T., Kwak D., Jin M. H., Cho K. *J. Am. Chem. Soc.* **2006**, *128*, 14458.

271. Lim H. S., Kwak D., Lee D. Y., Lee S. G., Cho K. *J. Am. Chem. Soc.* **2007**, *129*, 4128.

272. Matthews J. R., Tuncel D., Jacobs R. M. J., Bain C. D., Anderson H. L. *J. Am. Chem. Soc.* **2003**, *125*, 6428.

273. Ionov L., Minko S., Stamm M., Gohy J. F., Jerome R., Scholl A. *J. Am. Chem. Soc.* **2003**, *125*, 8302.

274. Julthongpiput D., Lin Y. H., Teng J., Zubarev E. R., Tsukruk V. V. *J. Am. Chem. Soc.* **2003,** *125*, 15912.

275. Yang J., Zhang Z., Men X., Xu X., Zhu X., Zhou X., Xue Q. *Journal of Colloid and Interface Science* **2012**, *366*, 191–195.

276. Zhao Y., Li M., Lu Q. *Langmuir* **2008**, 24, 3937.

277. Wang L., Lin Y., Su Z. Soft Matter **2009**, 5, 2072.

278. Wang L., Lin Y., Peng B., Su Z. *Chem. Commun.* **2008**, *44*, 5972.

279. Jiang C., Wang Q., Wang T., *New J. Chem.* **2012**, *36*, 1641–1645.

280. Pernites R. B., Ponnapati R. R., Advincula R. *C. Adv. Mater.* **2011**, *23*, 3207–3213.

281. Lahann J., Mitragotri S., Tran T.-N., Kaido H., Sundaram J., Choi I. S., Hoffer S., Somorjai G. A., Langer R. *SCIENCE* **2003**, *299*, 371-374.

282. Abbott N. L., Gorman C. B., Whitesides G. M. *Langmuir* **1995**, *11*, 16-18.

283. Lin P., Yan F., Chan H. L. W. *Langmuir* **2009**, *25*, 7465–7470.

284. Torres W., Donini J. C., Vlcek A. A., Lever A. B. P. *Langmuir* **1996**, *11*, 2920-2925.

285**.** Xu L., Chen W., Mulchandani A., Yan Y. *Angew. Chem. Int. Ed.* **2005**, *44*, 6009 –6012.

286. Xin B., Hao J. *Chem. Soc. Rev.* **2010**, *39*, 769–782.

287. Chunder A., Etcheverry K., Londe G., Cho H. J., Zhai L. *Colloids and Surfaces A: Physicochem. Eng. Aspects* **2009**, *333*, 187–193.

288. Takei G., Nonogi M., Hibara A., Kitamori T., Kim H. B. *Lab Chip* **2007**, *7*, 596–602.

289. Lippmann G. *Ann. Chim. Phys.* **1875**, *5*, 494–548.

290. Berge B *C. R. Acad. Sci.* II 1993, ***317,*** 157.

291. Gupta R., Olivier G. K., Frechette J. *Langmuir* **2010**, *26*, 11946–11950.

292. Dai W., Zhao Y. P. *Journal of Adhesion Science and Technology* **2008***, 22,* 217–229.

293. Prins M. W. J., Welters W. J. J., Weekamp J. W. *Science* **2001**, *291*, 277-280.

294. Cheng J.-Y., Hsiung L.-C., *Biomedical microdevices* **2004**, *6*, 341-347.

295. Gallardo B. S., Gupta V. K., Eagerton F. D., Jong L. I., Craig T. V. S., Shah R. R., Abbott N. L. *Science* **1999**, *283*, 57–61.

296. Bennett D. E., Gallardo B. S., Abbott N. L. *J. Am. Chem. Soc.* **1996**, *118*, 6499–6505.

297. Brown A. B. D., Smith C. G., Rennie A. R. *PHYSICAL REVIEW E* **2000**, *63*, 016305.

298. Trau M., Saville D. A., Aksay I. A. *Langmuir* **1997**, 13, 6375.

299. Yeh S.R., Seul M., Shraiman B. I. *Nature*, **1997**, *386*, 57.

300. Ristenpart W. D., Jiang P., Slowik M. A., Punckt C., Saville D. A., Aksay I. A. *Langmuir* **2008,** *24,* 12172-12180.

CHAPTER 2

CHAPTER 2

SMART ELECTRODES FOR STOP-GO FLUIDIC MANIPULATION IN ANALYTICAL MICROSYSTEMS

Alemayehu P. Washe,[a] P. Lozano,[b] D. Bejarano,[a] and Ioanis Katakis*[a]

[a] Bioengineering and Bioelectrochemistry Group, Department of Chemical Engineering, Universitat Rovira i Virgili, Avinguda Països Catalans, 26, 43007, Tarragona, Spain
[b] Current address: Integrated Microsystems for the Quality of Life S.L., C/del Ferro 6, Nave 7, 43006 Tarragona, Spain
*Corresponding author: Tel. +34 977 55 96 55, Fax + 34 977 55 96 21, E-mail: ioanis.katakis@urv.cat

Abstract

Taking advantage of electrochemically tunable wettability linked to reversible redox property of conducting polymers (e.g. poly(3-methylthiophene)), we demonstrated sequential stop-go fluidic operations in microfluidic systems. Electrical stimuli responsive superhydrophobic surface on screen printed carbon electrodes was produced via a prior construction of microscale roughness on electrode´s surface using selective solvent etching which simultaneously activates the electrodes. While the roughness is a precondition for producing superhydrophobicity, the activation facilitated electrodeposition of the polymer with the desired property. The performance of the SMART electrode was characterized in stop-go mode with response time between 2 and 10 sec depending on the actuation potential.

1 INTRODUCTION

Microfluidics offers very fascinating features for lab-on-a-chip (LOC) applications in sectors such as Point of Care (POC) diagnostics, food and environmental analysis.[1-7] Recent developments for LOC devices have shown a push towards user friendly devices (simple to operate, low cost and portable).[5, 8-13] Such devices require simple fluid manipulation and sensing principles lowering manufacturing costs and simplifying operation. The simplest such process consists of the movement of a fluid in a microchannel by capillary action. The ability to precisely control flow in such a simplistic microchannel could prove crucial for many LOC applications, particularly in bioanalytical applications where an analytical response depends on the extent of dissolution, mixing, and reaction of previously deposited molecules (antibodies, conjugates, oligonucleotides etc) with the analyte in the flow.[8] Flow control in such systems needs to be achieved with easily operated, effortlessly integrated valves. A large variety of valves with specific actuation methods including magnetic, pneumatic, piezoelectric, thermal, and electrochemical have been reported for flow control in microfluidic systems.[14,15] However, these solutions require mechanical operations with moving parts and applied mainly for gas flow control. Most reported valves for liquid flow control in microfluidic systems are based on stimuli responsive hydrogels.[16-20] Due to slow response of hydrogels to external stimuli; however, they are not suitable for fast actuations. The most appropriate flow control strategy for capillary force operated microfluidic devices is passive

56

mechanisms with no moving parts. Capillary flow is driven by capillary pressure which for rectangular microchannel of width (w) and depth (d) is given by the Young-Laplace equation:[9]

$$P_c = -\sigma_{lv}\left(\frac{Cos\theta_b + Cos\theta_t}{d} + \frac{Cos\theta_l + Cos\theta_r}{w}\right)$$

where P_c is the capillary pressure that drives capillary flow, γ_L is liquid-vapor interfacial energy, $\theta_{b,t,l,r}$ are the contact angles of the liquid on the bottom, top, left, and right channel wall surfaces, respectively. As per the Young-Laplace equation passive capillary flow control mechanisms can take advantage of the dependence of capillary flow on surface properties and dimensions of the microchannel. Variations in either wettability or geometry of the microchannel have been used as delay valves;[5, 8, 21] Delay valves, although can be effective with high affinity reaction that requires no longer than a minute of incubation, are not versatile and may not be reliable due to heterogeneous nature of most surfaces and anisotropy in dimensions of microchannels. On the other hand both experimental and theoretical works have indicated stringent dependence of sensitivity of microfluidic assays on flow rate in microchannels pointing to the importance of tight control of flow including stopping and restarting.[22, 23] Thus stopping the flow at the vicinity of the probe zone in the microchannel and restarting whenever required can provide reliable and precise control of the flow. Such operations can be performed using passive stop valves coupled to a fast actuation mechanism. Geometry based capillary stop valves actuated by centrifugal force as in lab on CD[24-27] and liquid triggering[28] mechanisms have been reported. In centrifugally operated valves, the rotation frequency is controlled but the liquid may fail to stop when rotation ceases because of heterogeneities resulting from anisotropy in dimension or wettability of the microchannel. In addition CD devices require external sources to operate the movement that limit miniaturization, integration and automation. Liquid triggered valves require a dedicated channel to introduce the liquid which may add operation complexity. On the other hand stimuli responding polymer based valves have been reported for on chip manipulation of capillary flow. The operation principle of such valves is based on change in wettability[29] of the polymer in response to external stimuli such as temperature,[30-31] and light.[32] In line with this approach electrical control of wettability is very attractive due to its simplicity to fabricate and operate and expediency to perform stop-go fluidic operations in microchannel. It can conveniently be applied in a programmable and automated fashion via individually addressable electrodes. To stop capillary flow a superhydrophobic surface is often required. Superhydrophobic surfaces provide distinct advantages. On one hand they provide reliable passive stopping. On the other hand they allow large range of contact angle changes via external signal. However, a low voltage actuation of the flow that stops at the superhydrophobic surface is not trivial. The surface has to be such that it

provides not only passive stopping but also prone to low voltage modulation of surface energy. Some reports have demonstrated electrically actuated flow using electrowetting on dielectric (EWOD).[33-34] Electrowetting techniques employed so far use mainly the prominent hydrophobic dielectric material-the poly (tetrafluoroethylene) (PTFE). However EWOD often requires high voltages (100s) and has associated problems including dielectric breakdown and contamination to the system, joule heating, and contact angle saturation.

Conducting polymers provide attractive opportunity to realize a low voltage actuated passive stop/go valves. In addition to their electronic conductivity and optical properties related to conjugated π-system, conducting polymers (also called synthetic metals) such as polythiophenes are able to retain the memory of their oxidation level. They can exist with a positively charged conjugated backbone and negatively charged counterions (dopants) or as neutral conjugated polymer- the two states displaying different wettability.[35] These properties make conducting polymers attractive for applications in corrosion protection,[36] conductive textiles,[37] and antistatic coatings,[38] and in the immobilization of biopolymers[39] and growth control of living cells.[40] Their ability to switch between two oxidation states corresponding to doped (oxidized) and undoped (neutral) states makes them particularly interesting for flow control in microfluidic systems. One possibility is therefore to construct superhydrophobic surfaces based on electrical stimuli responsive conducting polymers. Such superhydrophobic surfaces can provide passive stopping of capillary flow and also facilitate fast and low voltage actuation of the flow by virtue of their electrically tunable wettability. Among the electrical stimuli responsive conducting polymers, poly-3-methyl thiophene (P3MeT) has been the subject of extensive investigation due to their good environmental stability, relatively good electrical conductivity, and reliable mechanical adhesion to different surfaces.

The important step in the fabrication of stop-go valves envisaged in this study was the construction of the low-voltage responsive superhydrophobic surface. A model surface for superhydrophobicity is provided by the leaves of the Lotus plant (*Nelumbo nucifera*), which have an intrinsic hierarchical structure, built by convex cell papillae and randomly oriented hydrophobic wax tubules on it.[41, 42] Such surfaces display a rather very large values of water contact angle, usually above 150^0 giving the surface self cleaning property. Artificial superhydrophobicity have, therefore, been constructed by mimicking the characteristic surface features of Lotus leaves: i) constructing a nanoscale roughness on a low surface energy

(hydrophobic) material or ii) modifying previously roughness amplified surface with a material of low surface energy.[43-46] The most commonly employed method is the combination of fabrication of pillar arrays and the self-assembly technique which often involved complex and expensive fabrication techniques including lithography.[47, 48] One simple possibility to construct a SMART (specific and measureable action in real time) valve is construction of nanoscale roughness on a naturally hydrophobic screen printed carbon and modify the surface with stimuli responding conducting polymers (e.g. by electropolymerization).

Herein we demonstrate the design, fabrication, and integration of SMART superhydrophobic surface into capillary force operated microsystems for stop-go fluidic operations. A pair of electrodes, E1 and E2, with specific surface property deposited in microchannel constitutes the SMART valve. The liquid can flow across E1 surface by capillary action and stops at the SMART superhydrophobic E2 surface. A facile and low cost fabrication of roughness-enhanced hydrophobic surface is discussed. The decoration of the roughness amplified hydrophobic surface with electrical stimuli responsive conducting polymer (P3MeT) was described. Surface characterization was performed using scanning probe microscopy and FTIR. Stop-go fluidic operations were demonstrated in a microfluidic system incorporating the SMART valve. The key physicochemical change during the stop/go fluidic operation is superhydrophobic to superhydrophilic conversion corresponding to the neutral and oxidized forms of P3MeT film respectively as shown in Scheme 1. This simple and inexpensive method of fabricating surfaces with tunable wettability is effectively applied for stop-go fluidic operations in microfluidic systems. The simplicity of operation, low voltage and the versatility of the screen-printed carbon including the simplicity for mass production ensure wider applicability of our result.
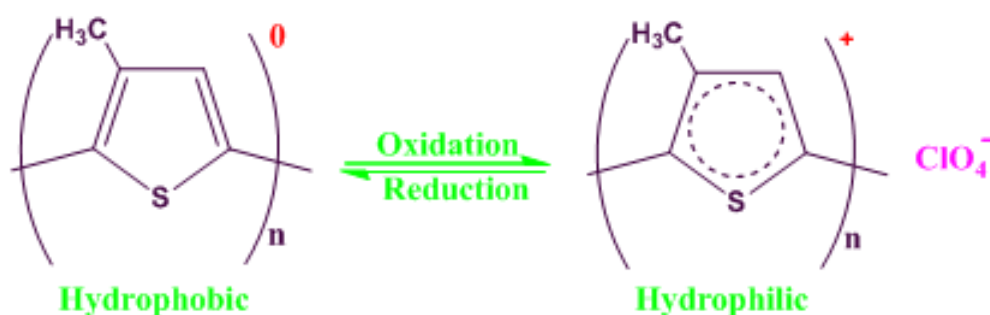
Scheme 1. Reversibly switching wettability of poly (3-methylthiophene)

2. Experimental

Materials and equipments

All the chemicals including 3-methylthiophene, LiClO$_4$, acetonitrile (CH$_3$CN), and N, N-dimethylformamide (DMF) were obtained from Sigma Aldrich. Distilled and de-ionized water (PURELAB UHQ II, ELGA) was used throughout the study. The substrate for printing was a polyester (PET) film with a thickness of 175 μm provided by ThyssenKrupp Plastic Iberica S.A. (Spain). The screen-printing apparatus used was DEK-248 (DEK International) equipped with a DEK Align 4 vision module (a two-point optical alignment system). The screen of a polyester mesh 305 (120/34), with an emulsion thickness of 13 μm was designed in-house and manufactured by DEK International (France). The squeegee used was made of polyurethane and provided by DEK International (model SQA152 with a contact angle of 45^0 and a hardness factor of 70). The inks (7102 conductor paste based on carbon and 5064 conductor paste based on silver) were provided by DuPont Ltd. (UK). The oven used for curing/ drying purposes was a Digiheat 150L oven provided by JP Selecta S.A, Spain.

Fabrication and characterization of SMART superhydrophobic surface

The printing was performed according to the procedure reported previously by our group.[49] The thickness (7.5 μm) of the SPCE film was measured using a Mitutoyo SJ-301 profilometer and the data received were analyzed with the software SURFPAK-SJ Version 1.401 (Mitutoyo Messgerate GmbH, Japan). Electropolymerization involved a prior activation and enhancement of the roughness of screen printed carbon. The plastics containing several screen printed carbon/silver electrode pairs were soaked in DMF placed in a rectangular chromatographic chamber for 20 minutes to expose all the electrodes entirely to the solvent to activate and enhance the roughness of the electrodes. The solvent treated electrodes were then cured at 100 ^{0}C for 20 minutes in the oven. Then electropolymerization was performed by recording cyclic voltammetry (CV) of 4 scans in the solution of CH$_3$CN containing the monomer (0.1 M 3MeT) and 0.2 M LiClO$_4$ along with 10^{-4} M FeCl$_3$. The chemical oxidant was incorporated to enhance porosity of the polymeric film as chemical polymerization co-occurs with electropolymerization as reported in Ref. 33. A one-compartment, three-electrode electrochemical cell consisting of SPCE (previously solvent treated) as working, screen printed Ag electrode as reference and common platinum electrode as counter were employed. After the electrochemical polymerization followed by in-situ

neutralization, the film was rinsed with acetonitrile to remove excess reactants and remaining LiClO$_4$, and then dried in N$_2$ atmosphere. Electrochemical measurements were performed using an Autolab PGSTAT10 with GPES (General Purpose Electrochemical System) software.

Characterization

Wettability of the electrodes was measured by recording the contact angles using video-based optical contact angle measuring goniometer (Model: OCA 15EC, supplier: NEURTEK instruments, Spain) with a Hamilton syringe attachment. Surface morphologies of roughness amplified SPCE and P3MeT film were investigated using environmental scanning electron microscopy (FEI model QUANTA 600 manufactured by FEI (USA). Further characterization of the polymer modified surfaces was carried out through FTIR-ATR.

Construction of Microchannel and characterization of flow rate

After the electropolymerization and subjecting the polymeric film to neutralizing potential, rinsing it in CH$_3$CN followed by drying in N$_2$ flow to produce superhydrophobicity, the microchannel was constructed.
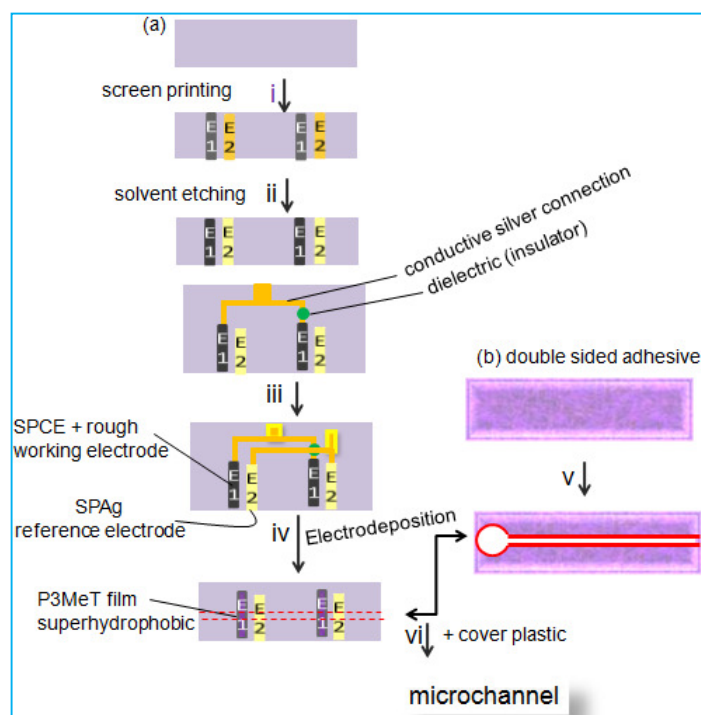

Fig. 1 Schematics of construction of microchannels incorporating SMART valves.

The microfluidic channels were fabricated by aligning and bonding two substrates, one previously patterned with the valving electrodes and the other acting as a cover via an interlayer of previously

patterned and machined double sided adhesive to form a microchannel containing the bottom wall patterned with arrays of electrodes. The double sided adhesive was patterned and machined with a *Fenix Flyer* CO_2 laser marker (Synrad) using 5 passes at 50% of power to produce *depth x width x length* = 100 μm x 500 μm x 6 cm open rectangular patterns with circular area of 12.56 mm^2 at one end to act as service port. Schematics of the steps for the fabrication of the microfluidic channel are shown in Figure 1. Flow rate in the microchannel was characterized by recording videos of flow of fluorescein dyed solution in the microchannel using a set up of LED light source, and inverted EO GigE camera interfaced with computer using a (μEye) software.

3. Results and Discussion

The fabrication of SMART superhydrophobic surface was carried out by electrodepositing electrical stimuli responsive P3MeT on previously microstructured screen printed carbon electrode surface. Fig. 2 (a) and (b) show environmental scanning electron microscopy (ESEM) image of screen printed carbon electrode (SPCE) surface and (b) that of microstructured surface obtained by subtractive etching of the former using DMF. The roughness enhancement apparent by the ESEM pictures is known to promote hydrophobicity. The water contact angles recorded on the untreated and 20 minutes DMF treated (and dried at 100^0C for 20 minutes) surfaces were 104^0 and 135^0 respectively as evident from the insets of 3 μL droplet of MQ water. The mechanism for the roughness enhancement using solvents can be explained by considering the fact that SPCE is a naturally hydrophobic (low surface energy) composite of graphite particles and organic resins as binding agents and other components for dispersion of the particles. Since not all the components dissolve in DMF, the most likely mechanism is that the solvent selectively and partially etches only the exposed soluble components (the organic resins or dispersion agents) during the controlled period of exposure. Interestingly the selective removal of nonelectroactive resins from the electrode´s surface also enhances the electrochemical performance of the electrodes by increasing graphitic loading and exposure (electrochemical accessibility) of the graphitic edges with electrocatalytic property[50] and facilitates the electropolymerization. Such strategies are amenable to the goal of producing polymers on electrode´s surface with desired tunable wettability property. The activation as well as roughness amplification strategy should not introduce nucleophilic functionalities on electrode´s surface. Functionalities as hydroxyl groups can render nucleophilic attack to the growing polymeric chain or charged intermediates of the polymerization and destroy the conjugation- the key requirement for the expected electrically tunable property of the polymer. Electrodeposition of the polymer on the microstructured

electrode´s surface was performed by cycling potential between -0.25 and 2 V at a scan rate of 50 mV/sec in a solution of 0.1 M 3-methylthiophene containing 0.2 M $LiClO_4$ and 10^{-4} M $FeCl_3$ in acetonitrile using a one-compartment three-electrode electrochemical cell consisting of SPCE (previously solvent treated) as working, screen printed Ag electrode as reference and common platinum electrode as counter to produce poly(3-methylthiophene). The CV displays broad anodic and cathodic peaks which could be due to a range of redox active species such as cation, radical, and dication of polymer.[51] As can be seen from Fig. 2 (c), the polymer exhibits a reduction peak around 0.2 V which was used as reference for neutralization. Investigation of the surface morphology of the polymer modified surface revealed a large enhancement of roughness as compared to the unmodified surfaces as can be seen in ESEM image, Figure 2 (d). The polymer modified surface display water contact angle of 154^0. Interestingly the static water contact angles were also found to decrease with increasing concentration of $LiClO_4$ solution which could be due to accumulation of the salt at the solid-liquid interface via the favorable interaction of the poorly solvated ClO_4^- with the hydrophobic porous structures.[52, 53] When using other salts (LiCl, NaCl, KCl, and $MgCl_2$), however, the water contact angle on the superhydrophobic porous surface showed slight increment as concentration increased from 0.001 to 0.1 but started to decrease gradually with further increment in concentration. The increasing order of static contact angles of 3 μL droplet of water on the superhydrophobic surface is KCl, NaCl, LiCl and $MgCl_2$ consistent with their order of free energies of interaction with hydrophobic pores.[53]
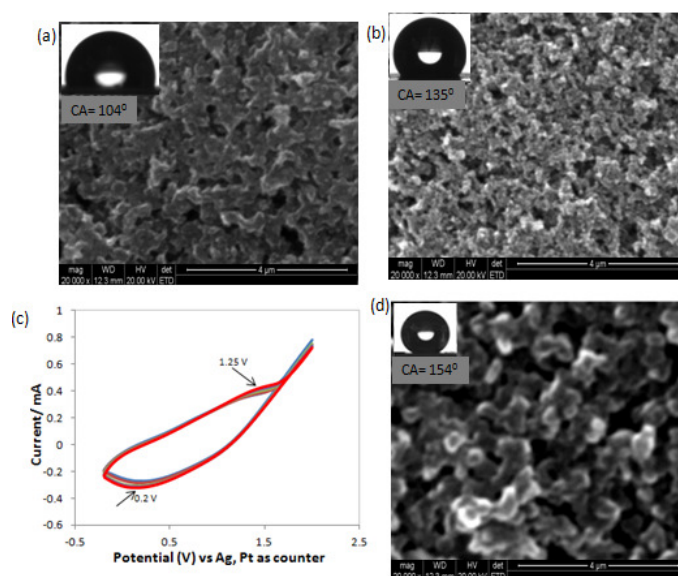

Fig. 2 (a) ESEM image of untreated screen printed carbon (CA = 104^0) and (b) ESEM image of 20 minutes DMF etched, dried at 100 ^{0}C for 20 minutes SPCE (CA = 135^0). The insets are photos of a 3 μL MQ water droplet on the corresponding surfaces. (c) Cyclic voltammetry of electropolymerization of 3-methylthiophene in 0.1 M of the monomer, 0.1 M $LiClO_4$ in CH_3CN. (d) ESEM image of electrodeposited P3MeT film (CA = 154^0) on a previously roughness amplified SPCE surface.

The presence of the polymer on electrode surface was confirmed by recording FTIR. As can be seen from Fig. 3, the FTIR of polymer modified surface exhibited characteristics peaks corresponding to P3MeT within the ranges 800-1800 and 2800-3100 cm-[1] for the so produced neutral 3-methylthiophene polymer. The FTIR spectrum was smoothed and baseline-corrected. Interestingly the FTIR of 3-methylthiophene (on SPCE surface previously DMF treated, dried, and coated with the monomer) and the P3MeT showed several peaks common to both the monomer and the polymer consistent with the literature. However, the presence of polymer on the electrode's surface was confirmed by comparison with the FTIR recorded using SPCE without any monomer or polymer as can be seen in Fig. 3.
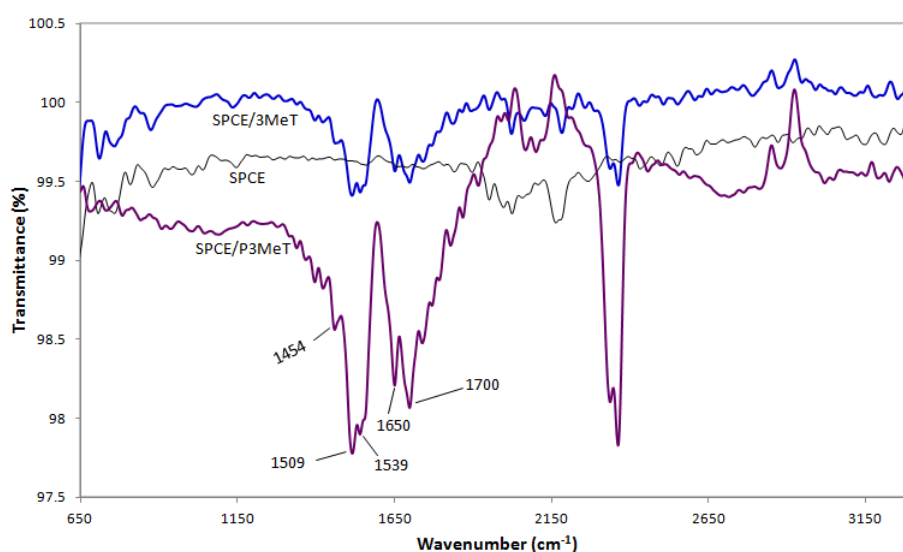

Fig. 3. FTIR spectrum of poly (3methylthiophene), unmodified SPCE surface, and a film of 3MeT dispensed on the surface of a previously solvent treated SPCE surface; the spectrum of the substrate (SPCE) was subtracted. The polymer was electrodeposited on electrode's surface from a solution of 0.1 M 3MeT, 0.2 M LiClO$_4$ containing the chemical oxidant FeCl$_3$, reduced to its neutral form, rinsed with CH$_3$CN, and dried in N$_2$ atmosphere.

Polythiophenes like other conducting polymers can be oxidized and reduced reversibly by controlling the potential. In general the oxidized polymeric films are more wettable than the neutral form. The wettability depends on the magnitude of potential applied and the nature of the dopant. On the other hand, the reversibility of potential induced wettability depends also on the mobility of the dopant (ions). The most frequently selected dopant is the perchlorate anion. This dopant can easily permeate into and out of the porous polymeric film thus facilitating the reversible wettability. When the polymer modified superhydrophobic surface was subjected to 1 V in 0.1 M LiClO$_4$, rinsed with acetonitrile and dried with N$_2$ flux, it converts into superhydrophilic. During this transformation, a contact angle change from 154^0 to 55^0 was recorded as shown in the

Fig. 4 (a). Fig. 4 (b) shows the reversible cycling of the wettability P3MeT film at neutralizing (0.2 V) and oxidizing (1V) potentials. The contact angle change, however, depends on the magnitude of potential applied and the duration of exposure. Fig. (c) shows the progressive decrease in contact angles on P3MeT as applied potential increases.
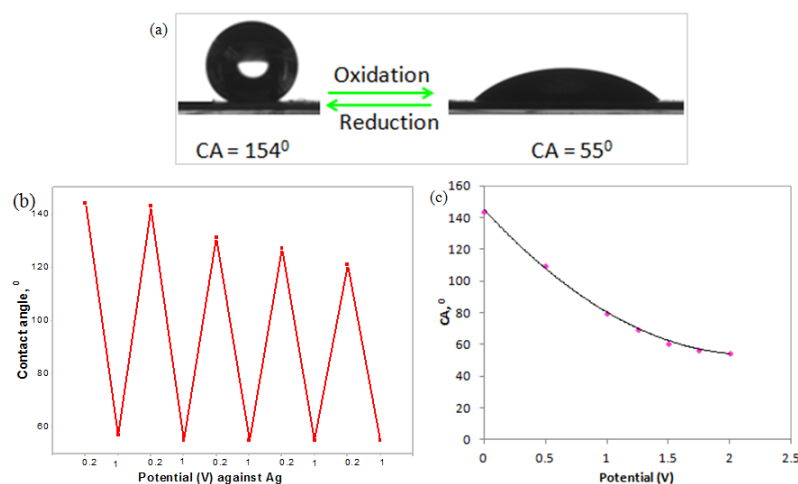

Fig. 4 (a) reversibly tunable wettability of P3MeT based superhydrophobic surface on screen printed carbon surface (b) Reversible superhydrophobic-to-superhydrophilic conversion of the porous film of P3MeT at oxidizing (1 V) and neutralizing (0.2 V) potentials (vs. Ag) in CH3CN containing 0.1 M LiClO$_4$. The contact angles correspond to a 3 L droplet of MQ water recorded after the redox process in CH$_3$CN, rinsing with CH$_3$CN followed by drying in N$_2$ flow.

Effect of type and concentration of electrolyte

The superhydrophobic-superhydrophilic reversible conversions of the P3MeT film depend critically on the type and concentration of electrolytes. Only with lower concentrations ($\leq$0.1M) of lithium perchlorate in CH$_3$CN maximum number of superhydrophobic-superhydrophilic cycling can be performed. When the concentration of LiClO$_4$ increases the reversibility of wettability conversion decreases. In 0.5 M LiClO$_4$ in CH$_3$CN solution, for instance, only two cycles of reversibility was achieved between superhydrophobic and hydrophilic. The number of reversible cycling also depends on the solvent employed. The superhydrophobic P3MeT film subjected to an oxidizing potential (1V) in aqueous solution of 0.1 M LiClO$_4$, for instance, becomes automatically superhydrophilic and didn´t become superhydrophobic again after neutralizing operation. A similar behavior was observed in aqueous solution of 0.1 M KCl. The one way superhydrophobic to superhydrophilic conversion is, however, adequate desirable operation for stop/go fluidic operations in microfluidic systems. Because such operation requires first superhydrophobic surface to stop the flow that when subjected to potential turns into superhydrophilic allowing the flow to resume.

The microfluidic device incorporating SMART stop-go valves

Having characterized the electrically tunable wettability via electrowetting on the SMART superhydrophobic electrode´s surface, two valves consisting of E1 (SMART superhydrophobic electrode) and E2 (wettable silver electrode) each were then incorporated into a capillary force operated microfluidic channel. Two main parts can be identified in this device (Fig. 5). The first is the entry part just after the service port where the relatively hydrophilic surfaces allow the liquid to penetrate the microchannel by capillary action, the second is the flow control zone where the two electrodes E2 followed by E1 were deposited in the microchannel. The flow crosses E2 by capillary action and stops at the SMART superhydrophobic E1 where the capillary pressure takes a positive value according to the Young-Laplace equation and acts as a barrier to flow. When the SMART superhydrophobic electrode is subjected to electrical signal (~1 V) the flow crosses the 1 mm hydrophobic barrier of E1 surface and reestablishes capillarity in the next zone until it encounters the second superhydrophobic surface where it stops passively and restarts only when stimulated by applied potential. The polymer based superhydrophobic surface provides a reliable stopping of the flow and allows the liquid to resume when subjected to an oxidizing potential (1V). In Fig. 5 (a-f) snapshots are shown as the fluorescein solution in 0.01 M PBS flows by capillary action in the entry zone (a), crosses the first (counter) electrode of the valving pair by capillary action (b), stopping at the SMART superhydrophobic electrode (c), flows by capillary action after crossing the valve under applied potential (d), crossing the second counter electrode by capillary action (e) and stopping at second SMART valve until stimulated to flow by electrical signal.
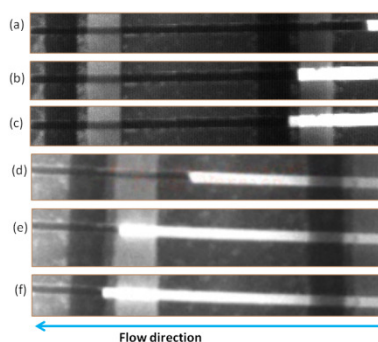

Fig. 5. Sequential stop/go fluidic operations in capillary force operated microfluidic systems. fluorescein solution in 0.01 M PBS flows by capillary action in the entry zone (a), crosses the first (counter) electrode of the valving pair by capillary action (b), stopping at the SMART superhydrophobic electrode (c), flow by capillary action after crossing the valve under applied potential (d), crossing the second counter electrode by capillary action (e) and stopping at second SMART valve until stimulated to flow by electrical signal.

Each electrode (E2 or E1) has a width corresponding to the microchannel width (500 μm) and a length of 1 mm. The separation between the two electrodes is 200 μm. Both the autonomous and potential induced flow rates depend on the channel dimension which is expected from the Washburn equation.[54] The valve performance was characterized by recording response time. It showed a positive dependence on the potential when tested in solution of 0.01 and 0.1 M KCl and 0.1 M LiClO$_4$. The response of the flow actuation was found to depend on the geometry of the microchannel. The potential-induced flow rate in the valves increases with decreasing dimensions of the microchannel. The flexibility of fabrication allowed us to incorporate multiple on-off fluidic manipulations along the microchannel by printing several pairs of the electrodes with proper treatment of the surface.

4. Conclusion

A facile approach to the fabrication of stimuli responsive superhydrophobic surface and implementation in microfluidic systems for stop/go fluidic operations was reported. Electrodeposition of conducting polymer (P3MeT) on a previously microstructured SPCE surface gave superhydrophobic surface that displays superhydrophobic-superhydrophilic reversible wettability. The extremely simple approach of enhancing the microscale roughness by just soaking in DMF followed by drying drastically reduces the cost of fabrication of superhydrophobic surfaces. While the superhydrophobicity provides passive stopping of capillary flow, the ability to convert the superhydrophobic surface wettability into superhydrophilic facilitated the low voltage actuation of the flow. Taking advantage of possibility of printing multiple electrode pairs on a plastic substrate that can be modified at the same time by the solvent treatment followed by electropolymerization allowed constructing multiple stop/go valves in microchannels. Our approach greatly simplifies system construction and assembly as the functional components are fabricated prior to channel sealing and same technique as flow actuation can be used for sensing.

Acknowledgements

References

[1] L. Santiago, D. Bejarano, P. Lozano, I. Katakis, Analyst 135 (2010) 1276. D.

[2] D. Mata, D. Bejarano, M. L. Botero, P. Lozano, M. Constantí, and I. Katakis, *Electrochim. Acta* 2010, 55, 4261–4266.

[3] G. Vladimir, L. F. Harris, A. J. Ricco, M. X. Tan, and D. E. Williams, *Anal. Chem.* 2012, 84, 487–515.

[4] L. Gervais, N. de Rooij , and E. Delamarche, *Adv. Mater.* 2011, 23, 151–176.

[5] T. J. Clark, P. H. McPherson, and K. F. Buechler, *Point of Care* 2002, 1, 42–46.

[6] S. Choi, M. Goryll, L. Y. M. Sin, P. K. Wong, J. Chae, Microfluid Nanofluid (2011) 10:231–247.

[7] C. D. Chin, V. Linder and S. K. Sia, *Lab Chip* 2012, 12, 2118–2134.

[8] D. Juncker, H. Schmid, U. Drechsler, H. Wolf, M. Wolf, B. Michel, N. Rooij, and E. Delamarche, *Anal. Chem.* 2002, 74, 6139-6144

[9] L. Gervais, E. Delamarche, Lab Chip 9 (2009) 3330–3337.

[10] Z. Nie, F. Deiss, X. Liu, O. Akbulut and G. M. Whitesides, Lab Chip, 2010, 10, 3163–3169.

[11] A. W. Martinez, S. T. Phillips, Z. Nie, C.-M. Cheng, E. Carrilho, B. J. Wiley, and G. M. Whitesides, Lab Chip, 2010, 10, 2499–2504.

[12] Z. Nie, C. A. Nijhuis, J. Gong, X. Chen, A. Kumachev, A. W. Martinez, M. Narovlyanskya and G. M. Whitesides, Lab Chip, 2010, 10, 477–483.

[13] H. Hisamoto, Y. Nakashima, C. Kitamura, S. Funano, M. Yasuoka, K. Morishima, Y. Kikutani, T. Kitamori, and S. Terabe, Anal. Chem. 2004, 76, 3222-3228.

[14] K. W Oh, and C. H Ahn, J. Micromech. Microeng. 16 (2006) R13–R39

[15] A. K. Au, H. Lai, B. R. Utela and A. Folch, *Micromachines* 2011, *2*, 179-220.

[16] Beebe D J, Moore J S, Bauer J M, Yu Q, Liu R H, Devadoss C and Jo B H 2000 *Nature* 404 588–90

[17] Liu R, Yu Q and Beebe D J 2002 *J. Microelectromech. Syst.* 11 45–53

[18] Harmon, M.E., Tang, M. & Frank, C.W. (2003). *Polymer*, Vol. 44, No. 16, pp. 4547-4556.

[19] Harmon, M.E., Tang, M. & Frank, C.W. (2003). *Polymer*, Vol. 44, No. 16, pp. 4547-4556.

[20] Richter A, Kuckling D, Howitz S, Gehring T and Arndt K-F 2003 *J. Microelectromech. Syst.* 12 748–53.

[21] Suk J. W., Cho J.-H., J. Micromech. Microeng. 2007, 17, N11-N15.

[22] Zimmermann M., Delamarche E., Wolf M., Hunziker P. *Biomed. Microdevices* **2005**, *7*, 99–110.

[23] Rossier J. S., Gokulrangan G., Girault H. H., Svojanovsky S., Wilson G. S. *Langmuir* **2000**, 16, 8489.

[24] Duffy, D.C., Gillis H. L., Lin J., Sheppard N. F., Jr., Kellogg G. J., Anal. Chem. 1999, 71, 4669-4678.

[25] Park J., Sunkara V., Kim T.-H., Hwang H., Cho Y.-K., Anal. Chem. 2012, 84, 2133–2140.

[26] Gustafsson, M., Hirschberg D., Palmberg C., Jornvall H., Bergman T., Anal. Chem. 2004, 76, 345-350.

[27] Chen, J.M.; Huang, P.C.; Lin, M.G. *Microfluid. Nanofluid.* 2008, *4*, 427-437.

[28] Zimmermann M., Hunziker P., Delamarche E., Microfluid Nanofluid 2008, 5, 395-402.

[29] Bingwei Xin and Jingcheng Hao Chem. Soc. Rev., 2010, 39, 769–782

[30] A. Chunder, K. Etcheverry, G. Londe, H. J. Cho, and L. Zhai, *Colloids Surf., A* 2009, 333, 187–193.

[31] G. Chen, F. Svec and D. R. Knapp, *Lab Chip*, Vol. 8, No. 7, pp. 1198-1204.

[32] Go Takei, Mari Nonogi, Akihide Hibara, Takehiko Kitamori and Haeng-Boo Kim Lab Chip, 2007, 7, 596–602.

[33] Prins M. W. J., Welters W. J. J., Weekamp J. W., Science 2001, 291, 277-280.

[34] Cheng J.-Y., Hsiung L.-C., Biomedical microdevices 2004, 6, 341-347.

[35] L. Xu, W. Chen, A. Mulchandani, and Y. Yan, Angew. Chem. Int. Ed. 2005, 44, 6009 –6012.

[36] G. Kousik, S. Pitchumani, N. G. Renganathan, Prog. Org. Coat. 2001, 43, 286 – 291.

[37] H. H. Kuhn, A. D. Child, W. C. Kimbrell, Synth. Met. 1995, 71, 2139 – 2142.

[38] D. Mecerreyes, V. Alvaro, I. Cantero, M. Bengoetxea, P. A. Calvo, H. Grande, J. Rodriguez, J. A. Pomposo, Adv. Mater. 2002, 14, 749 – 752.

[39] A. Azioune, M. M. Chehimi, B. Miksa, T. Basinska, S. Slomkowski, Langmuir 2002, 18, 1150 – 1156.

[40] J. Y. Wong, R. Langer, D. E. Ingber, Proc. Natl. Acad. Sci. USA 1994, 91, 3201 – 3204.

[41] W. Barthlott, C. Neinhuis, *Planta* 1997, *202*, 1.

[42] H. J. Ensikat, P. Ditsche-Kuru, C. Neinhuis, W. Barthlott, *Beilstein J. Nanotechnol.* 2011, *2,* 152–161.

[43] L. Feng, S. Li, Y. Li, H. Li, L. Zhang, J. Zhai, Y. Song, B. Liu, L. Jiang, D. Zhu, *Adv. Mater.* 2002, *14*, 1857.

[44] X.-M. Li, D. Reinhoudt, M. Crego-Calama, Chem. Soc. Rev., 2007, 36, 1350–1368.

[45] G. McHale, N. J. Shirtcliffe, M. I. Newton, *Analyst,* 2004, 129, 284-287.

[46] M. Ma, R. M. Hill, Current Opinion in Colloid & Interface Science 11 (2006) 193–202.

[47] Nicholas L. Abbott, Christopher B. Gorman, and George M. Whitesides *Langmuir 1995,11,* 16-18

[48] Peng Lin, Feng Yan,* and Helen L. W. Chan Langmuir 2009, 25(13), 7465–7470.

[49] D. Bejarano, P. Lozano, D. Mata, S. Cito, M. Constanti, I. Katakis, *J. Micromech. Microeng.* 2009, *19*, 115007.

[50] Alemayehu P. Washea, Pablo Lozano-Sánchez, Diego Bejarano-Nosas, Ioanis Katakis, Electrochemical Acta 91 (2013) 166– 172.

[51] D. Singh, S. Dubey, B.M. Prasad and R.A. Mısra, *J. Appl. Polym. Sci.,* 73 (1999) 91)

[51] B. Xin, and J. Hao, *Chem. Soc. Rev.* 2010, 39, 769–782.

[53] J. Dzubiella, and J.-P. Hansen, *J. Chem. Phys.* 2005, 122, 234706.

[54] Y. Zhu, K. Petkovic-Duran, *Microfluid Nanofluid* 2010, *8*, 275-282.

CHAPTER 3

CHAPTER 3

ELECTROCHEMICALLY ACTUATED STOP-GO VALVES FOR CAPILLARY FORCE-OPERATED DIAGNOSTIC MICROSYSTEMS

Alemayehu P. Washe,[a] P. Lozano,[b] D. Bejarano,[a] and Ioanis Katakis*[a]

[a] Bioengineering and Bioelectrochemistry Group, Department of Chemical Engineering,

Universitat Rovira i Virgili, Avinguda Països Catalans, 26, 43007, Tarragona, Spain

[b] Current address: Integrated Microsystems for the Quality of Life S.L., C/del Ferro 6, Nave 7, 43006 Tarragona, Spain

*Corresponding author: Tel. +34 977 55 96 55, Fax + 34 977 55 96 21, E-mail: ioanis.katakis@urv.cat

(This work is dedicated to Professor Adam Heller on the occasion of his 80th birthday)

ABSTRACT

Lateral flow immunosensing devices continue to be the most successful commercial realization of analytical microdevices. They owe their success to their simplicity that significantly depends on the capillary-driven flow and versatile technological platform that lends itself to fast and low cost product development. In order to compete with such a convenient product microsystems can benefit from simple to operate fluid manipulation. We show that capillary-driven flow in microchannels can be manipulated with electrochemically activated valves with no moving parts. These valves consist of screen printed electrode pairs that are transversal to the flow. One of the electrodes is solvent-etched to produce a superhydrophobic surface that provides passive stopping and facilitate low voltage (~1V) actuation of the flow via electrowetting. The operation of such valves in the stop/go mode with response time between 2 and 45 sec depending on the type and concentration of salt is demonstrated. Mechanistic invetsigation indicated that the response depends on at least three phenomena that contribute to electrocapillarity: the electrochemical double layer capacitance, specific counterion adsorption, and possibly electrohydrodynamic effects.

1. Introduction

There is a growing demand for simple, easy to use and operate, low-cost, fast-responding, and portable devices for semiquantitative analysis with applications in Point of Care (POC) diagnostics, food safety, and environmental monitoring. As a result, great interest has been shown for the development of analytical microsystems.[1-3] Microsystems have advantages resulting from miniaturization, including use of very small volume of samples and reagents, less waste, short analysis time, portability and improved analytical separation and sensitivity. However, operation of microsystems require fluidic manipulations and integration of all the analytical procedures including sampling, transport, mixing, incubation, reaction and analysis on the microfluidic device. Despite great advances in microfabrication and instrumentation, the most successful commercially portable food analysis and POC diagnostic devices are still lateral flow devices, and more specifically, lateral flow immunoassays (LFIA).[4-6] This success is probably due to the

foolproof operation, low cost, and short development time required for development of products based on this platform. Although microsystems are expected to overcome some intrinsic limitations[7] of LFIAs such as low sensitivity and difficulty of quantitative testing, the 3-dimensional nature of their porous membrane bestows special advantage to LFIAs; it not only allows slow passive/capillary movement of the liquid, but also facilitates separation, mixing, interaction and detection. When trying to transform such assays into a microfluidic channel, challenges resulting from the laminar behavior of microscale flows have to be overcome and fluid movement has to be induced, usually by means of external gradients that require coupling with instruments that eventually counter many of the portability, low cost, easy operation advantages of analytical microsystems.

We are therefore interested in platforms that allow effortless fluid movement and control in simple microfluidic devices. Such microfluidic immunoassays most probably should mimic LFIAs exploiting capillary phenomena for sample movement. In such an integrated device immunochemical reagents are previously deposited in the microchannel and, as the solution containing the analyte is introduced, undergo dissolution, mixing, and reaction with the analyte yielding an immunocomplex that is detected at the detector located downstream.[8-12] Both theoretical and experimental works have indicated the stringent dependence of sensitivity of such immunoassays on the flow rate in the microchannel.[10, 13-17] Variations in either wettability or geometry of the microchannel have been used as delay[4,8] valves for flow control. Delay valves, although can be effective with high affinity reaction that require no longer than a minute of incubation, are not versatile and may not be reliable due to the heterogeneous nature of most surfaces. In addition, slow dissolution and mixing in the laminar regime most likely obliges to complete stopping of the flow. Thus a precise control over flow rates including stopping and restarting in microfluidic devices should provide a flexible tool that allows versatility in the development of products based on such a platform.

Passive stop valves coupled to a fast actuation mechanism provide attractive avenue for flow control in capillary force-operated diagnostic microsystems. A large variety of valve specific actuation methods including magnetic, pneumatic, piezoelectric, electrostatic, and bimorph have been reported for miniaturized microvalves.[18] However, these solutions require mechanical operations with moving parts and bulky peripherals that limit miniaturization. On the other hand, the dependence of microscale flow on interfacial energy has been used for on-chip actuation of

flow because interfacial energy can be modulated by electrical[19] photochemical,[20] thermal,[21] or electrochemical methods.[22]

We are particularly interested in electrically-driven solutions because we develop electrochemical sensors for the downstream detection and quantification of analytes; since a hand held potentiostat will invariably be used for reading, the same instrument could be programmed to operate such passive valves. Unlike other methods, electrical control of interfacial energy (electrowetting) has advantages including miniaturizability, simplicity and absence of moving parts. In addition to electrowetting on electrode in direct contact with electrolyte electrowetting on dielectric (EWOD) has been investigated as a method to avoid problems of electrolysis-possible scenario in direct electrowetting. Notwithstanding remarkable improvements and applications, however, EWOD often requires high voltage and suffers joule heating, contact angle saturation and dielectric break down.[23, 24] Unlike smooth surfaces which can provide only small range of contact angle changes, special attention has been given to electrowetting on superhydrophobic nanoporous surfaces.[25-32] When a droplet of electrolytic liquid is placed over superhydrophobic electrode surface, the droplet levitates on the top of the asperities due to air trapped in the pores.[33] Application of a critical low voltage (V_c)[34] across this electrode-electrolyte interface could enhance the surface charge and lead to modulation of interfacial energy resulting in the wettability transition[25-32] from a relatively less stable Cassie-Baxter regime[35-37] to Wenzel regime;[38] then a complete wetting can be achieved when the potential is increased above V_c. When the superhydrophobic porous graphitic surface is incorporated into a microchannel it was envisaged that the surface could provide not only passive stopping of the flow (in absence of potential) but also a low voltage actuation of the flow.

In this work we demonstrate that taking advantage of the superhydrophobic porous graphitic carbon, we can induce multiple stop/go operations of the flow in a microfluidic system. The large potential window of the electrode material and its intrinsic charge accumulation capacity[39] facilitate the wettability transition and hence the flow actuation at extremely low voltage. We also report on our efforts to characterize and rationalize the behavior of these superhydrophobic, potential-activated valves, especially by varying the type and ionic strength of the fluid supporting electrolytes. The reported scheme is directly applicable to capillary force operated diagnostic microsystems, particularly to those that mimic LFIAs. The deposition of electrode arrays (valves) on a plastic substrate was performed using a low cost and versatile thick film technology (screen printing).[40] The superhydrophobic surface on electrode material was fabricated by selective and

controlled solvent etching of the screen printed carbon (SPC) electrodes. Surface characterization was performed using scanning probe microscopy. The electrochemical characteristics of the electrode and the wettability transitions were studied using electrochemical impedance spectroscopy. Porosity was further characterized using BET (Brunauer, Emmett and Teller) method. Mechanistic insights regarding effect of concentration and type of electrolytes on the flow actuation were gathered through in situ electrowetting experiments. Flow rates in the microchannel were characterized by recording videos of the meniscus position in the presence and absence of potential.
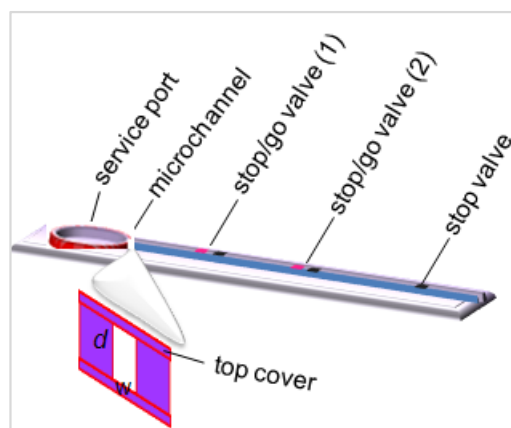

Figure 1. Schematic view of the capillary force operated microsystem incorporating stop/go valves developed in current work. The device has a service port where sample liquid is pipetted; three valves-two stop/go and the third just stop valve incorporated along fluidics to perform sequential flow control operations.

Figure 1 shows a schematic view of the capillary force operated microsystem incorporating stop/go valves developed in this work. The device has a service port where sample liquid is pipetted, three valves (two stop/go and the third just stop valve) to perform sequential stop/go operations. The zone before the first valve can be used for immunochemical deposition and the zone between the first stop/go and second stop/go valves can be dedicated for the detection. The zone between the second stop/go valve and just stop valve can be dedicated for control test. The valving operation is compatible to any assay that involves aqueous electrolytes including colorimetric or optical but is particularly attractive for electrochemical detections where the same technique of valve operation is used for detection.

2. Theoretical Background

Laminar flow in a horizontal microchannel depends on the geometry and wettability of the microchannel surfaces. As the liquid wets the dry part of the microchannel it overcomes the Gibbs free energy cost corresponding to change in interfacial area:

$$dG = (\gamma_{SL} - \gamma_S)dA_{SL} + \gamma_L dA_L \ldots\ldots\ldots. (1)$$

For equilibrium condition, dG = 0, equation 1 can be rearranged to Young´s equation:

$$\gamma_S = \gamma_{SL} + \gamma_L Cos\theta_0 \ldots\ldots\ldots. (2)$$

Where γ_S, γ_{SL}, and γ_L are the interfacial energies at the solid-vapor, solid-liquid, and liquid-vapor interfaces respectively. $Cos\theta_0$ is the cosine of the contact angle that the liquid-vapor interface forms with the solid-liquid interface. The contact angle provides a measure of the wettability of a surface. Capillary flow is driven by capillary pressure which is related to the geometry and wettability of the microchannel as given by Young-Laplace equation; which for a rectangular[41] microchannel of width (w) and depth (d) is:

$$P_c = \gamma_L \left(\frac{Cos\theta_b + Cos\theta_t}{d} + \frac{Cos\theta_l + Cos\theta_r}{w} \right) \ldots\ldots\ldots. (3)$$

where P_c is the capillary pressure that drives capillary flow, γ_L is liquid-air interfacial energy, $\theta_{b,t,l,r}$ are the contact angles of the liquid on the bottom, top, left, and right channel wall surfaces, respectively. Modulation of the interfacial energy of a system consisting of an electrolyte and the other immiscible phases (solid and vapor) in contact to each other is related to interfacial excess by the Gibbs adsorption isotherm; which at constant temperature is given by:

$$d\gamma = -\sum \Gamma_i d\mu_i \ldots\ldots\ldots. (4)$$

where γ is the interfacial energy of two immiscible phases, μ_i is the chemical potential (partial molar free energy at constant temperature and pressure) of a component x_i, Γ_i is the excess of that component at the interface, in moles per unit area of interface. Γ_i may take positive or negative values corresponding to positive or negative adsorption respectively and dictates the effect of type and concentration of added salt on the interfacial energy. On the other hand, it is well known that charges on electrode surface form an electrical double layer (EDL) with counter ions from the solution. Considering the EDL as a parallel plate capacitor, Lippmann[42] developed an electrocapillarity (electrowetting) equation:

$$(\partial\gamma/\partial V)_{\mu,P,T} = -\sigma \ldots\ldots\ldots. (5)$$

where σ is the surface charge density of the counter-ions at applied potential V. Equation (5) can be extended to the well-known Lippmann–Young[24] equation:

$$Cos\,\theta(V) = Cos\,\theta_0 + \frac{\varepsilon_0\,\varepsilon V^2}{2\lambda\gamma_L} \dots\dots (6)$$

Where λ is the Debye length, ε_0, and ε are the dielectric permittivity of vacuum and water respectively. Equation (6) has been used to describe electrowetting phenomena in microchannels. The above theories are mainly based on the Young´s equation that is a thermodynamic description of the wettability of smooth surfaces. For rough surfaces, the Wenzel[39] and Cassie-Baxter[38] models should be considered. The Wenzel model introduces a roughness factor ´R´ to account for the effect of roughness on contact angle. Accordingly the effective contact angle is given by:

$$Cos\,\theta = RCos\,\theta_0 \dots\dots (7)$$

For smooth surface R = 1, and $\cos\theta = \cos\theta_0$. When the surface is highly rough and porous, due to the air trapped in the pores a composite interface of solid-liquid and liquid-vapor can be imagined beneath a liquid droplet resting on such surface. On such surface the droplet levitates on the top of the asperities and the liquid partially contacts the area beneath it leaving open air spaces. The contact angles on such surfaces are usually above 150^0, in which case the surface is classified as superhydrophobic. Taking into account both the roughness and open air space at the composite interface of the superhydrophobic surface, thus, the contact angle is given by: [43]

$$Cos\,\theta = Rf_1 Cos\,\theta_0 - f_2 \dots\dots (8)$$

Where f_1 is the total area of solid–liquid interface and f_2 is the total area of liquid–air interface beneath the droplet. The wettability transition from the Cassie-Baxter to Wenzel state can lead to increased area of solid-liquid by the expense of liquid-vapor interfaces beneath the liquid. Due to the metastable nature of the Cassie state of the droplet, a low voltage transition to Wenzel regime is expected to yield large changes in contact angles. The corresponding change in capillary pressure is expected to facilitate flow actuation in microchannels at low voltage.

3. Results and Discussion

Superhydrophobic nanoporous electrode: characterization

The superhydrophobic surface is produced by increasing the roughness/porosity of a low surface energy composite material. Screen printed carbon is a naturally hydrophobic (low surface energy) composite of graphite particles and organic resins as binding agents and other components for dispersion of the particles. Since not all the components can dissolve in a selective solvent, etching of the surface with the solvent can promote hydrophobicity through amplification of the roughness.[44-46] Figure 2 (a) shows an environmental scanning electron microscopy (ESEM) image of a naturally hydrophobic screen printed carbon (SPC) surface and (b) shows that of the

superhydrophobic porous surface obtained by the solvent etching of the former using DMF. The water contact angles (CA) recorded on the untreated and treated surfaces were 104^0 and 151^0 respectively. The level of roughness and nature of the porosity varies with duration of exposure to the solvent. It was found that the contact angle increases with increasing duration of exposure in the solvent reaching a plateau after 40 minutes.
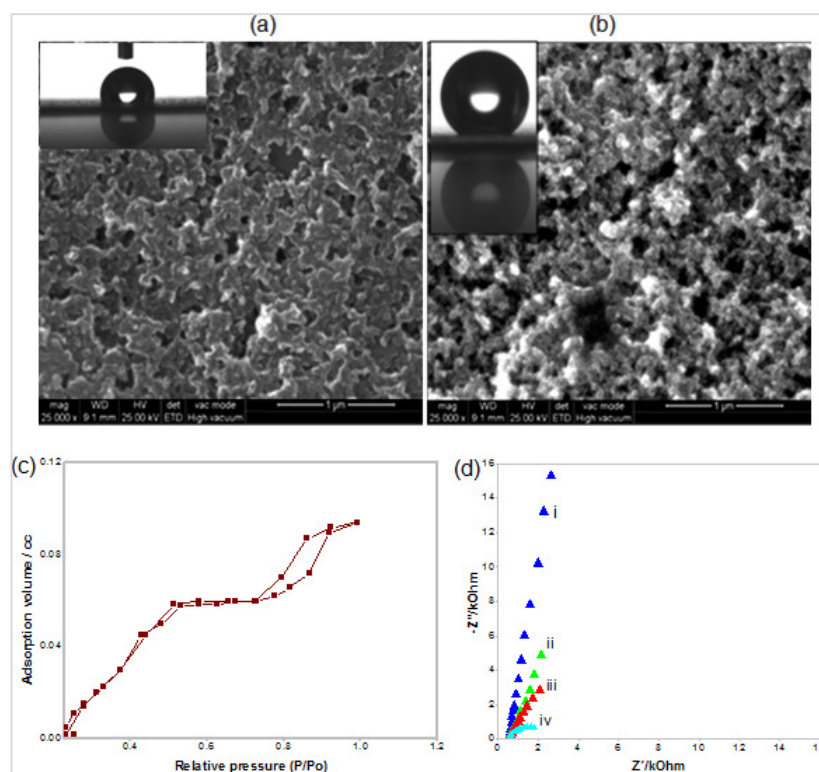

Figure 2. (a) ESEM image of naturally hydrophobic screen printed carbon (CA = 104^0 left) and (b) ESEM image of superhydrophobic (CA = 151^0 right). The insets are photos of a 3 μL MQ water droplet on the corresponding surfaces. (c) Nitrogen adsorption-desorption isotherm of mesoporous solvent etched SPCE surface. (d) Nyquist impedance plot of the superhydrophobic nanoporous carbon electrode recorded in same solution of 0.5 M $LiClO_4$ by varying E_{dc} (= 0.5 (i), 0.8 (ii), 1 (iii), and 1.5 V (iv) with all other conditions remained the same; frequency range 100 kHz to 0.1 Hz, ΔE_{ac} = 10 mV.

BET surface area analysis using nitrogen adsorption-desorption experiments on the superhydrophobic surface (CA=151^0) obtained after 40 minutes of exposure to DMF followed by 20 minutes drying at 100 ^{0}C, yielded a type-IV curve (Figure 2c), with a slight hysteresis loop at relative pressures (P/P0) about 0.8 which is indicative of the predominant contribution of mesoporous structures (2 to 50 nm) to the adsorption isotherm.[47-49] Figure 2 (d) shows a Nyquist plot of the impedance recorded in 0.5 M $LiClO_4$ under varying E_{dc} (0.5 up to 1.0 V) keeping all other experimental conditions the same (amplitude of excitation 10 mV in the frequency range 100 kHz-0.1 Hz) using the superhydrophobic nanoporous electrode as working, the untreated screen

printed electrode as reference and a platinum rod as counter. The impedance revealed a nearly vertical line reflecting a predominant capacitive behavior of the porous electrode at V≤1. The progressive decrease in phase angle as E_{dc} was increased from 0.5 V up to 1 V clearly suggests enhanced finite diffusion of ions in the porous structures as they become more accessible to the liquid via electrowetting. The EIS results reinforce the expected electrowetting transition of the interface from the less wetted Cassie-Baxter regime to more wetted Wenzel regime that occurs, in this case, at a critical low voltage $V_c = 1V$.

Electrowetting on superhydrophobic nanoporous electrode

In order to verify the facile wettability changes on the superhydrophobic nanoporous carbon electrode at applied potential, in situ electrowetting experiments were performed. Some judiciously selected salts with varying concentrations were investigated for ion specific effects to decipher the mechanism. Figure 3 (a) shows the set up of the in-situ electrowetting experiment where a droplet of a liquid is in direct contact with the two electrodes, E1 and E2: E1 is the DMF modified superhydrophobic porous electrode and E2 is the unmodified SPCE. The contact angles before and after application of a potential at E1 was recorded. Figure 3 (b) shows the recorded contact angles against applied potentials in KCl solutions. The curves correspond to concentrations: 0.01, 0.1 0.5 and 1 M of KCl from bottom to top respectively. Each point in the curve corresponds to the mean of at least three repetitions. It can be seen from the Figure that as the concentration of KCl increases the potential-induced change in contact angle decreases. The observed trends are the same for other tested salts: LiCl, NaCl, $MgCl_2$, and phosphate buffer saline (PBS) solution-a common electrolyte used to simulate physiological sample matrices in miniaturized microfluidic systems. The decreasing order of recorded change in contact angle at 1 V in 0.01 N is: KCl > NaCl > LiCl > $MgCl_2$. Among the tested salts $MgCl_2$ showed significantly reduced CA changes at a given potential and ionic strength as compared to the monovalent salts. These results are consistent with the fact that the screening (of the electric field) length around an ion depends on the local concentration of ions which is given by the Debye length.[50] The other interesting observation is the relatively larger change in CA at negative applied potential as compared to that when positive potential is applied. This leads us to believe that in addition to the screening effect, the potential-induced electrowetting effect also depends on specific adsorption.[51] The higher potential requirement to induce a given change in CA at a positive potential as compared to when negative potential is applied, reflects specific adsorption of cations on the surface. This hypothesis is reinforced by the results obtained with $MgCl_2$: during adsorption

on a surface, the ion may have to shed some of its hydration shell a process whose free energy varies with ion solvation.[52] The relatively high free energy of solvation of the highly charged, small sized Mg^{+2} makes it less prone to desolvation when potential is applied, leading to less pronounced CA changes when compared to the CA change of the less solvated ions. The larger effect of negative potential than positive on CA may also be attributed the nature of surface charges, most likely negative charges, on the so printed screen printed carbon. Such charges are related to zeta potential and could arise, among others, due to dissociation of surface moities such as amines or carboxyls. Anticipating the effect of zeta potential on the wettability-swtiching potential and vice versa, we performed elemental analysis using ESEM to examine significant presence of such functionalities as amines or carboxyl groups on electrode´s surface. Our results indicated the % of nitrogen and oxygen go way down to be ignored effectively and % of carbon way up consistent with the recorded superhydrophobicity of the solvent etched surface suggesting that the role of zeta potential of moieties on the surface not very significant. However, a determination of the zeta potential of the surface might be necessary to rule out purely surface effects on the observed switching.

 The large changes in contact angles at such low potentials are probably due to the electrowetting transition from the less stable Cassie Baxter to Wenzel regime on the superhydrophobic porous surface. If this is so, solutions of $LiClO_4$ whose poorly solvated ClO_4^- has hydrophobic character[53] should give larger contact angle changes relative to the other tested salts at a given ionic strength and potential. As can be seen in Figure 3c, indeed this result was obtained with $LiClO_4$: not only larger contact angle changes are observed, but also they seem to be symmetric with respect to the sign of potential. Interestingly, the potential-induced changes in contact angle increases with both concentration and potential in $LiClO_4$ solution. These results seem to contradict the expectation; since the Debye length is expected to decrease with increasing concentration of ions, reduced changes in contact angle can be expected as concentration increases. Both trends in the results can be explained considering the mobility and permeation capability of Li^+ and ClO_4^- ions into the hydrophobic porous film instead as the principal effect of the Debye-length effect of the more hydrophilic ions. In other words, the adsorption effect overcomes in importance the EDL effect in the case of $LiClO_4$.

Such facile movement of ions into and out of the porous film has been the key factor in the electrically tunable wettability of some porous films of conducting polymers.[53] The permeation ability of ions into a porous matrix is a function of interrelated parameters: size, charge, forces of

interaction with the solid surface, and free energy of solvation[52] and therefore difficult to quantify. Still, some general trends are clearly observed and give support to our hypothesis: the ClO_4^- which is poorly solvated and interacts effectively with the hydrophobic surface can easily permeate into the hydrophobic pores and thus an increased adsorption with increasing concentration is expected in accordance with Gibbs adsorption isotherms. The other interesting phenomena observed when using $LiClO_4$ was a complete spreading of the droplet as the potential is increased above a certain potential at which a large change in contact angle was observed. This large change in contact angle is expected to correspond to the expected facile transition from superhydrophobic Cassie-Baxter to complete wetting through the Wenzel regime as ions permeate into the grooves.
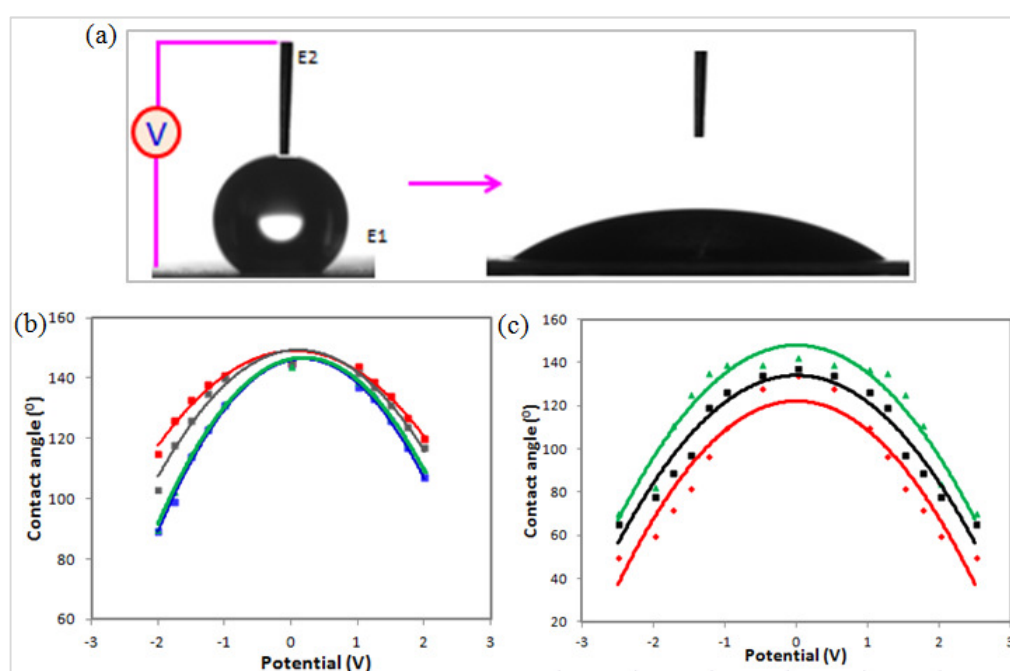

Figure 3 (a) A 3 μL droplet of aqueous solution of 0.1 M KCl in contact with E1 (superhydrophobic nanoporous electrode) and E2 just SPC representing the experimental set up and typical changes in contact angles as potential is applied at E1. Figure (b) and (c) shows contact angle as a function of applied potential obtained by applying a potential at E1 in KCl and $LiClO_4$ of different concentrations respectively. The curves in Figure (b) correspond to 0.1, 0.5 and 1 M of KCl from bottom to top respectively. Those in Figure 2 (c) correspond to 1, 0.5 and 0.1 M of $LiClO_4$ from bottom to top respectively.

Figure 4 (a) shows image of a 3 μL droplet of 0.01 M PBS placed between coplanar electrodes: E1 and E2 of pitch of separation 200 μm. The electrodes were previously deposited on a poly (ethylene terephthalate) substrate by screen printing and then modified with the solvent to produce the required hydrophobicity and porosity. When a potential ≤ -1 V was applied at E1 against E2 for 10 seconds, the liquid began to expand and wetted the dry zones of the electrodes. Interestingly

the droplet deforms and advances towards the negatively polarized electrode. This phenomenon is consistent with the above results and reported works.[54]
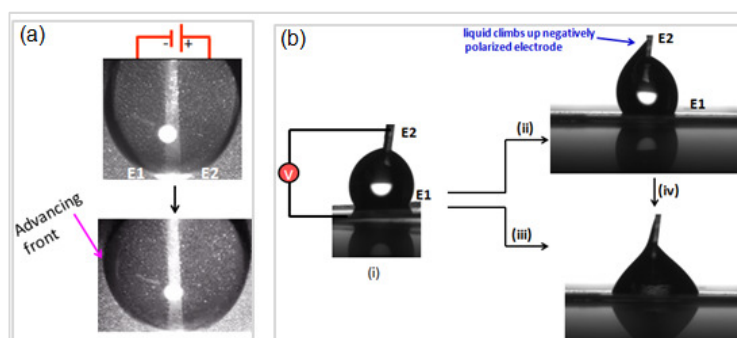

Figure 4 (a) shows image of a 3 µL droplet of 0.01 M PBS placed between E1 and E2 of pitch 200 µm advancing toward a negatively polarized (E1) electrode. (b) Shows set up of 3 µL droplet of 0.1 M KSCN solution on the superhydrophobic (E1) electrode and contacting counter electrode (E2) (i); the directional effect of potential induced flow of 0.1 M KSCN solution when E1 is positively biased against E2; the droplet starts to climb up the negatively polarized electrode-E2 (ii). When E1 is negatively biased against E2 the droplet spreads on E1 surface (iii). The liquid climbing up E2 can be made to spread on E1 by changing the direction of polarity (iv).

From these results it is difficult to ascribe the contact angle changes as the only cause of bulk flow; other possible forces such as electrohydrodynamic[55-58] and Marangoni effects could also contribute to flow actuation when the valving electrodes are placed in such close proximity. Marangoni effects are expected to arise when there is a non uniform distribution of counter ions of opposite effect on interfacial tension as determined by their position in the *Hofmeister series* at electrodes in close proximity. In order to confirm this we further considered KSCN, a salt whose cation and anion belong to the extremes of the Hofmeister series-structure forming and structure breaking respectively. This liquid "climbs up" the negatively polarized electrode as shown in Figure 4b, i.e when a positive potential is applied at E1 or alternatively a negative potential at E2. This dramatic movement is more observable with KSCN than KCl as expected. However, with LiClO$_4$ there was not any observable directionality as the driving force, in this case, is the affinity adsorption of ClO4$^-$ to hydrophobic porous matrix. The asymmetric chemical process across the two electrodes corresponding to preferential adsorption of ClO4$^-$ on the positively polarized superhydrophobic porous electrode and lack of counter process at the other electrode can cause concentration gradients across the closely placed electrodes giving rise to electrohydrodynamic flow.

These experiments indicate that there are at least three phenomena driving the induced electrowetting behavior observed on such superhydrophobic surfaces. The use of different electrolytes helps separate them; however an attempt to quantifiably predict the importance of

each one would require a more controlled superhydrophobic surface. Instead, we are more interested in achieving flow manipulation in a microsystem and for this reason we turned our attention to incorporating the "valves" in simple microfluidic channels as described below.

The microfluidic device incorporating stop-go valves

Having optimized the electrowetting on the electrode´s surface, two valves consisting of E1 (superhydrophobic nanoporous) and E2 (wettable) each and the third just a stop valve (E1) were then incorporated into a capillary force operated microfluidic channel. Two main parts can be identified in this device (Figure 1). The first is the entry part just after the service port where the relatively hydrophilic surfaces allows the liquid to penetrate the microchannel by capillary action, the second is the flow control zone where the two electrodes E2 followed by E1 are deposited in the microchannel. The flow crosses E2 by capillary action and stops at the superhydrophobic E1 until stimulated by applied voltage as shown in Figure 5. In this figure snapshots are shown as the fluorescein solution in 0.01 M PBS flows through the microchannel and reaches the first two zones followed by the valve activation: Figure 5(a) shows the solution at the capillary-driven flow entry part, Figure 5(b) as it stops at E1 and (c) shows the fluid crossing E1 (passive stop valve) under applied negative potential at E1 or alternatively positive potential at E2. Each electrode (E2 or E1) has a width corresponding to the microchannel width (500 μm) and a length of 1 mm. The separation between the two electrodes is 200 μm. The liquid crosses E2 driven by capillarity and stops when it reaches the superhydrophobic carbon surface where the capillary pressure takes a positive value according to the Young-Laplace equation and acts as a barrier to flow. When an electrical potential ($\leq$ -1V) is applied at E1 against E2, the liquid rapidly crosses the 1 mm hydrophobic barrier of the superhydrophobic surface of E1. Once the liquid crosses the hydrophobic barrier, it reestablishes capillarity in the next zone until it encounters E1 of second valve at same flow rate as the entry part. The flow rate also depends on the channel dimension which is expected from the Washburn equation:[59]

$$x^2 = a_0 \frac{\gamma r^2 P_c}{4\mu} t \ldots \ldots \ldots . (9)$$

where x is the displacement of meniscus at time t, r is channel radius, P_c is capillary pressure, a_0 is a constant associated with the channel cross section shape, μ viscosity of the liquid, γ is surface tension of water. The potential-induced flow rate in the valves increases with decreasing dimensions of the microchannel. The flexibility of fabrication allowed us to incorporate multiple on-off fluidic manipulations along the microchannel by printing several pairs of the electrodes with proper treatment of the surface.
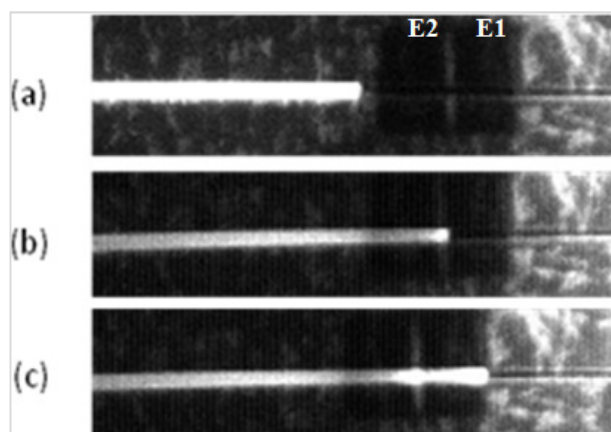
Figure 5 Snapshots taken while recording the video as a 10 µL fluorescein dyed solution of 0.1 M phosphate buffer saline (PBS) solution - (a) enters and flows through the microchannel by capillary action in the first part of the microchannel, (b) stopping at the superhydrophobic carbon (E1) surface. (c) Crossing the hydrophobic barrier of E1 under applied voltage.

Ion-specific effects on the valve operation

A limited number of electrolytes were used to characterize their effects on the efficiency of the valve operation. This was done to verify the qualitative predictions that could be drawn by the contact angle measurements. In order to define a quantitative comparison metric between different channels we chose to measure the "response time" of the valve. We define as "response time" the time elapsing between the application of the potential and the moment the meniscus front reaches and crosses the end of the 1 mm hydrophobic barrier of the valve (E1). Videos of the flow of fluorescein dyed solution were recorded to track the position of the meniscus as a function of time. Figure 6(a) and (b) shows the response time against the concentration and applied potential respectively in the tested electrolytes. Not surprisingly, KCl and PBS solutions cross E1 only when a negative potential was applied at E1 or alternatively a positive potential at E2. The "response time" in KCl or PBS showed positive concentration dependence, i.e. the flow was slower as the concentration increased as shown in Figure 6(a). When a positive potential is applied at E1, regardless of the magnitude of potential and concentration, however, practically no response was observed not only in KCl and PBS but also NaCl, $MgCl_2$ or $LiSO_4$. As positive potential > 1.5 V was applied at E1 the liquid front momentarily readjusted but did not show any movement. These results are expected and consistent with the results presented in Figure 3b. The sudden readjustment that ceases quickly at positive potential at E1 is expected as there is contact angle change at this potential for concentrations ≤ 0.1 N (see Figure 3b) but not sufficient to induce flow. Even at potentials where there is sufficient change in contact angle, however, the potential induced flow occurs only when E1 is biased negatively with respect to E2. The results reinforce

our hypothesis that the flow actuation using such coplanar electrodes with very close proximity may not only involve contact angle changes but also is subjected to other forces proposed above that might contribute to the electrocapillarity phenomena and hydrodynamic forces. Further to the point, when LiClO$_4$ was the electrolyte, the flow rate increased with increasing concentration and potential, regardless of the sign, again consistent with the result in Figure 3c. The observed results are characteristic of the superhydrophobic nanoporous electrode and may change completely with change in electrode type. Interestingly, when both E1 and E2 were the non etched SCPE, neither electrowetting nor the potential induced flow over the electrodes were observed.
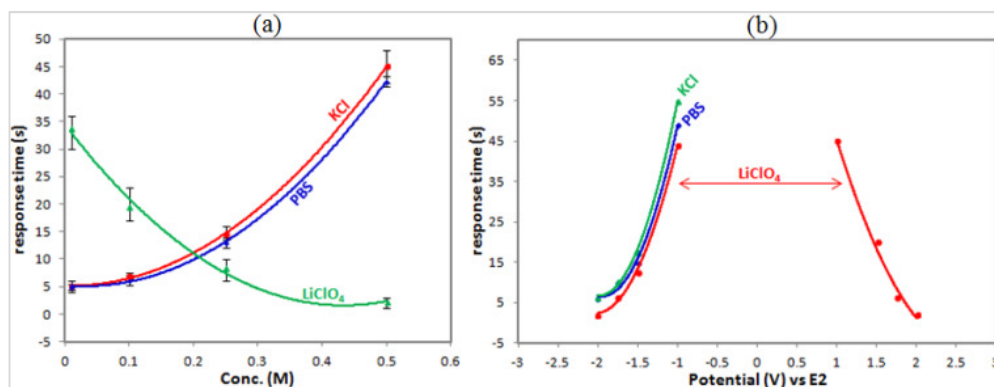

Figure 6 (a) Response time against concentration as -1.5 V is applied at E1 in KCl, PBS, and LiClO$_4$. (b) response time vs potential applied at E1 in 0.2 M solution of KCl, PBS, and LiClO$_4$.

Manipulation of real liquid

In order to demonstrate the direct applicability of the stop-go operations for the said application we considered, in addition to the above representative test liquids, PBS buffers containing proteins at pH 5 to 8. The PBS solutions containing proteins of interest such as β-lactoglobulin or bovine serum albumin (BSA) can be stopped and restarted at potential activation of the valves. The stop-go operations of the valves in the protein containing solution coincides with the conditions discussed above for PBS.

4 Conclusion

We show that superhydrophobic nanoporous carbon based surfaces display unique electrowetting behaviour with respect to the type and concentartion of electrolytes. The droplet placed between two such closely spaced electrodes shows directionality of flow when a potential is applied. The directional flow behaviour of the droplet is suggested other forces such as Marangoni or electrohydrodynamic effects playing a role. Such superhydrophobic nanoporous electrodes fabricated via a facile selective and controlled solvent etching of SPCE surface can be easily incorporated in microchannels for a stop/go fluidic operations. We show all low cost approach in

the fabrication of either the microfluidic channels or the flow control mechanisms through reel-to-reel or other manufacturing methods. The stop/go valves that are electrochemically activated and therefore can be operated by potentitostats that can also be used for signal generation and reading when such microchannels are used as simple analytical microsystems. When such devices can operate by capillarity, the ability to control the flow can provide important versatility for product design allowing complete reagent dissolution, mixing and reaction time manipulation. We have seen that the activation of the valves does not follow simple electrowetting principles dependent on the electrical double layer capacitance, and it appears that specific adsorption phenomena and possibly electrohydrodynamic or Marangoni-type effects play a role. The flowing electrolyte (and therefore the sample matrix in real applications) can thus signficantly influence the behaviour of these valves. An important challenge is to better understand all the driving forces so that eventually we could be able to influence their importance and achieve a valve behavior independent of the nature of the sample matrix. We have started work using urine and food samples and we have been able to maintain a predictable behavior for the valves, and are incoprorating immunosensors downstream from the valves that will eventually result in an integrated analytical device. However, signficant work is needed for such devices to reach the robustness and versatility of lateral flow immunosensing devices.

Experimental Section

Materials and methods

All the chemicals including N, N-dimethylformamide (DMF), phosphate buffer saline solution (PBS) and fluorescein isothiocyanate I 98 % (HPLC) were obtained from Sigma Aldrich. Distilled and de-ionized water (PURELAB UHQ II, ELGA) was used throughout the study. The substrate for printing was a poly (ethylene terephthalate) (PET) film (thickness: 175 μm) provided by ThyssenKrupp Plastic Iberica S.A. (Spain). The screen-printing apparatus used was DEK-248 (DEK International) equipped with a DEK Align 4 vision module (a two-point optical alignment system). The screen of a polyester mesh 305 (120/34), with an emulsion thickness of 13 µm was designed in-house and manufactured by DEK International (France). The squeegee used was made of polyurethane and provided by DEK International (model SQA152 with a contact angle of 45^0 and a hardness factor of 70). The inks (7102 conductor paste based on carbon and 5064 conductor paste based on silver) were provided by DuPont Ltd. (UK). The curing/ drying of the ink was carried out in a Digiheat 150L oven (JP Selecta S.A, Spain). The adhesive used to bond the

components was commercial Nactac-T9020 provided by MACtac, Spain. It is a 100 μm thick PET film coated on both sides with pure acrylic adhesive.

Fabrication of the microsystem

The printing of the carbon ink deposit to pattern the PET plastic with screen printed electrodes (SPCE) was performed according to the procedure reported previously.[40] The superhydrophobic surface on electrode material was fabricated by dipping the SPCE surface in N, N-dimethylformamide (DMF) for 40 minutes and drying at 100 ^{0}C for 20 minutes. Solvent etching followed by drying is a straight forward method similar to thermal[60] methods for producing porous materials. The microfluidic channels were fabricated by aligning and bonding two substrates, one previously patterned with the valving electrodes and the other acting as a cover, via an interlayer of previously patterned and machined double sided adhesive to form a microchannel containing the bottom wall patterned with arrays of electrodes. The double sided adhesive was patterned and machined with a *Fenix Flyer* CO_2 laser marker (Synrad) using 5 passes at 50% of power to produce *depth x width x length* = 100 µm x 500 µm x 6 cm open rectangular patterns with circular area of 12.56 mm^2 at both ends. Schematics of the steps for the fabrication of the microfluidic channel are shown in Figure 7.


Figure 7.Fabrication of the microsystems incorporating electrochemically actuated valves

Characterization

Wettability of both as printed and DMF-modified carbon electrode surfaces was measured by recording the contact angles using video-based optical contact angle measuring goniometer (Model: OCA 15EC, supplier: NEURTEK instruments, Spain) with a Hamilton syringe attachment. Surface morphology of roughness amplified carbon surface was investigated using environmental scanning microscopy (FEI model QUANTA 600 manufactured by FEI (USA). The thickness (7.5 µm) of the SPCE film was measured using a Mitutoyo SJ-301 profilometer and the data received were analyzed with the software SURFPAK-SJ Version 1.401 (Mitutoyo Messgerate GmbH, Japan). Snapshots of the flow of fluorescein dyed solution in the microchannel were taken using a set up of LED light source, and inverted EO GigE camera interfaced with computer using a (µEye) software.

Keywords: Microsystems, capillary flow control, stop-go valve, electrochemically actuated, superhydrophobic nanoporous

References

[1] D. Mata, D. Bejarano, M. L. Botero, P. Lozano, M. Constantí, I. Katakis, *Electrochim. Acta* **2010**, *55*, 4261–4266.

[2] V. Gubala, L. F. Harris, A. J. Ricco, M. X. Tan, D. E. Williams, *Anal. Chem.* **2012**, *84*, 487–515.

[3] L. Gervais, N. de Rooij, E. Delamarche, *Adv. Mater.* **2011**, *23*, 151–176.

[4] T. J. Clark, P. H. McPherson, K. F. Buechler, *Point of Care* **2002**, *1*, 42–46.

[5] C. D. Chin, V. Linder, S. K. Sia, *Lab Chip* **2012**, *12*, 2118–2134.

[6] A. Warsinke, *Anal. Bioanal. Chem.* **2009**, *393*, 1393-1405.

[7] G. A. Posthuma-Trumpie, J. Korf, A. van Amerongen, *Anal. Bioanal. Chem.* **2009**, *393*, 569–582.

[8] L. Gervais, E. Delamarche, *Lab Chip* **2009**, *9*, 3330–3337.

[9] B. S. Lee, J.-N. Lee, J.-M. Park; J.-G. Lee, S. Kim, Y.-K. Cho, C. Ko, *Lab Chip* **2009**, *9*, 1548–1555.

[10] J. Park, V. Sunkara, T.-H. Kim, H. Hwang, Y.-K. Cho, *Anal. Chem.* **2012**, *84*, 2133–2140.

[11] A. H. C. Ng, U. Uddayasankar, A. R. Wheeler, *Anal. Bioanal. Chem.* **2010**, *397*, 991–1007.

[12] A. Bange, H. B. Halsall, and W. R. Heineman, *Biosens. Bioelectron.* **2005**, *20*, 2488–2503.

[13] S. Assadollahi, C. Reininger, R. Palkovits, P. Pointl, T. Schalkhammer, *Sensors* **2009**, *9*, 6084-6100.

[14] M. Zimmermann, E. Delamarche, M. Wolf, P. Hunziker, *Biomed. Microdevices* **2005**, *7*, 99–110.

[15] T. G. Henares, F. Mizutani, H. Hisamoto, *Anal. Chim. Acta* **2008**, *611*, 17–30.

[16] J. S. Rossier, G. Gokulrangan, H. H. Girault, S. Svojanovsky, G. S. Wilson, *Langmuir* **2000**, *16*, 8489-8494.

[17] A. L. Brøgger, D. Kwasny, F. G. Bosco, A. Silahtaroglu, Z. Tü̈mer, A. Boisen, W. E. Svendsen, *Lab Chip* **2012**, *12*, 4628–4634.

[18] K. W. Oh, C. H. Ahn, *J. Micromech. Microeng.* **2006**, *16*, 13–39.

[19] H. Salimi.-Moosavi, T. Tang, D. J. Harrison, *J. Am. Chem. Soc.* **1997**, *119*, 8716-8717.

[20] K. Ichimura, S. K. Oh, M. Nakagawa, *Science* **2000**, *288*, 1624-1626.

[21] A. Chunder, K. Etcheverry, G. Londe, H. J. Cho, L. Zhai, *Colloids Surf., A* **2009**, *333*, 187–193.

[22] B. S. Gallardo, V. K. Gupta, F. D. Eagerton, L. I. Jong, V. S. Craig, R. R. Shah, N. L. Abbott, *Science* **1999**, *283*, 57-60.

[23] F. Mugele, J. C. Baret, *J. Phys.: Condens. Matter* **2005**, *17*, 705–774.

[24] H. Moon, S. K. Cho, *J. Appl. Phys.* **2002**, *92*, 4080-4087.

[25] T. N. Krupenkin, J. A. Taylor, T. M. Schneider, S. Yang, *Langmuir* **2004**, *20*, 3824-3827.

[26] V. Bahadur, S. V. Garimella, *Langmuir* **2007**, *23*, 4918-4924.

[27] Z. Han, B. Tay, C. Tan, M. Shakerzadeh, K. Ostrikov, *ACS Nano* **2009**, *3*, 3031–3036.

[28] C. H. Lee, S. K. Kang, J. A. Lim, Y.-J. Kwark, H. S. Lim, J. Kim, J. H. Cho, *J. Mater. Chem.* **2012**, *22*, 14656-14660.

[29] C. Ran, G. Ding, W. Liu, Y. Deng, W. Hou, *Langmuir* **2008**, *24*, 9952-9955.

[30] R. I. Revilla, L. Guan, X.-Y. Zhu, B.-G. Quan, Y.-L. Yang, C. Wang, *J. Phys. Chem. C* **2012**, *116*, 14311–14317.

[31] D. L. Herbertson, C. R. Evans, N. J. Shirtcliffe, G. McHale, M. I. Newton, *Sens. Actuators A* **2006**, *130*, 189–193.

[32] B. Kakade, R. Mehta, A. Durge, S. Kulkarni, V. Pillai, *Nano Lett.* **2008**, *8*, 2693-2696.

[33] Y. Lai, X. Gao, H. Zhuang, J. Huang, C. Lin, L. Jiang, *Adv. Mater.* **2009**, *21*, 3799–3803.

[34] W. Dai, Y.-P. Zhao, *J. Adhes. Sci. Technol.* **2008**, *22*, 217–229.

[35] G. Whyman, E. Bormashenko, *Langmuir* **2011**, *27*, 8171–8176.

[36] A. B. D. Cassie, S. Baxter, *Trans. Faraday Soc.* **1944**, *40*, 546–551.

[37] E. Bormashenko, *Langmuir* **2011**, *27*, 12769–12770.

[38] Wenzel, *Ind. Eng. Chem.* **1936**, *28*, 988-994.

[39] H . LI, L. ZOU, L. PAN, Z. SUN, *Environ. Sci. Technol.* **2010**, *44,* 8692–8697.

[40] D. Bejarano, P. Lozano, D. Mata, S. Cito, M. Constanti, I. Katakis, *J. Micromech. Microeng.* **2009**, *19*, 115007.

[41] D. Juncker, H. Schmid, U. Drechsler, H. Wolf, M. Wolf, B. Michel, N. Rooij, E. Delamarche, *Anal. Chem.* **2002**, *74*, 6139-6144.

[42] G. Lippmann, *Ann. Chim. Phys.* **1875**, *5*, 494–548.

[43] A. W. Adamson, *Physical Chemistry of Surfaces*, Wiley-Interscience, New York, 1990.

[44] M. Ma, R. M. Hill, *Curr. Opin. Colloid Interface Sci.* **2006**, *11*, 193–202.

[45] X. Feng, L. Jiang, *Adv. Mater.* **2006**, *18*, 3063–3078.

[46] A. P. Washe, P. Lozano-Sánchez, D. Bejarano-Nosas, I. Katakis, *Electrochim. Acta* **2013**, *91*, 166– 172.

[47] Z. Peng, D. Zhang, L. Shi, T. Yan, S. Yuan, H. Li, R. Gao, J. Fang, *J. Phys. Chem. C* **2011**, *115*, 17068–17076.

[48] F. Lufrano, P. Staiti, *Int. J. Electrochem. Sci.* **2010**, *5*, 903 – 916.

[49] K. S. W. Sing, D. H. Everett, R. A. W. Haul, L. Moscou, R. A. Pierotti, J. Rouqerol, T. Siemieniewska, *Pure Appl. Chem.* **1985**, *57*, 603-619.

[50] H.-J. Butt, K. Graf, M. Kappl, *Physics and Chemistry of Interfaces*, Wiley, New York, **2003**, p. 45.

[51] D. C. Grahame, *Chem. Rev.* **1947**, *41*, 441-502.

[52] J. Dzubiella, J.-P. Hansen, *J. Chem. Phys.* **2005**, *122*, 234706.

[53] B. Xin, and J. Hao, *Chem. Soc. Rev.* **2010**, *39*, 769–782.

[54] C. D. Daub, D. Bratko, K. Leung, A. Luzar, *J. Phys. Chem. C* **2007**, *111,* 505-509.

[55] W. D. Ristenpart, P. Jiang, M. A. Slowik, C. Punckt, D. A. Saville, I. A. Aksay, *Langmuir* **2008**, *24,* 12172-12180.

[56] A. B. D. Brown, C. G. Smith, A. R. Rennie, *Phys. Rev. E* **2000**, *63*, 016305.

[57] N. Sasaki, T. Kitamori, H.B. Kim, *Lab Chip* **2006**, *6*, 550-554.

[58] W.Y. Ng, S. Goh, Y.C. Lam, C. Yang, I. Rodríguez, *Lab Chip* **2009**, *9*, 802–809.

[59] Y. Zhu, K. Petkovic-Duran, *Microfluid Nanofluid* **2010**, *8*, 275-282.

[60] A. P. Washe, S. Macho, G. A. Crespo, F. X. Rius, Anal. Chem. **2010**, *82* 8106–8112.

CHAPTER 4

CHAPTER 4

ELECTROCHEMICALLY ACTUATED PASSIVE STOP-GO MICROVALVES FOR FLOW CONTROL IN MICROFLUIDIC SYSTEMS

Alemayehu P. Washe, P. Lozano-Sánchez[¥], D. Bejarano-Nosas, B. Teixeira-Dias and Ioanis Katakis*

Bioengineering and Bioelectrochemistry Group, Department of Chemical Engineering, Universitat Rovira i Virgili, Avinguda Països Catalans, 26, 43007, Tarragona, Spain

¥ Current address: Integrated Microsystems for the Quality of Life S.L., C/del Ferro 6, Nave 7, 43006 Tarragona, Spain

*Corresponding author: Tel. +34 977 55 96 55, Fax + 34 977 55 96 21, E-mail: ioanis.katakis@urv.cat

Abstract

Flow manipulation is a critical expected capacity for integrated microsystems. One way to realize low cost devices is to take advantage of capillary forces for fluid movement. In such systems, flow manipulation should be achieved with easily operated, effortlessly integrated valves. One advantageous method to operate sensors and actuators in microsystems is electrochemistry. Here, the design, fabrication and implementation of low voltage electrochemically actuated passive stop-go microvalves for on-off fluidic manipulations in microfluidic systems are reported. Two closely spaced electrodes (one of which has superhydrophobic surface) were fabricated by screen printing followed by surface structuring in a microchannel. The fabrication of the superhydrophobic surface (water contact angle (CA) 152 ^{0}) was performed by selective and controlled solvent-etching of a naturally hydrophobic (CA = 105 ^{0}) screen printed carbon surface. The process increased the roughness and porosity of the surface that caused the superhydrophobic effect. The superhydrophobic surface of the carbon electrode, in addition to functioning as passive stop valve (PSV), facilitates the flow actuation using low applied voltage avoiding observable electrochemical reactions in aqueous solutions. When a low voltage (~ - 1 V) was applied at the carbon electrode against a silver electrode, the flow of such solutions (e.g. 0.01 M phosphate buffer saline solution) that was stopped at the PSV, resumed, crossing the 1 mm pitch of hydrophobic barrier of the PSV in 1 sec and reestablishing capillary flow downstream. The low cost and flexibility of fabrication, facile integration and miniaturization, and reproducible performance of such on/off valves make this configuration promising for the development of low cost microfluidic devices for point-of-care diagnostics, food analysis, and environmental monitoring.

Keywords: Microfluidics, fluid control, passive microvalve, electrochemically actuated, superhydrophobic

1. Introduction

For more than ten years the microfluidics community is anticipating an impressive market domination of lab-on-a-chip (LOC) devices in sectors such as Point of Care (POC) diagnostics, food and environmental analysis. Expectations of market volumes in excess of several billion dollars have not materialized in part due to the high manufacturing costs of the disposables with many current production processes. One possible enabling development for LOC devices is to break down their overall performance in simpler "unit operations" and use simple fluid manipulation and sensing principles lowering manufacturing costs and simplifying operation. The simplest such process consists of the movement of a fluid in a microchannel where simple operations take place (for example, dilution, dissolution of solids, metering, and detection). The ability to precisely control flow in such a simplistic microchannel could prove crucial for many LOC applications, particularly in bioanalytical applications where an analytical response depends on the dissolution of previously deposited reagents, the kinetics of biological affinity and enzymatic reactions, and mass transport of products to a transducer [1]. A miniaturized microfluidic immunoassay, for instance as reported in Ref. [2], involves an immunochemical previously deposited in the microchannel which, as the solution containing the analyte is introduced, undergoes–dissolution, mixing, and reaction with the analyte yielding an immunocomplex that is detected at the detector located downstream. Therefore the success of detection depends critically on the extent of dissolution, mixing, and immunoaffinity binding, all of which require enough residence time due to the laminar nature of microscale flow. To this end, two key on-chip fluidic operations are required: stopping the flow at the vicinity of the probe zone in the microchannel and a fast and reliable flow actuation mechanism. Such operations can be performed in the microchannels using microvalves.

A number of miniaturized microvalves (active and passive) with a variety of actuation methods including magnetic, pneumatic, piezoelectric, electrostatic, and bimorph have been reported [3]. Most of these solutions require mechanical operation with moving parts and bulky peripherals that limit miniaturization. On the other hand, the dependence of microscale flow on surface property, particularly wettability, has been used to either generate passive flow as in capillary driven microfluidic systems or to passive stop-go control of the flow in the microchannel [4-6]. The capillary pressure (Pc) that governs capillary flow is given for a rectangular microchannel [7] of width (w) and depth (d) by the Young-Laplace equation:

$$P_c = -\sigma_{lv}\left(\frac{Cos\theta_b + Cos\theta_t}{d} + \frac{Cos\theta_l + Cos\theta_r}{w}\right)$$

Where σ_{lv} is liquid-air interfacial energy and $\theta_{b,t,l,r}$ are the contact angles of the liquid on the bottom, top, left, and right channel wall surfaces, respectively, are the radii of curvature in the directions vertical and parallel to the liquid stream. It can be clearly seen that through precise control of the surface wettability (keeping the microchannel dimension constant) the desirable flow behavior including flow stopping can be achieved. Superhydrophobic surfaces of conductive material provide an attractive opportunity for passive stopping as well as flow actuation using extremely low voltage, permitting in situ control of wettability using nothing more than a potentiostat, which is already connected to the microsystem if electrochemistry is used for transduction of sensor output.

In this work we report on a highly sensitive, low-voltage electrochemically actuated, passive stop-go microvalve produced through a novel design and fabrication of superhydrophobic carbonaceous surface of electrodes that provide both passive stopping of the capillary driven flow and facilitate low voltage electrochemical actuation of the flow. The horizontally placed superhydrophobic electrode, Scheme 1-E2, and the wettable screen printed silver electrode (Scheme 1-E1) with a pitch of 200 μm separation incorporated into a microchannel constitute the electrochemically actuated passive stop-go microvalve. We describe the fabrication, characterization, and operation of this geometry as a microfluidic component that can be key in facilitating the development of low cost LOC devices for point-of-care diagnostics, food, and environmental monitoring.
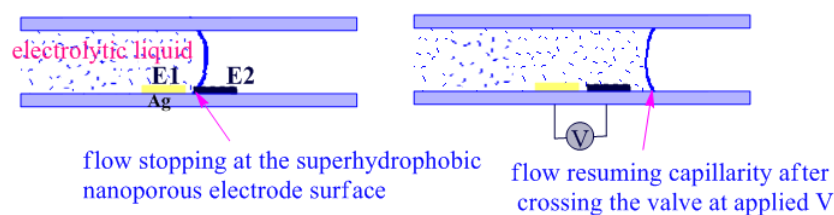
Scheme 1. Side view of the rectangular microchannel consisting of two closely spaced electrodes, E1 (screen printed silver) and E2 (superhydrophobicly modified screen printed carbon), on the bottom wall constituting the low voltage actuated passive stop-go microvalve.

2. Materials and methods

All the chemicals including N, N-dimethylformamide (DMF), phosphate buffer saline solution (PBS) and fluorescein isothiocyanate I 98 % (HPLC) were obtained from Sigma Aldrich. Distilled and de-ionized water (PURELAB UHQ II, ELGA) was used throughout the study. The substrate for printing was a poly (ethylene terephthalate) (PET) film with a thickness of 175 μm provided by ThyssenKrupp Plastic Iberica S.A. (Spain). The screen-printing apparatus used was DEK-248

(DEK International) equipped with a DEK Align 4 vision module (a two-point optical alignment system). The screen of a polyester mesh 305 (120/34), with an emulsion thickness of 13 μm was designed in-house and manufactured by DEK International (France). The squeegee used was made of polyurethane and provided by DEK International (model SQA152 with a contact angle of 45^0 and a hardness factor of 70). The inks (7102 conductor paste based on carbon and 5064 conductor paste based on silver) were provided by DuPont Ltd. (UK). The curing/ drying of the ink was carried out in a Digiheat 150L oven (JP Selecta S.A, Spain). The adhesive used to bond the components was commercial Nactac-T9020 provided by MACtac, Spain. It is a 100 μm thick PET film coated on both sides with pure acrylic adhesive.

2.1. Fabrication

The printing of the carbon ink deposit to pattern the PET plastic with screen printed electrodes (SPCE) was performed according to the procedure reported previously [8]. The superhydrophobic surface on electrode material was fabricated by dipping the SPCE surface in N, N-dimethylformamide (DMF) for 40 minutes and drying at 75 ^{0}C for 30 minutes. The microfluidic channels were fabricated by aligning and bonding two substrates, one previously patterned with the valving electrodes and the other acting as a cover, via an interlayer of previously patterned and machined double sided adhesive to form a microchannel containing the bottom wall patterned with arrays of electrodes. The double sided adhesive was patterned and machined with a *Fenix Flyer* CO_2 laser marker (Synrad) using 5 passes at 50% of power to produce *depth x width x length* = 100 μm x 500 μm x 6 cm open rectangular patterns with circular area of 12.56 mm^2 at both ends. Schematics of the steps for the fabrication of the microfluidic channel are shown in Figure 1.


Fig. 1. (a) PET plastic. i. Screen printing ii. 40 minutes exposure to DMF followed by curing/ drying at 75 ^{0} C for 30 minutes to produce superhydrophobic surface. iii. Screen printing of silver electrode. (b) the double sided adhesive tape iv. Laser ablation of double sided adhesive tape v. aligning and bonding the substrate patterned with the valving electrodes with the plastic lid via an interplay of the previously patterned and machined double sided adhesive to produce the microchannel with patterned flow behavior including stopping and restarting. The circular heads at the beginning and end of the microchannel serve as inlet and outlet reservoirs.

2.2. Characterization

The thickness (7.5 μm) of the SPCE film was measured using a Mitutoyo SJ-301 profilometer and the data received were analyzed with the software SURFPAK-SJ Version 1.401 (Mitutoyo Messgerate GmbH, Japan). Wettability of both as printed and DMF modified carbon and silver electrode surfaces was measured by recording the contact angles using video-based optical contact angle measuring goniometer (Model: OCA 15EC, supplier: NEURTEK instruments, Spain) with a Hamilton syringe attachment. Surface morphology of roughness amplified carbon surface was investigated using environmental scanning microscopy (FEI model QUANTA 600 manufactured by FEI (USA). Snapshots of the flow of fluorescein dyed solution in the microchannel were taken using a set up of LED light source, and inverted EO GigE camera interfaced with computer using a (μEye) software.

3. Results and Discussion

3.1 Superhydrophobic surface-The passive stop valve

The key step in the fabrication of a passive stop-go microvalve reported in this work was the fabrication of the superhydrophobic surface on conductive material surface. Figure 2 (a) shows environmental scanning electron microscopy (ESEM) image of a naturally hydrophobic screen printed carbon (SPC) surface and (b) that of the superhydrophobic surface obtained by subtractive etching of the former using DMF. The roughness enhancement apparent by the ESEM pictures was confirmed by BET surface area analysis (results not shown) is known to promote hydrophobicity [9, 10]. The water contact angles recorded on the untreated and treated surfaces were 105^0 and 152^0 respectively. The enhanced hydrophobicity of the solvent-treated surface is consistent with the increase of roughness as evidenced by the ESEM image. The mechanism for the roughness enhancement using solvents can be explained by considering the initial screen printed carbon surface; SPC is a naturally hydrophobic (low surface energy) composite of graphite particles and organic resins as binding agents and other components for dispersion of the particles. Since not all the components dissolve in DMF, the most likely mechanism it that the solvent selectively and partially etches only the exposed soluble components (the organic resins or dispersion agents) during the controlled period of exposure. We tried to reproduce the effect with other solvents including dimethylsulfoxide (DMSO), acetonitrile (CH_3CN), and acetone. Figure 2 (c) shows the recorded contact angles using a 3 μL sessile droplet of MQ water on the 40 minutes solvent treated and dried surfaces. Although DMSO showed a similar effect of enhancing surface hydrophobicity as DMF, it was less efficient in doing so than DMF and also it acts by

precipitating some of the components on the surface which required further steps of rinsing. Acetonitrile and acetone do not produce any significant hydrophobicity enhancement; rather were observed to have adverse effect on the adhesivity of the carbon or silver to the plastic surface. Thus DMF was selected for further experiments. It did not have any peeling or disconnecting effect either on the ink deposit or on the plastic when the strips were exposed to it for as long as 24 hours, and the surface slackened by DMF treatment cures immediately by thermal treatment. Interestingly, the contact angle increases progressively with duration of exposure of the surface to DMF to reach a maximum and start to decrease when the exposure time was prolonged as shown in Figure 2 (d) pointing to the effect of the nature of nanoscale roughness (porosity) on the contact angle. Our approach, although follows a novel strategy, is consistent with the general method of amplification of nanoscale roughness as has been reported using lithography [11] and phase separation [12].
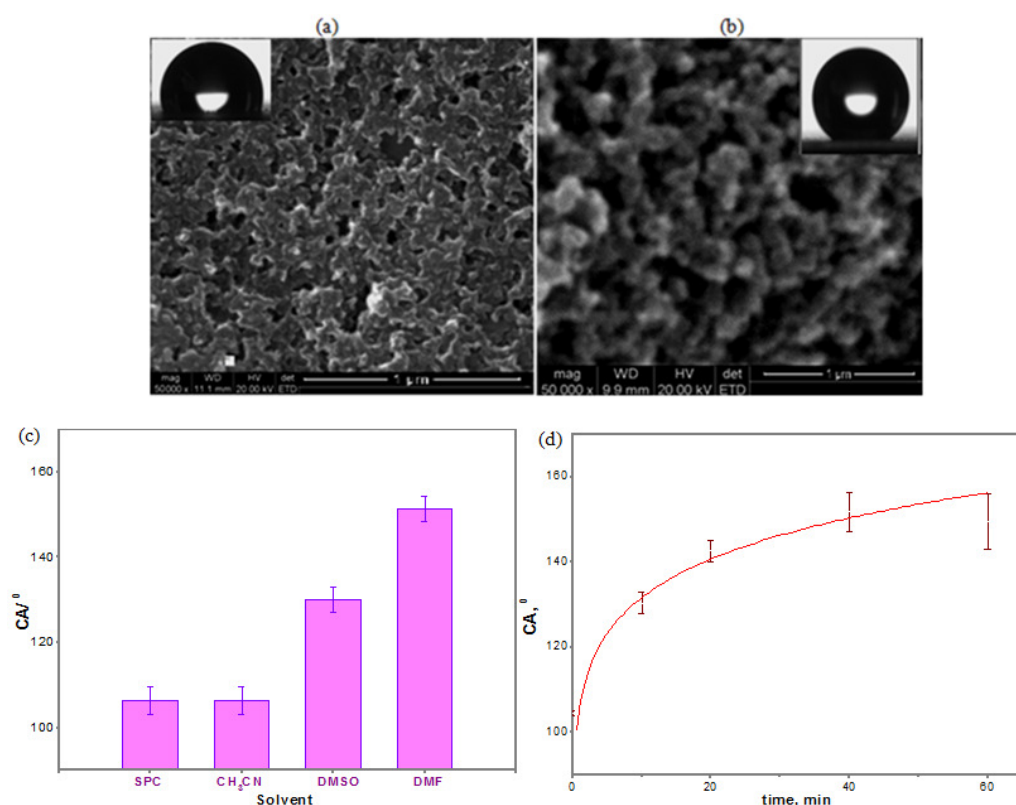

Figure 2. (a) ESEM image of naturally hydrophobic screen printed carbon (CA = 105^0 left) and (b) ESEM image of superhydrophobic (CA = 152^0 right). The insets are photos of a 3 μL MQ water droplet on the corresponding surfaces. (c) Comparison of contact angles recorded on untreated SPC and the 40 minute solvent -exposed SPC surfaces for different solvents. (d) Contact angle as a function of duration of exposure of the SPC surface to DMF.

3.2. The microfluidic device and operation of the microvalve

The fluid flow in the microfluidic device fabricated in this work can be considered to take place in three different zones; the first is the entry part with relatively hydrophilic surfaces that allows the liquid to penetrate the microchannel autonomously by capillary action, the second is the flow control zone where the flow stops until stimulated by applied voltage, and the third the capillary driven flow zone that displays similar flow behavior as the entry part. Incorporated in the flow control zone is the microvalve consisting of two closely placed electrodes- the silver (Ag) and the superhydrophobic carbon electrode as shown in Figure 3. In this figure snapshots are shown as the liquid reaches the two first zones and the valve activation- (a) at the capillary driven flow entry part, (b) crossing the silver surface and (c) stopping at the superhydrophobic carbon of fluorescein dyed solution of 0.01 M phosphate buffer saline (PBS) solution as it flows through the microchannel. As can be seen from Figure 3 (c), the stopping state of the liquid is marked by the formation of a shiny ring at the meniscus which could be due to accumulation of the fluorescing molecules just behind the meniscus [13]. The silver electrode pad has a width corresponding to the microchannel width (500 μm) and a length of 1.5 mm. Similarly the carbon electrode pad has a width corresponding to the microchannel width (500 μm) and a length of 1 mm. The pitch of separation (labeled `$d$` in Figure 3 (c)) between the two electrodes is 200 μm. The liquid crosses the silver electrode driven by capillarity and stops when it reaches the superhydrophobic carbon surface where the capillary pressure takes a positive value according to the Young-Laplace equation and acts as a barrier to flow. When an electrical potential (~-1V) is applied at the carbon electrode against the silver electrode, the liquid rapidly crosses the 1 mm hydrophobic barrier of the superhydrophobic surface. Once the liquid crosses the hydrophobic barrier, it reestablishes capillarity in the third zone at the same flow rate as the entry part as set during the design. The flexibility of fabrication allowed us to incorporate multiple on-off fluidic manipulations along the microchannel by printing several pairs of the electrodes (results no shown).

3.3. Electrolyte effects on microvalve activation

A limited number of electrolytes were used to observe their effects on the efficiency of the valve operation. The response time of the valve was used as a criterion. Videos of the flow of fluorescein solution were recorded to track the position of the meniscus as a function of time to characterize the flow rate at different zones in the microchannel. Accordingly, the flow rate of 1 mm/sec at the capillary driven zone was measured during the play back of the videos. Such flow rate, however, can vary depending on the dimensions of the microchannel provided that the

wettability remains the same. Although the nature and concentration of electrolytes may be expected to affect the flow rate, we didn´t observe significant changes in the flow rate of the tested solutions (NaCl, KCl, and PBS) in the concentration ranges 0.01 to 0.5 molar. While the flow stops completely at the PSV until stimulated by applied potential, it was found that the potential-induced flow through the superhydrophobic barrier of the PSV depends on the magnitude of potential applied, concentration and nature of electrolytes. Figure 4 (a) and (b) shows variation of flow rate through the valve surface as a function of concentration of different electrolytes and applied potential respectively. Error bars at each point in Figure 4 (a) correspond to the standard deviation of 12 measurements [12 microvalves from four batches (each 3 microvalves, N = 12] constructed and tested at different periods of the work reflecting a very good reproducibility and repeatability. Figure 4 (b) shows an increase in flow rate of potential-induced flow with increasing potential as can be expected. The flow rate measurement involves recording response time of the valve that can be defined as the time elapsing between the turning on of the potential and the time the meniscus front reaches and crosses the end of the 1 mm hydrophobic barrier of the valve surface. Different electrolytes including KCl, NaCl and PBS were considered in order to demonstrate the applicability of the valves to the development of miniaturized microfluidic systems for biodetection that commonly employs PBS solutions. Except a slightly faster speed of the PBS solution no significant difference was observed in response times between the solutions of NaCl and KCl.
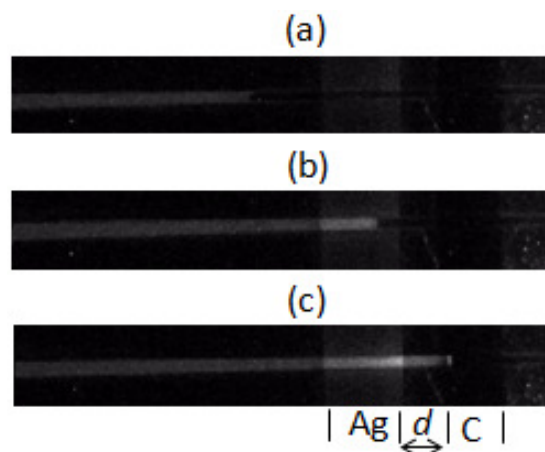

Fig. 3. Snapshots taken while recording the video as the fluorescein solution of 0.01 M phosphate buffer saline (PBS) solution - (a) enters and flows through the microchannel by capillary action in the first part of the microchannel, (b) crossing the silver electrode surface by capillary action, (c) stopping at the superhydrophobic carbon (C) surface.
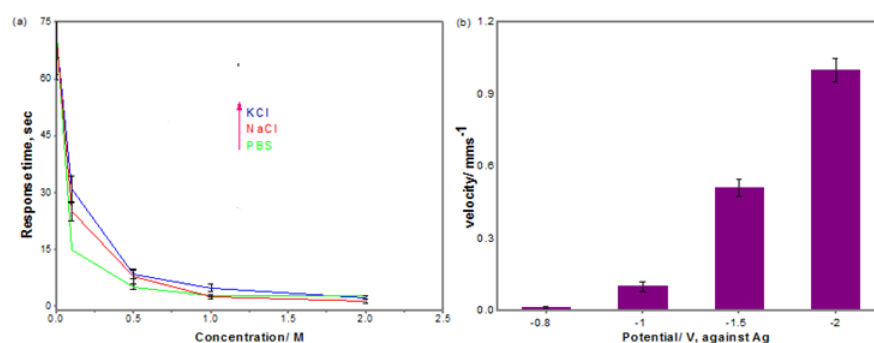
Fig. 4. (a) Response time of the microvalve as a function of the concentration of different electrolytes [KCl, NaCl, PBS] when -1.5 V applied at C against Ag. (b) The velocity of a 0.5 M KCl solution over the hydrophobic barrier of passive stop valve as a function of applied voltage on the C against Ag.

Mechanism

For all chloride based salts tested-KCl, NaCl, LiCl, $MgCl_2$ and PBS the higher the concentration the faster the response of the valves at negative potential at E1(carbon) or alternatively positive potential at E2(Ag).The operation showed preferential response to positive potential applied at Ag, regardless of its relative position (in place of E1or in place of E2) or alternatively a negative potential at C. Surprisingly, when Ag is placed at E1 position, the liquid crosses Ag at a positive potential against E2 (carbon) but never stops again at other valves located down fluidics. But when Ag replaces E2, the flow that has crossed E1(carbon) at a positive potential at Ag or alternatively a negative potential at E1 stops as usual at E1 of the second valve located down fluidics (videos in supporting information). The former could be attributed to charging of the meniscus as chloride adsorbs on Ag surface. Thus the mechanism for the Ag-C valve is linked to the presence of chloride in the solution. Chloride ions can specifically adsorb on Ag surface. This adsorption can be enhanced at positive potential at which Ag is oxidized into Ag^+[14]. The very fast adsorption of chloride at the oxidized Ag surface can create large columbic force corresponding to local gradients in concentration that can propel the liquid in similar fashion as electrohydrodynamic effect [15-18].

Table 1 shows summary of ESEM elemental analysis results for percent chloride adsorbed/desorbed, see supporting information, in presence and absence of potential. The Ag surface previously subjected to +1V for 30 seconds in 0.5 M KCl against carbon electrode, rinsed with MQ water and dried at 80 ^{0}C for 20 minutes showed a relatively large amount of chloride adsorbed. Interestingly the adsorbed chloride can be desorbed from the surface by subjecting the electrode in situ at -1 V, a potential decided based on cyclic voltammetry. A control experiment by just soaking the electrode in the test solution (0.5 M KCl) for 30 seconds followed by rinsing with

MQ water and drying at 80 ^{0}C for 20 minutes confirmed very low level of chlorides on the surface as compared to the potential induced adsorption.

Table 1. Summary of ESEM elemental analysis of Ag surface for adsorbed chlorides after exposure to KCl solution in presence and absence of potential.

[KCl], M	Potential, V	% Cl$^-$	% Ag	% C
0.5	1[a]	13.23	82.53	4.24
0.5	-1[b]	1.36	95.91	2.73
0.5	0[c]	1.18	96.38	2.44

[a] Ag previously subjected to +1V in against carbon electrode, rinsed with MQ water and dried at 80 ^{0}C for 20 minutes. [b] step [a] followed by -1 V for 30 seconds in situ [c] Ag soaked in 0.5 M KCl for 30 seconds + rinse with MQ water + 80 ^{0}C for 20 minutes.

4. Conclusion

This work demonstrates the on-off fluidic manipulations in basic microfluidic systems through the design of microchannel that displays capillarity and integration of a low voltage electrochemically actuated passive stop-go microvalve fabricated on microchannel walls through screen printing followed by surface structuring. The use of solvents to produce superhydrophobic surfaces on composite material surfaces introduces a novel low cost approach for surface structuring. Superhydrophobic conductive surfaces allow to reliably stop the flow for as long as required and facilitate very fast actuation. Multiple on-off fluidic manipulations can be performed by replicating the same architecture at multiple specific locations along the fluidics which reinforces the applicability of the stop-go microvalve developed in this work to miniaturized microfluidic systems for biodetection. A deeper understanding of the mechanism of actuation should allow the tuning of the valves so that their operation be independent of the composition of the matrix.

Acknowledgements

100

References

[1] L. Gervais, N. Rooij, E. Delamarche, Adv. Mater 23 (2011) 151–176.

[2] L. Gervais, E. Delamarche, Lab Chip 9 (2009) 3330–3337.

[3] K. W. Oh, C. H. Ahn, J. Micromech. Microeng. 16 (2006) 13–39.

[4] K. Ichimura, S.K. Oh, M. Nakagawa, Science 288 (2000) 1624-1626.

[5] G. Takei, M. Nonogi, A. Hibara, T. Kitamori, H. Kim, Lab Chip 7 (2007) 596–602.

[6] A. Chunder, K. Etcheverry, G. Londe, H. J. Cho, L. Zhai, Colloids and Surfaces A: Physicochem. Eng. Aspects 333 (2009) 187–193.

[7] D. Juncker, H. Schmid, U. Drechsler, H. Wolf, M. Wolf, B. Michel, N. Rooij, E. Delamarche, Anal. Chem. 74 (2002) 6139-6144.

[8] D. Bejarano, P. Lozano, D. Mata, S. Cito, M. Constanti, I. Katakis, J. Micromech. Microeng. 19 (2009) 115007.

[9] M. Ma, R. M. Hill, Current Opinion in Colloid & Interface Science 11 (2006) 193–202.

[10] X. Feng, L. Jiang, Adv. Mater. 18 (2006) 18, 3063–3078.

[11] G. Scheen, K. Ziouche, Z. Bougrioua, P. Godts, D. Leclercq, T. Lasri, Langmuir 27 (2011) 6490–6495.

[12] J. T. Han, X. R. Xu, K. W. Cho, Langmuir 21 (2005) 6662-6665.

[13] R. Fahraeus, T. Lindqvist, Am J Physiol 96 (1931) 562–568.

[14] P. Bro, and N. Marincic, *J. Electrochem. Soc.* **1969**, 116, 1338-1341.

[15] W. D. Ristenpart, P. Jiang, M. A. Slowik, C. Punckt, D. A. Saville, and I. A. Aksay, *Langmuir* **2008**, 24, 12172-12180.

[16] A. B. D. Brown, C. G. Smith, and A. R. Rennie, *Phys. Rev. E* **2000**, 63, 016305.

[17] N. Sasaki, T. Kitamori and H.B. Kim, *Lab Chip* **2006**, 6, 550-554.

[18] W.Y. Ng, S. Goh, Y.C. Lam, C. Yang, I. Rodríguez, *Lab Chip* **2009**, 9, 802–809.

CHAPTER 5

CHAPTER 5

Facile and versatile approaches to enhancing electrochemical performance of screen printed electrodes

Alemayehu P. Washe[a,*], Pablo Lozano-Sánchez[b,1], Diego Bejarano-Nosas[a], Ioanis Katakis[a,**]

[a] Bioengineering and Bioelectrochemistry Group, Department of Chemical Engineering, Universitat Rovira i Virgili, Avinguda Països Catalans, 26, 43007 Tarragona, Spain
[b] Integrated Microsystems for the Quality of Life S.L., C/del Ferro 6, Nave 7, 43006 Tarragona, Spain

ABSTRACT

Screen printed carbon electrodes provide attractive opportunity for the development of miniaturized low cost electrochemical sensors. However, the electrodes display very low level of electrochemical performance due to the nonelectroactive components in the ink formulation and relatively low graphitic carbon content imposed by the constraints of screen-printing. In this work, selective etching action of a judiciously selected solvent was envisaged to improve the electrochemical characteristics of the electrodes. The procedure involves soaking the electrode strips in N, N-dimethylformamide (DMF) for just minutes of etching followed by drying. Five minutes DMF treated electrode, for instance, showed a 100-fold increase in the heterogeneous charge transfer kinetics compared to the untreated electrodes. The effective area of the solvent treated electrode was 57- fold of its apparent geometric area. The solvent treated electrodes also showed a dramatically decreased charge transfer resistance from ca. 18 000 Ohm to 180 Ohm. The results of surface examination using scanning probe microscopy and electrochemical impedance spectroscopy revealed enhancement in the porosity of the solvent treated electrodes. The procedure is versatile and applicable to other screen printed electrodes such as gold, silver or silver/silver chloride to improve the performance characteristics including stability. The ability to activate several electrodes simultaneously and multiple re-usability of the solvent makes this approach cost effective and very promising to facilitate mass production of miniaturized and disposable electrochemical sensors.

Key words: Screen-printed electrodes, solvent etching, electrode kinetics, electrochemical performance

1. Introduction

Disposable screen-printed carbon electrodes (SPCEs) fabricated via thick-film (screen-printing) technology offers the most promising route for the development of miniaturized sensors for the detection of different analytes including microorganisms [1,2], proteins [3–7], glucose [8–10], or nucleic acids [11,12], among others, in point-of-care testing and on-site monitoring. The low cost of the material (SPC) and its compatibility for mass production make SPCEs the primary choice

for researchers and diagnostic companies, particularly for electrochemistry driven applications. The great interest in the SPCEs is also due to attractive features of the carbon: chemically inert, low background currents and wide potential window [13, 14]. The performance of SPCEs, however, depends critically on the surface properties and the nature of the carbon ink. Due to the nonelectroactive additives in the inks and hence the relatively low graphitic carbon content imposed by the constraints of screen-printing, the redox activity and the overall analytical performance of the electrodes are compromised [15, 16]. The nonelectroactive components (or simply contaminants) including the polymeric binders in the ink block the electrochemically active graphitic particles leading to slower rates of heterogeneous charge transfer kinetics and seriously affect reversibility of electrochemical reactions at the electrodes. In addition to the impeding nature of the ink, commercial SPCEs exhibit wide range of electrochemical reactivities for benchmark redox systems. SPCEs from different commercial supplier display different background currents and have varying performance depending on the type of specific electrochemical techniques employed [15,17]. Such differences in the performance of the electrodes have been ascribed to variations in: (i) the graphitic loading, (ii) degree of electrochemical accessibility of the graphitic edges and (iii) the nature of the graphite particles and its functionalization [15]. These characteristics the electrodes, however, can be tuned using proper surface pretreatment methods. The surface pretreatment methods for SPCE employed to-date including electrochemical, chemical treatments prior to electrochemical, and exposure to UV and oxygen plasma are usually based on either increasing the density of oxygenated groups on the electrode surface or increasing the exposure of the electroactive graphitic particles. Wang et al. [17] proposed a short electrochemical pre-anodization of the electrodes for improved electrochemical performance. Cui et al. [18] described pretreatment procedure in saturated Na_2CO_3 solution at 1.2 V as a mild and effective condition for improving the electrochemical performance of SPCE. Wei et al. [19] showed further improvement in the heterogeneous charge transfer rate constant and electrochemical reversibility by soaking fresh SPCEs into concentrated NaOH for tens to hundreds of minutes prior to pre-anodization in low concentration NaOH. Notwithstanding the enhancement in the electrode performance, NaOH treatment may have problem of detaching the SPCEs from the substrate [18]. Kostaki et al. reported the possibility to improve electrochemical characteristics of SPCEs based on galvanostatic treatment (5 μA for 6 min in 0.1 M H_2SO_4) [20]. Osbome et al. [21] described activation of SPCEs based on the use of UV light from an excimer laser source to selectively etch the organic binding polymer from the composite surface thereby exposing sub-layers of carbon particulates. Wang et al. [22] reported

the use of plasma treatment to increase the graphitic edge planes as effective mechanism to enhance the electrochemical performance of screen-printed electrodes. These activation procedures may enhance the performance of the electrodes, but may either require cost intensive instrumentation, or not suitable for mass production or introduce surface functionalities that may lead to loss of stability of the performance of the electrodes.

Therefore, a simple, low cost and yet effective strategy for the activation of screen printed electrodes without compromising the stability is continuously being sought. Here, we report a new approach to enhance the electrochemical performance of SPCEs via the mechanism of increasing graphitic loading and exposure of more pristine graphitic edges. SPCE is a typical composite material composed of graphite particles and organic resins as binding agents and other components for dispersion of the particles. Thus it was envisaged that, since not all the components can dissolve in a judiciously selected organic solvent, a controlled and selective etching of the SPCEs' surface can increase the graphitic loading and exposure of more pristine graphitic edges. Scanning probe microscopes and electrochemical methods were used to characterize surface morphology and enhancements in the area of the solvent treated electrodes as compared to the untreated electrodes. The electrochemical characteristics including charge transfer kinetics and reversibility at the solvent treated electrodes were studied using electrochemical impedance spectroscopy (EIS) and cyclic voltammetry. The experimental results strongly reinforced the proposed mechanism. This simple, low cost and yet effective surface pretreatment procedure is more generic and can be applied as a versatile approach to enhance the electrochemical characteristics of other screen printed electrodes such as screen printed gold, silver or silver/silver chloride given the composite nature of all the electrodes and the presence of such contaminants as binders or dispersion agents in all of the inks. The proposed mechanism, although follows novel approach, is consistent with the previous reports [21–27].

2. **Experimental**

2.1. *Materials and equipments*

All the chemicals including $K_4[Fe(CN)_6]\cdot 3H_2O$, $K_3[Fe(CN)_6]$, $Sr(NO_3)_2$ and N,N-dimethylformamide (DMF) were obtained from Sigma Aldrich. Distilled and de-ionized water (PURELAB UHQ II, ELGA) was used throughout the study. The substrate for printing was a polyester (PET) film with a thickness of 175 μm provided by ThyssenKrupp Plastic Iberica S.A. (Spain). The screen-printing apparatus used was DEK-248 (DEK International) equipped with a

DEK Align 4 vision module (a two-point optical alignment system). The screen of a polyester mesh 305 (120/34), with an emulsion thickness of 13 μm was designed in-house and manufactured by DEK International (France). The squeegee used was made of polyurethane and provided by DEK International (model SQA152 with a contact angle of 45° and a hardness factor of 70). The inks (7102 conductor paste based on carbon and 5874 conductor paste based on Ag/AgCl) were provided by DuPont Ltd. (UK). Although SPCEs based on other types of commercially available inks including conductor inks-C2030519P4 carbon/graphite and 26-9203 conductive carbon from Gwent and SunChemical respectively were also tried, the proof-of-concept results were obtained mainly with 7102 conductor paste based on carbon provided by DuPont Ltd. (UK). The oven used for curing/drying purposes was a Digiheat 150 L oven provided by JP Selecta S.A., Spain.

2.2. Fabrication, surface pretreatment and characterization

The printing was performed according to the procedure reported previously by our group [28]. The thickness (7.5 μm) of the SPCE film was measured using a Mitutoyo SJ-301 profilometer and the data received were analyzed with the software SURFPAK-SJ Version 1.401 (Mitutoyo Messgerate GmbH, Japan). The plastics containing several screen-printed electrodes were placed vertically in a rectangular chromatographic chamber containing N, N-dimethylformamide for 5 min to expose all the electrodes entirely to the solvent. The solvent treated electrodes were then cured at 100 °C for 20 min in the oven. The surface area enhancement resulting from the solvent treatment was characterized using electrochemical methods (electrochemical impedance spectroscopy (EIS), and cyclic voltammetry (CV)), environmental scanning electron microscopy (FEI model QUANTA 600 manufactured by FEI (USA)) and atomic force microscopy. The adhesive single-side coated with acrylic (Adhesive research; ARCARE8565) was patterned and machined with a Fenix Flyer CO_2 laser marker (Synrad) using 4 passes at 50% of power to produce a circular opening of radius = 1.5 mm which when pasted on the electrode surface delimits a constant geometric area of the electrode to be 7.07 mm^2.

2.3. Electrochemical studies

Electrochemical studies involved a prior preparation of the solvent treated and untreated electrodes to delimit a constant area of the electrode surface as described in the previous section. The electrochemical performance of the solvent activated electrode surface of fixed area was investigated by recording cyclic voltammetry (CV) and EIS of $Fe(CN)_6^{3-/4-}$ redox couple. All the

106

electrochemical measurements including EIS were recorded in a 2 mM $Fe(CN)_6^{3-/4-}$ solution containing, unless otherwise stated specifically, 0.1 M $Sr(NO_3)_2$. A one-compartment, three-electrode electrochemical cell consisting of SPCE (either solvent treated or untreated) of geometric area 7.07 mm^2 as working, screen printed Ag/AgCl electrode (of geometric area 7.07 mm^2) as reference and platinum electrode as counter were employed. All dc potentials (E_{dc}) were referred to this reference electrode. A general purpose electrochemical system, the Autolab PGSTAT12 (Ecochemie) with frequency response analyzer (FRA2), was used. The impedance spectra were recorded in the 100 kHz–0.1 Hz frequency range. The amplitude for the sinusoidal excitation signal was 10 mV and the temperature was 20–23 $^\circ$C. The spectra were then fitted to an equivalent electrical circuit model using the Autolab impedance analysis software.

3. Results and discussion

3.1. Microscopic characterization

Surface characteristics of composite electrode materials can be tuned effectively using solvents. Fig. 1(a) and (b) show the environmental scanning electron microscopy (ESEM) images of the untreated and solvent treated SPCE surfaces respectively. The untreated surface, Fig. 1(a), is relatively smoother and has denser matrix that could be due to excess presence of the polymeric binders. The 5 min solvent treated electrode surface, Fig. 1(b), exhibited discernible topographic features with increased porosity and morphological alterations corresponding, most likely, to the subtracted components. The ESEM images also revealed a progressive increase in surface porosity with increasing duration of exposure to the solvent (data not shown). Topographic analysis of the 5 min DMF treated electrode using atomic force microscopy (AFM), Fig. 1(c), provided peak-to-peak roughness and the rms to be 1430 nm and 210 nm, respectively, pointing to increased fractal dimensions resulting from DMF treatment and is consistent with the ESEM results.

3.2. Electrochemical impedance spectroscopy

In order to investigate the charge transfer kinetics of the sol-vent treated porous electrodes as compared to that of untreated electrodes, impedance was recorded under specific operating conditions. Fig. 2(a) shows Nyquist impedance plot of 2 mM $Fe(CN)_6^{3-/4-}$ using 5 min DMF treated and untreated SPCEs (b) shows that of SPCE exposed to DMF for different durations of time; 1-30 min. In all cases the geometric area of the working electrode (the DMF treated or untreated) and the reference electrode (Ag/AgCl) were 7.07 mm^2. Impedance was recorded at E_{dc} = 0.12 V, E_{ac} = 10 mV, frequency range 100 kHz–0.1 Hz. Two distinct regions typical of rough/porous electrodes can be seen in the Nyquist plots: (i) a depressed semicircle in the high

frequency region corresponding to charge transfer process and (ii) a 45° line in the low frequency region defining a Warburg region of semi-infinite diffusion of species at electrode/electrolyte interfaces.
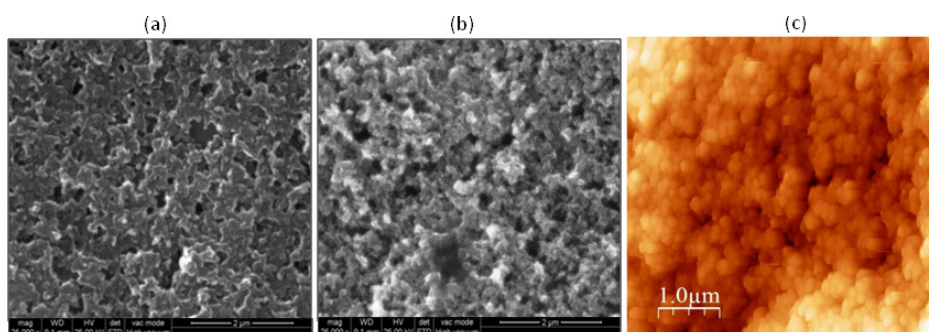

Fig. 1. (a) ESEM image of untreated screen printed carbon electrode surface and (b) ESEM image of 5 min DMF treated SPCE surface. (c) Atomic force microscopy topography image of 5 min DMF treated SPCE surface. The AFM image was taken in a tapping mode using a silicon tip-BCB350.

A dramatic decrease in the charge transfer resistance (R_{ct}, diameter of the semi-circles) can be achieved by just 5 min exposure of the SPCE surface to DMF, Fig. 2(a). A ~100 fold increased rate ($k°$) of the heterogeneous charge transfer kinetics at the 5 min DMF activated SPCE as compared to untreated SPCE was calculated using the values of R_{ct} from the EIS measurements based on Eq. (1) [29].

$$k^O = \frac{RT}{F^2 R_{ct} AC} \tag{1}$$

where R is the gas constant, T the temperature (296 K), F the Faraday constant, C is the concentration (mol cm^{-3}) of Fe(CN)$_6^{3-/4-}$, and A is the geometric area (cm^2) of the electrode. $k°$ was obtained as 1.3×10^{-2} cm s^{-1} and 1.04×10^{-4} cm s^{-1} for 5 min solvent treated and untreated electrodes, respectively. Fig. 2(b) shows the different high frequency intersection with Z′ axis of the electrodes exposed to DMF for different durations of time. The gradual increase in the Z′ values (real component of the impedance) with duration of expo-sure suggests alterations in the porosity of the electrodes and hence the corresponding ohmic resistance of the porous matrix [30]. The inset in Fig. 2(b) shows the R1(Q[R_{ct}W]) modified Randles circuit model where R1 represents the ohmic resistance of the electrolyte in solution and in the pores; Rct represent charge transfer resistance; and W is the Warburg element corresponding to a nearly 45^0 line in the low frequency region of the impedance. Q is the constant phase element, CPE, which accounts for electrode roughness. The experimental data fits well with the modified Randles circuit model. The average error (χ^2) of fits for 10 different impedance spectra of the DMF treated/untreated electrodes was 2.1×10^{-4}. These results from EIS are consistent with the results from cyclic voltammetry as can be seen in subsequent sections.
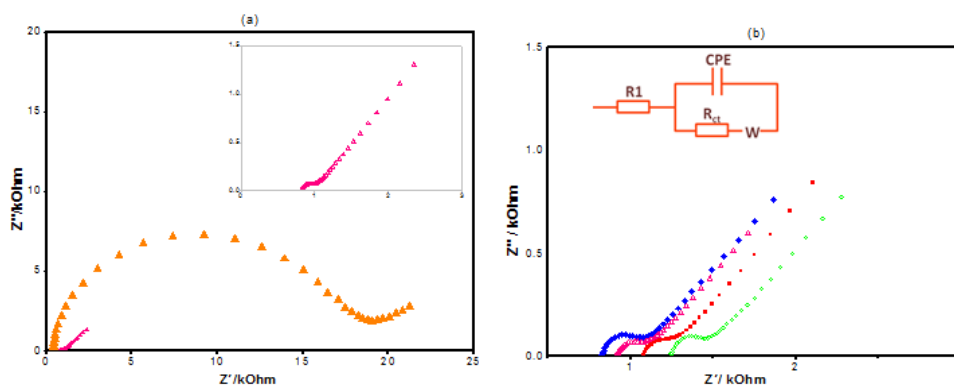
Fig. 2. (a) Nyquist impedance plot of 2 mM $Fe(CN)_6^{3-/4-}$ using (a) raw (▲) and 5 min (△) DMF treated SPCEs, (b) SPCEs treated in DMF for different duration of time: 1 min (◆), 5 min (△), 20 min (■), and 30 min (□). In all cases the geometric area of working electrode and reference electrode (Ag/AgCl) were 7.07 mm^2 each and platinum rod was employed as counter. Impedance was recorded at E_{dc} = 0.12 V, E_{ac} = 10 mV, frequency range 100 kHz–0.1 Hz. The temperature was 23 °C.

3.3. CV characterization of electrode performance

It is apparent that reducing the nonelectroactive components from the electrode surface could proportionally increase the graphitic loading and expose more electrochemically useful graphitic edges. This expectation was also realized through the CVs of $Fe(CN)_6^{3-/4-}$ redox couple recorded using the solvent treated and untreated SPCEs. As can be seen in Fig. 3(a), dashed line, the CV recorded using the general-purpose carbon inks (DuPont) based untreated electrodes did not show any sharp redox peaks. The i_{pa} and i_{pc} of 13.3 μA and 11.789 μA, respectively, and the peak-to-peak separation of 400 mV at a scan rate of 20 mV s^{-1} were roughly estimated for these electrodes. As scan rates increases, however, the CVs of the untreated electrodes exhibit indiscernible peaks. The 5 min DMF treated electrode, on the other hand, showed a very sharp anodic (i_{pa}) and cathodic (i_{pc}) peaks and a highly improved electrochemical reversibility. Although the values of peak-to-peak separation (ΔEp) appears to depend slightly on scan rates, ΔEp can be decreased from 400 mV of the untreated electrode to 100 mV of 5 min DMF treated SPCE electrodes (DuPont) at scan rate of 20 mV s^{-1}. Fig. 3(b) shows CVs of 2 mM $Fe(CN)_6^{3-/4-}$ at 5 min DMF modified SPCE at scan rates of 25, 50, 75, and 100 mV s^{-1} from inner to outer. The slight variations in the positions of peak currents with scan rates suggest the quasireversible nature of the electrode processes.

CV measurements were also adapted to determine the enhancement in the electrochemically active area and compare the results with the data obtained from EIS measurement to validate the importance of charge transfer kinetics and effective area of the electrode in accounting for the recorded enhancement in the performance of the solvent treated electrodes. Since capacitive current, $i_c = CV(t)^{-1}$ where C is the
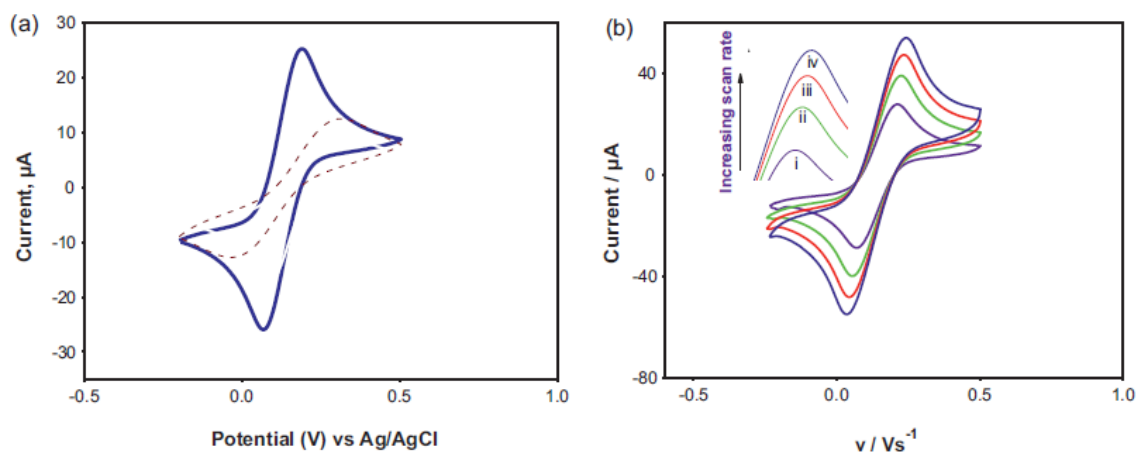
Fig. 3. (a) CVs of 2 mM $Fe(CN)_6^{3-/4-}$ redox couple at scan rate 20 mV s^{-1} using raw SPCE (dashed line), 5 min DMF modified (solid line). (b) CVs of 2 mM $Fe(CN)_6^{3-/4-}$ at 5 min DMF modified SPCE at scan rates of 25, 50, 75, and 100 mV s^{-1} from inner to outer (i–iv).

capacitance, V is the potential, t is time is also expected to increase with increasing area of the electrode, it was important to record the cyclic voltammograms in the background solution to determine the corresponding capacitive currents. Fig. 4(a) shows comparison of the cyclic voltammograms recorded in presence and absence of the redox couples in the solution. Fig. 4(a) curve 'a2' corresponds to the CV of 2 mM $Fe(CN)_6^{3-/4-}$ in 0.1 M $Sr(NO_3)_2$ solution recorded at the 20 min DMF treated electrode at scan rate of 20 mVs^{-1} whereas curve 'a1' correspond to several CVs recorded in 0.1 M $Sr(NO_3)_2$ at 0, 1, 5, 10, 20, 30, and 60 min DMF treated electrode surfaces at same scan rate. As can be seen from the figure the capacitive currents are negligible com-pared to faradaic currents, particularly in the important region of $Fe(CN)_6^{3-/4-}$ redox process (0.1–0.2 V) and are effectively ignored. Compared to the untreated electrodes, however, the DMF treated electrodes displayed higher level of capacitive current at higher potentials (>0.3 V) as shown in Fig. 4(b) curves 'b1'for DMF treated and curves 'b2'for the untreated. Interestingly, however, the capacitive currents recorded using DMF treated electrodes did not vary significantly among the electrodes with varying duration of exposure to DMF. For instance, the capacitive currents of 1 min DMF treated and untreated electrodes of same geometric area were 20 nA and 1.3 nA respectively but other DMF treated electrodes displayed very closer values of 25, 27, 29, 27 and 30 nA corresponding to 5, 10, 20, 30, and 60 min durations of exposure to the solvent respectively at 0.15 V. These results indicate that although further increment of the exposure time than required is expected to increase the total area, the resulting porous structures may not all be accessed by the test liquid/ions. This is clearly reflected in the effective areas of the DMF treated electrodes estimated using the modified Randles-Sevĉik equation for quasireversible reaction by

110

adapting the methods described in Refs. [31–33]. The modified Randles-Sevĉik equation for quasireversible reaction is given by [29]:

$$i_p = K(\Lambda, \alpha) \times (2.69 \times 10^5)n^{3/2}A_{eff}C\sqrt{D}\sqrt{v} \qquad (2)$$

where i_p is the peak current in amperes obtained from CV, D is diffusion coefficient of the 2 mM $Fe(CN)_6^{3-/4-} = 7.6 \times 10^{-6}$ cm^2 s^{-1}) which is assumed to be equal to $D_{ox} = D_{Red}$ [15], C is the concentration of the probe species in the bulk solution (mol cm−3) and $K(\Lambda, \alpha)$ is a modified parameter for quasireversible reaction with function of Λ, defined as $k°/[D_{ox}(nF/RT)v]^{1/2}$, transfer coefficient ($\alpha = 0.5$), v is the scan rate in V s^{-1}, A_{eff} is effective electrode area (cm2). The parameter $K(\Lambda, \alpha)$ was determined from the ΔE_p and $(E_{p/2} - E_{pc})$ of same cyclic voltammograms recorded to obtain Fig. 4(c) [29]. First, the dimensionless parameter $\Delta(\Lambda, \alpha)$ was determined from the $(E_{p/2} - E_{pc})$ of same cyclic voltammograms where $E_{p/2}$ and E_{pc} are the half-wave and cathodic potentials, respectively, and Λ $(=\psi\pi^{1/2})$ was extracted from the working curve of ΔE_p vs ψ based on method developed by Nicholson [31]. From the $\Delta(\Lambda, \alpha)$ and Λ, therefore the values of α was determined for DMF modified and unmodified screen printed carbon electrodes to be from 0.33 to 0.63. The parameter $K(\Lambda, \alpha)$, ranging from 0.70 to 0.81, was then obtained from the corresponding values of Λ and α [32]. Fig. 4(c) shows a nearly linear plot of $i_{pc}K(\Lambda, \alpha)^{-1}$ of the redox process against the square root of the scan rate- the slope of which was used to estimate the effective areas of the electrodes. Error bars at each point correspond to the standard deviation of the measured peak currents obtained, after effectively ignoring capacitive currents, using 9 DMF activated SPCE from 3 batches (each 3 electrodes, N = 9).

Fig. 4(d) shows the effective area of the electrodes as a function of duration of exposure to the solvents. Clearly, the solvent treated electrodes display very large electrochemically active area than the untreated electrodes. The effective area of a 5 min DMF treated electrode, for instance, was 57-fold of its apparent geometric area. This result is consistent with the EIS data that the charge transfer resistances of the solvent treated electrodes were very low as compared to that of the untreated ones. Thus the observed improvement in the electrochemical performance of the solvent treated electrodes can be ascribed to the fastest charge transfer process at the increased electrochemically active electrode surface resulting from the selective etching action of the solvent. In an attempt to reproduce the findings with other solvents, we tried DMSO, acetonitrile and acetone.
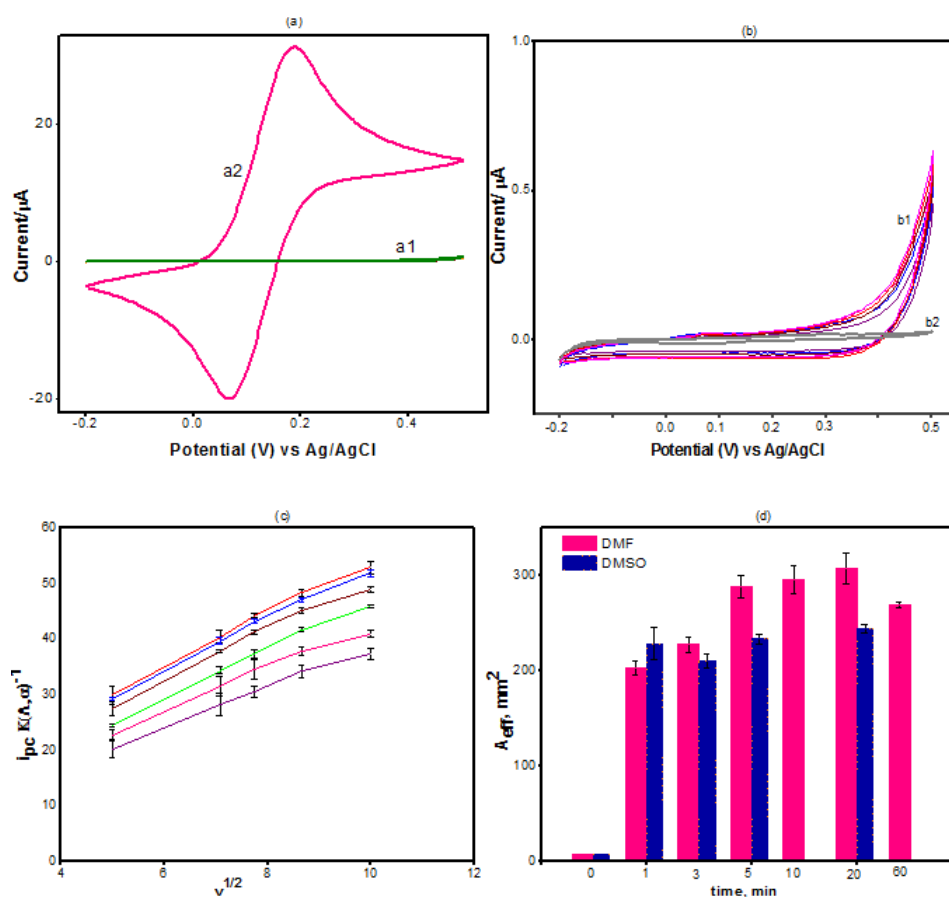
Fig. 4. (a) curve 'a2' corresponds to the CV of 2 mM $Fe(CN)_6^{3-/4-}$ in 0.1 M $Sr(NO_3)_2$ solution recorded at 20 min DMF treated electrode at scan rate of 20 mVs^{-1} whereas curve 'a1' correspond to several closely spaced CVs recorded in 0.1 M $Sr(NO_3)_2$ at 0, 1, 5, 10, 20, 30, and 60 min DMF treated electrode surfaces at same scan rate. (b) Shows the expanded version of the capacitive currents where the difference between the DMF treated (curves 'b1') and untreated (curve 'b2') electrodes become clear at higher potentials (>0.3 V). (c) Plot of $i_pK(\Lambda, \alpha)^{-1}$ obtained from the CVs of 2 mM $Fe(CN)_6^{3-/4-}$ in 0.1 M $Sr(NO_3)_2$ against the square root of the scan rate at the, bottom to top, 1, 3, 60, 5, 10, and 20 min DMF treated electrodes, respectively. (d) Comparison of electrochemically active area resulting from activation by DMF (■) and DMSO (■–dashed border) for different duration of exposure.

As can be seen from Fig. 4(d) both DMF and DMSO treated electrodes display dramatic enhancement in effective areas as compared to the untreated electrodes. Although DMSO has a similar effect of enhancing the electrochemical performance of the electrode, the improvement was not as high as that obtained with DMF. Moreover, during the prolonged duration of exposure than 20 min DMSO precipitates the etched contaminants on the electrode surface instead of dissolving entailing a rinsing step. Acetonitrile and acetone showed adverse effect on the adhesion of the screen printed film to the substrate. The electrodes soaked in DMSO looks like a wet paste. After the drying step, however, the electrode cures immediately and displays a highly reproducible improved level of performance. In both DMSO as well as DMF, the adverse flaking effect of acetone/acetonitrile is totally not observed. Based on the relatively better electrochemical characteristics of DMF treated electrodes, however, DMF can be selected as effective solvent for

further experiments. It did not have any peeling or disconnecting effect on either the plastic or electrodes when the strips were subjected to it for as long as 24 h. Since thermal effects on composite material surface has been reported to enhance porosity and enable sensing application [34], it was important to test if the lower working temperature (<100 ∘C) in the current study might have contributed to the recorded improvement in the performance of the electrodes. However, the electrodes treated at temperatures up to 120 ∘C for several minutes to hours did not exhibit any significant change in the electrochemical characteristics. Use of elevated temperature was not possible due to the temperature effects on the integrity of the substrates. Table 1 provides summary of kinetic and electrochemical reversibility data obtained for $Fe(CN)_6^{3-/4-}$ at SPCEs after pretreatment methods presented in current work and previous reports. In addition to the improved electrochemical performances demonstrated, current approach has advantages of simplicity, low cost, versatility, and direct industrial application for mass production of disposable electrochemical sensors and increases the potential of screen printed electrodes in facilitating further electrochemical novel-ties/applications.

Table 1

Comparison of the electrochemical performance of SPCEs activated via different procedures for $Fe(CN)_6^{-3/-4}$

Pretreatment procedure	Reference	ΔE_p (mV)	k^0 (cms^{-1})
0.05 M PBS, 1.5 V, 2 min	[17]	100[a]	3 x 10^{-3}
Saturated Na$_2$CO$_3$, 1.2 V, 5 min	[18]	61[b], 72, 105	6.5 x 10^{-3}
1 hr soaking in 3 M NaOH plus 1.2 V for 20 s in 0.5 M NaOH	[19]	67[c], 75[d], 80[a]	1.2 x 10^{-2}
UV excimer laser exposure	[21]	140[a]	2.5 x 10^{-3}
0.5 M H$_2$SO$_4$, -2 to +2 V, 20 cycles	[35]	121	-
Saturated Na$_2$CO$_3$, 1.2 V, 5 min	[35]	113	-
5 min DMF exposure, drying at 100 ∘C, 20 min	Current work	87	1.3 x 10^{-2}

Scan rates: [a]100 mVs^{-1}, [b]SPCEs of three different carbon inks at 60 mVs^{-1}, [c]10 mVs^{-1}, [d]50 mVs^{-1} and others at 20 mVs^{-1}.
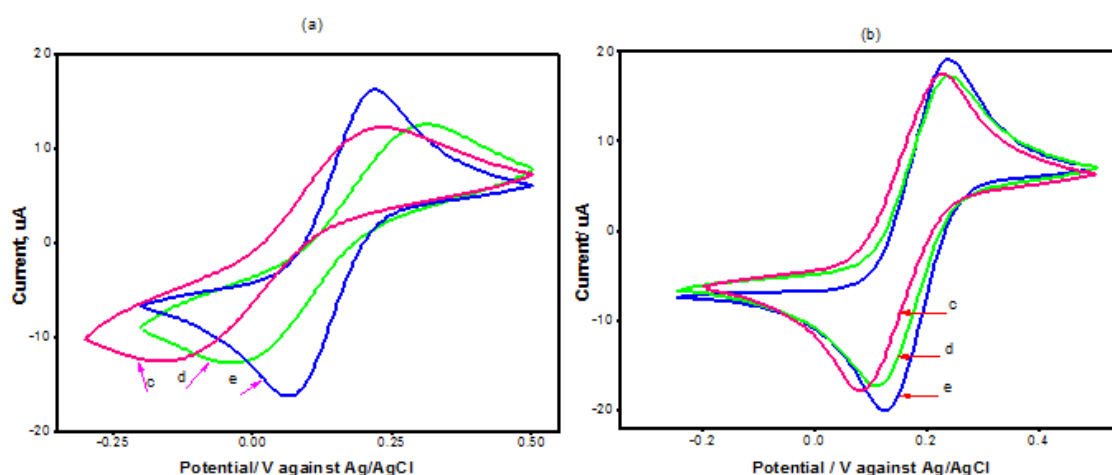

Fig. 5. Comparison of CVs of 2 mM $Fe(CN)_6^{3-/4-}$ redox couple at scan rate of 20 mVs^{-1} using (a) untreated, (b) 5 min DMF treated SPCEs from (c) Sunchemical, (d) DuPont and (e) Gwent.

113

In addition to the 7102 conductor paste based on carbon pro-vided by DuPont Ltd. (UK) used for the proof-of-concept results discussed above, other types of commercially available SPCEs were also tried to assess the versatility of the activation procedure. They include the C2030519P4 carbon/graphite provided by Gwent and 26-9203 conductive carbon obtained from SunChemical. Fig. 5 shows representative cyclic voltammograms of the 2 mM $Fe(CN)_6^{3-/4-}$ redox couple recorded using each type of carbon electrodes. As can be seen from the figure, the CVs recorded at untreated electrodes exhibit large differences in the peak currents and their position. Only Gwent electrode gave discernible redox peaks before pretreatment. Among, the DMF treated electrodes too, Gwent electrodes exhibited high peak currents. A peak-to-peak separation of 87 mV can be recorded at lower scan rates at the DMF treated Gwent electrodes. Notwithstanding the better performances of Gwent electrodes, all of the tested electrodes always exhibit improved level of electrochemical performance after pretreatment with DMF. These results strongly support the fact that the differences in the electrochemical performances of SPCEs are ascribed to the proportional graphitic loading and level of exposure of the electroactive sites. The solvent treatment appears to increase such sites through cleaning and etching of the surface contaminants.

4. Conclusion

We report that solvents can be used to modify surface characteristics of composite electrode materials through their selective etching action. Specifically, we demonstrated that selective etching action of a judiciously selected solvent (DMF) on the surfaces of screen-printed carbon electrodes greatly improves the electrochemical characteristics of the electrodes. The recorded improvement in the performance characteristics of the electrodes after pretreatment with DMF is proposed to be due to increased loading and exposure of the electroactive graphitic particles as the solvent selectively removes the surface blocking binders/resins. This superficial subtraction of certain but not all components from the surface of the electrodes affords a morphologically modified surface with improved pristine characteristics of the electroactive components. The proposed mechanism can be extended to other screen-printed electrodes including gold, silver, silver/silver chloride etc. The ability to activate several screen-printed electrodes simultaneously via the extremely simple, fast and yet effective activation procedure makes this approach cost effective and very promising to facilitate the development of disposable and miniaturized electrochemical biosensors for point-of-care diagnostics, food analysis, and environmental monitoring.

Acknowledgements

References

[1] D. Mata, D. Bejarano, M.L. Botero, P. Lozano, M. Constantí, I. Katakis, Screen-printed integrated microsystem for the electrochemical detection of pathogens, Electrochimica Acta 55 (2010) 4261.

[2] P. Ertl, M. Wagner, E. Corton, S.R. Mikkelsen, Rapid identification of viable Escherichia coli subspecies with an electrochemical screen-printed biosensor array, Biosensors and Bioelectronics 18 (2003) 907.

[3] L. Santiago, D. Bejarano, P. Lozano, I. Katakis, Screen-printed microsystems for the ultrasensitive electrochemical detection of alkaline phosphatase, Analyst 135 (2010) 1276.

[4] T. Montesinos, S.P. Munguia, F. Valdez, J.L. Marty, Disposable cholinesterase biosensor for the detection of pesticides in water-miscible organic solvents, Analytica Chimica Acta 431 (2001) 231.

[5] C. Bonnet, S. Andreescu, J.L. Marty, Adsorption: an easy and efficient immobilisation of acetylcholinesterase on screen-printed electrodes, Analytica Chimica Acta 481 (2003) 209.

[6] F. Darain, S.-U. Park, Y.-B. Shim, Disposable amperometric immunosensor system for rabbit IgG using a conducting polymer modified screen-printed electrode, Biosensors and Bioelectronics 18 (2003) 773.

[7] O. Bagel, B. Limoges, B. Schollhorn, C. Degrand, Subfemtomolar determination of alkaline phosphatase at a disposable screen-printed electrode modified with a perfluorosulfonated ionomer film, Analytical Chemistry 69 (1997) 4688.

[8] Q. Gao, Y. Guo, W. Zhang, H. Qi, C. Zhang, An amperometric glucose biosensor based on layer-by-layer GOx-SWCNT conjugate/redox polymer multilayer on a screen-printed carbon electrode, Sensors and Actuators B 153 (2011) 219.

[9] D.R. Matthews, E. Bown, A. Watson, R.R. Holman, J. Steemson, S. Hughes, D. Scott, Pen-sized digital 30-second blood glucose meter, Lancet 1 (1987) 778.

[10] F. Ge, X.E. Zhang, Z.P. Zhang, X.M. Zhang, Simultaneous determination of maltose and glucose using a screen printed electrode system, Biosensors and Bioelectronics 13 (1998) 333.

[11] M. Dequaire, A. Heller, Screen printing of nucleic acid detecting carbon electrodes, Analytical Chemistry 74 (2002) 4370.

[12] J. Wang, D.K. Xu, A.N. Kawade, R. Polsky, Metal nanoparticle-based electrochemical stripping potentiometric detection of DNA hybridization, Analytical Chemistry 73 (2001) 5576.

[13] Q. Gao, X. Cui, F. Yang, Y. Ma, X. Yang, Preparation of poly(thionine) modified screen-printed carbon electrode and its application to determine NADH in flow injection analysis system, Biosensors and Bioelectronics 19 (2003) 277.

[14] H.C. Yoon, H.S. Kim, Electrochemical characteristics of a carbon-based thickfilm L-lactate biosensor using L-lactate dehydrogenase, Analytica Chimica Acta 336 (1996) 57.

[15] P. Fanjul-Bolado, D. Hernández-Santos, P. José Lamas-Ardisana, A. Martín- Pernía, A. Costa-García, Electrochemical characterization of screen-printed and conventional carbon paste electrodes, Electrochimica Acta 53 (2008) 3635.

[16] B.D. Malhotra, A. Chaubey, Biosensors for clinical diagnostics industry, Sensors and Actuators B 91 (2003) 117.

[17] J. Wang, M. Pedrero, H. Sakslund, O. Hammerich, J. Pingarron, Electrochemical activation of screen-printed carbon strips, Analyst 121 (1996) 345.

[18] G. Cui, J.H. Yoo, J.S. Lee, J. Yoo, J.H. Uhm, G.S. Cha, H. Nam, Effect of pre-treatment on the surface and electrochemical properties of screen-printed carbon paste electrodes, Analyst 126 (2001) 1399.

[19] H. Wei, J.J. Sun, Y. Xie, C.G. Lin, Y.M. Wang, W.H. Yin, G.N. Chen, Enhanced electrochemical performance at screen-printed carbon electrodes by a new pretreating procedure, Analytica Chimica Acta 588 (2007) 297.

[20] V.T. Kostaki, A.B. Florou, M.I. Prodromidis, Electrochemically induced chemical sensor properties in graphite screen-printed electrodes: The case of a chemical sensor for uranium, Electrochimica Acta 56 (2011) 8857.

[21] M.D. Osbome, B.J. Seddon, R.A.W. Dryfe, G. Lagger, U. Loyall, H. Schafer, H.H. Girault, Excimer laser-induced electrochemical activity in carbon ink films, Journal of Electroanalytical Chemistry 417 (1996) 5.

[22] S.C. Wang, K.S. Chang, C.J. Yuan, Enhancement of electrochemical properties of screen-printed carbon electrodes by oxygen plasma treatment, Electrochimica Acta 54 (2009) 4937.

[23] C.E. Banks, R.G. Compton, New electrodes for old: from carbon nanotubes to edge plane pyrolytic graphite, Analyst 131 (2006) 15.

[24] M. Rubianes, G.A. Rivas, Carbon nanotubes paste electrode, Electrochemistry Communications 5 (2003) 689.

[25] M.D. Rubianes, G.A. Rivas, Enzymatic biosensors based on carbon nanotubes paste electrodes, Electroanalysis 17 (2005) 73.

[26] C.H. Lee, S.C. Wang, C.J. Yuan, M.F. Wen, K.S. Chang, Comparison of amperomet-ric biosensors fabricated by palladium sputtering, palladium electrodeposition and nafion/carbon nanotube casting on screen-printed carbon electrodes, Biosensors and Bioelectronics 22 (2007) 877.

[27] R.J. Bowling, R.T. Packard, R.L. McCreery, Mechanism of electrochemical acti-vation of carbon electrodes: role of graphite lattice defects, Langmuir 5 (1989) 683.

[28] D. Bejarano, P. Lozano, D. Mata, S. Cito, M. Constanti, I. Katakis, Screen prin-ting as a holistic manufacturing method for multifunctional microsystems and microreactors, Journal of Micromechanics and Microengineering 19 (2009) 115007.

[29] A.J. Bard, L.R. Faulkner, Electrochemical Methods: Fundamentals and Applica-tions, Wiley, New York, 2001.

[30] S. Devan, V.R. Subramanian, R.E. White, Analytical solution for the impedance of a porous electrode, Journal of the Electrochemical Society 151 (2004) 905.

[31] R.S. Nicholson, Theory and application of cyclic voltammetry for measurement of electrode reaction kinetics, Analytical Chemistry 37 (1965) 1351.

[32] H. Matsuda, Y. Ayabe, Zur theorie der randles- sevcik schen kathodenstrahl-polarographie, Zeitschrift für Elektrochemie 59 (1955) 494.

[33] S.H. Lee, H.Y. Fang, W.C. Chen, Electrochemical characterization of screen-printed carbon electrodes by modification with chitosan oligomers, Electro-analysis 17 (2005) 2170.

[34] A.P. Washe, S. Macho, G.A. Crespo, F.X. Rius, Potentiometric online detection of aromatic hydrocarbons in aqueous phase using carbon nanotube-based sensors, Analytical Chemistry 82 (2010) 8106.

116

[35] E. Dock, T. Ruzgas, Screen-printed carbon electrodes modified with cellobiose dehydrogenase: amplification factor for catechol vs. reversibility of ferricyanide, Electroanalysis 15 (2003) 492.

117

CHAPTER 6

GENERAL CONCLUSION

Flow control is critical expected operation in the development of microfluidic devices. The manner of flow control can be different depending on whether the final microfluidic device is intended for analysis of gas or liquid samples. Flow control strategies intended to accompany the development goal of simple and low cost devices should consider simple and all low cost approaches in fluid pumping and valving mechanisms. As a power free pumping mechanism capillary force is frequently selected for the development of microfluidic devices for applications that require user friendly devices. As a microscale flow, however, capillary flow is also laminar and consequently is bad mixer. To promote dissolution, mixing, and reaction in microchannels, especially when these operations have to be performed in the vicinity of chemicals previously deposited in microchannels, precise manipulation of capillary flow including stopping and restarting is very important.

While capillary flow can be controlled either by controlling the surface property or geometry of microchannel when using a liquid of constant surface property, wettability based approaches are more flexible and can be accomplished in simpler and cheaper steps. In stop/go fluidic operations in capillary force driven microfluidic systems, the first step is to design and produce microsystems and test capillarity. In this thesis through careful selection of materials based on wettability characteristics and some well established theories such as the Young-Laplace equation microsystems that display capillarity has been constructed from low cost materials such as plastics bonded via adhesives. To stop capillary flow at a specific location in microchannels of such devices, a superhydrophobic surface is often required. Superhydrophobic surface is desired for some more reasons: it allows large range of contact angle changes and change in capillary pressure and it displays a favorable low voltage wettability transition to more wettable states which is expected to facilitate the flow actuation. Although numerous methods have been reported demonstrating the fabrication of superhydrophobic surfaces, most of the reported methods are just proof of concepts and are not suitable for specific application such as flow stopping and restarting by a low voltage approach. Needles to mention, low voltage is selected in this thesis for flow actuation because of its simplicity to operate, miniaturize (both size and cost) and integrate into microfluidic devices. All what was required is to produce a superhydrophobic surface that provides passive stopping of capillary flow and that also facilitates the low voltage actuation of the flow.

118

Superhydrophobic surfaces are usually produced by either of the two methods: constructing a nanoscale roughness on a hydrophobic material of modifying low surface energy rough materials with hydrophobic materials. In this thesis both approaches were implemented through simple and low cost approach to produce superhydrophobic surface that is suitable for the intended passive stopping and low voltage actuation of the flow. In the first approach SMART superhydrophobic surface was constructed by modifying a previously roughness amplified and activated screen printed carbon electrode with electrically responsive polymer. Because it is superhydrophobic it provides passive stopping. Because the polymer undergoes wettability switching from superhydrophobic to superhydrophilic under applied potential the flow restarts at extremely low voltage (<1V). As the fabrication of the polymer based superhydrophobic surface had to be accomplished by electropolymerization on a previously roughness amplified surface, the screen printed carbon electrode´s surface needed to be modified first. In addition to this, untreated screen printed carbon does not allow direct electropolymerization because of its reduced electrochemical characteristics imposed by contaminants. The electrode needs to be activated. Thus prior to electropolymerization the screen printed carbon electrode surface was activated in a manner that simultaneously enhances roughness. However, this task had to be done in a specific manner. The activation as well as roughness amplification strategy should not introduce nucleophilic functionalities on electrode´s surface. Such functionalities as hydroxyl groups can render nucleophilic attack to the growing polymeric chain during the electropolymerization and destroy the conjugation- the key requirement for the expected electrically tunable property of the polymer. This is achieved in this work by a new procedure that involves controlled and selective subtraction of nonelectroactive components from the electrode's surface based on solubility principles. The selective subtraction enhances surface roughness and also activates the electrodes for electropolymerization by increasing graphitic loading and exposure (electrochemical accessibility) of the graphitic edges with electrocatalytic property. Electrodeposition of the polymer was then performed on the previously roughened and activated screen printed carbon electrode´s surface through controlled cycling of potential to produce poly(3-methylthiophene) based superhydrophobic surface that displays passive stopping of capillary flow and facilitate low voltage actuation of the flow. While the polymer based valve is attractive, it suffers from the lack of stability of the polymer as it grows by electropolymerization. The polymer can simply get oxidized preferentially to monomers. This problem was overcome during this thesis by subjecting the polymeric film to a neutralizing potential just after the polymerization. This approach is very attractive to provide proof of concept but may be difficult if mass production is required.

119

Alternatively, therefore, and with the objective of simplifying procedures to facilitate mass production and producing a more robust superhydrophobic surface, superhydrophobic nanoporous electrode was produced via controlled etching of a composite electrode surface (screen printed electrode). This approach boasts simplicity and is based on the favorable wettability transition from the less stable Cassie-Baxter wettability regime of superhydrophobic nanoporous electrode with no further modification to a more stable and more wettable Wenzel regime of wettability by electrowetting. By virtue of superhydrophobicity the electrode stops the flow and by virtue of the high conductivity, large potential window and intrinsic charge accumulation capacity of carbonaceous material it facilitates the low voltage actuation through electrowetting transitions at extremely low voltage. In this case both electrodes involved in the valving operation are based on screen printed carbon-one wettable and the other superhydrophobic nanoporous in each stop/go valving electrode pair. This valve showed a strong dependence of the type and concentration of ions. For common salts including NaCl, KCl, $MgCl_2$, the lower (≤ 0.1) the concentration the better the flow actuation. The valve response to applied potential is also sensitive to the porosity nature of the electrode which is difficult to control with solvent etching approach. At least three phenomena that can contribute to electrocapillarity have been revealed: the electrical double layer capacitance, specific counterion adsorption, and possibly electrohydrodynamic effects corresponding to on-chip generated gradients.

In the third scheme the same superhydrophobic surface developed on carbon electrode was used but couple to screen printed silver. This is the simplest approach and provides faster responses that show positive dependence on concentration, especially of chloride salts. The superhydrophobic electrode as usual provides passive stopping of the flow and facilitates low voltage actuation of the flow but in this case in different manner. The asymmetric electrode configuration is expected to cause asymmetric electrochemical process giving rise to gradients across the two electrodes that can propel the liquid. In this way stop/go fluidic operations were successfully demonstrated in capillary force operated microfluidic devices.

In conclusion three different strategies were investigated to produce electrochemically actuated capillary flow control in a way that facilitates the development of capillary force operated integrated microfluidic devices. The operation of the valves is successfully demonstrated in the expected manner. The performance characteristics of the valves were investigated in a stop/go mode through response time measurements. Mechanistic investigations on the operation principles

were carried out through electrowetting and other methods including but not limited to electrochemical impedance spectroscopy and BET methods. The investigation has revealed new insights into electrical actuation of flow based on electrowetting mechanisms. Factors that were not given due attention appeared to play significant role in electrochemical actuation of microscale flow. At least three phenomena that contribute to electrocapillarity: the electrical double layer capacitance, specific counterion adsorption, and possibly electrohydrodynamic effects corresponding to on-chip generated gradients have been found to play significant role in the flow actuation.

CHAPTER 7

FUTURE OUTLOOK

Flow control is critical expected operation in the development of microfluidic devices. Thus the electrochemically actuated capillary flow control developed in this study is directly applicable to capillary force operated microfluidic devices not only originally intended electrochemical microfluidic immunosensor but also other microfluidic systems for bioanalytical analysis where stopping of flow at a specific location in microchannel and restarting is required. The device may find application in all areas of research that tries to develop microfluidic systems based on the principle of lateral flow devices-be it calorimetric, optical, and electrochemical or just agglutination assays. The electrochemically actuated valves may also be applicable in reactant-in product-out microfluidic synthesis; which involves a sequence of elementary reactions to be performed downstream. In this case catalysts, instead of immunochemical can be previously deposited in microchannels to realize miniaturization, integration and automation the synthetic routes.

The ability to move protein containing solution over a porous carbon-based surface under applied potential, demonstrated in this study, may find application in protein separation or in separation and analysis of other biomolecules such as DNA/RNA. Probably such simply produced porous network of carbon, if occurred in column, could also compete with current technology for electrophoresis because charged species will move with different degree over such surface under applied potential. The superhydrophobic porous carbonaceous surface may also find application in other electrokinetic applications such as electroosmotic or electrohydrodynamic. It can replace porous membranes or glass frits used in such applications. The superhydrophobic nanoporous carbon developed in this study may also be applied as perchlorate (ClO_4^{-1}) sensor. The superhydrophobic carbon coupled to silver may be applied for chloride removal applications. The porous carbon developed in this study may also find application in heterogeneous catalysis especially solid supported catalysis as the porous structures can provide supports to such catalyst.

All electrochemistry based sensors and biosensors require activation of the electrode´s surface. In view of the highly attractive avenue that screens printed electrodes provides for the development of low cost electrochemical biosensor, the developed electrode surface modification strategy may find application in the development of sensors/biosensors. Electrowetting is currently investigated for various applications. The mechanistic investigations carried out in this study may add new insights into the understanding and improvement of such applications.